# Statistical mechanics of boundary driven systems


Thomas Stephen Welsh

Submitted in accordance with the requirements
for the degree of Doctor of Philosophy

The University of Leeds

School of Physics and Astronomy

June 2012

The candidate confirms that the work submitted is his/her own and that appropriate credit has been given where reference has been made to the work of others.

# Acknowledgements

Many thanks go to my supervisor Mike Evans for much guidance and support. I am also very grateful to John Williamson for helpful discussions and less helpful but necessary distractions from work.

Thank you to my parents, who provided the foundation for everything I do.

Finally and most importantly, I must thank my family: my wife for putting up with me and my obsessions, and especially my children for letting me forget about the rest of the world while I am with them.

# Abstract

Statistical mechanics is concerned with finding the macroscopic behaviour of a physical system given its microscopic characteristics. At equilibrium there is a general framework given in terms of the various statistical ensembles that describes how to calculate the macroscopic quantity that is desired. Out of equilibrium there is no such framework, leading to the treatment of microscopic models on an individual basis and the investigation of arbitrarily defined models. However, there exists a recent theory of boundary driven steady states and an associated nonequilibrium counterpart to detailed balance due to Evans.

In this thesis I first review this theory of boundary driven steady states and the associated nonequilibrium counterpart to detailed balance due to Evans, before applying the theory to some toy models of driven athermal systems. These initial attempts do not reproduce the qualitative behaviour of granular systems such as jamming but are a valuable and novel starting point for a more thorough investigation of this technique.

I then move on to the general theory of boundary driven systems and formulate a nonequilibrium free energy principle. The physical content of this is illustrated through a simple diffusion model. I then provide a reformulation of the principle which is more suitable for calculation and demonstrate its validity in a more complex model.

Finally I investigate a particular example of a boundary driven system, a toy model of a complex fluid called the rotor model. I first use simulation to investigate the model and its phase behaviour, before using an analytical approach to do the same. This approach takes the form of a nonequilibrium real space renormalisation group calculation, and qualitatively reproduces some of the features seen in the simulations.

# Contents

# List of Figures

# Abbreviations

| | |
|---|---|
| NCDB | Nonequilibrium Counterpart to Detailed Balance |
| ODE | Ordinary Differential Equation |
| DPD | Dissipative Particle Dynamics |

# Chapter 1

# Introduction

It is a fact observed for centuries that macroscopic amounts of matter, typically but not limited to solids, liquids or gases, if left unperturbed, will generally settle down into an unchanging state. When this is the case, such systems can typically be described by a small number of variables such as energy, volume and temperature. Thermodynamics describes how these few variables change and are related to each other using the ideas of heat and work; despite the vast array of systems governed by thermodynamics, the main features of the theory can be summed up by just four laws. As science progressed it was found that this everyday matter actually consisted of an unimaginable number of atoms or molecules undergoing rapid motion, on the scale of Avogadro's number or of the order of $10^{23}$. A new challenge emerged: the alternative description of these systems starting from the microscopic level. The field of statistical mechanics is primarily concerned with such systems containing a large number of elements.

The microscopic state of a system can be described by a microstate - a list of all microscopic properties of the system such as the position, velocity and angular momentum of every particle. Given the equations of motion of the particles the system is completely specified, and the evolution of the microstate of the system will be given by these equations. They are of course impossible to solve for practically all realistic systems due to the fantastically large number of them.

Fortunately, in practice we never care about exactly which microstate the system is in at a given time, but instead the values of quantities we measure at the macroscopic scale such as pressure and volume. Statistical mechanics approaches this question by introducing probabilistic assumptions into the theory and asking the

question: what is the probability of finding the system in a particular microstate? For systems at equilibrium with a heat bath of temperature $T$, the answer has been known for over a century and is given by the Boltzmann distribution. If each microstate $\mathbf{x}$ is assigned an energy $E(\mathbf{x})$, then the probability of observing that microstate is proportional to $e^{-\beta E(\mathbf{x})}$, where $\beta = 1/k_B T$ and $k_B$ is Boltzmann's constant:

$$p(\mathbf{x};\beta) = \frac{e^{-\beta E(\mathbf{x})}}{Z}, \quad Z = \sum_{\mathbf{x}} e^{-\beta E(\mathbf{x})}. \tag{1.1}$$

$Z$ is a normalisation factor called the partition function. This probability distribution can then be used to calculate the values of quantities that an experimenter will actually observe, if that quantity can be connected with an appropriate function over the microstates of the system, and given that the calculation can actually be performed. An equivalent formulation is in terms of the free energy $F$, defined by

$$F = -\beta^{-1} \ln Z. \tag{1.2}$$

This microscopic definition of the free energy provides a link to thermodynamics, where the macroscopic quantities such as pressure and internal energy are calculated as appropriate derivatives of the free energy. Using either of these approaches, the problem appears to be solved.

This statement does not by itself answer all of our questions, however. One of the most striking features of equilibrium physics is the existence of phase transitions, whereby a system changes from one state to a qualitatively different one upon variation of some control parameter such as temperature. The transition is characterised by an order parameter, a quantity that changes qualitatively upon crossing the transition, for example by moving from zero to a nonzero value. Thermodynamically, this qualitative change is captured by a non-analytic free energy, that is, a free energy for which one or more of the derivatives with respect to the control parameter is undefined.

A deep insight into phase transitions is gained by one of the most important ideas in physics of the previous century: renomalisation group theory. Used extensively in the physics of criticality (continuous phase transitions) and particle physics, it is based on the changes upon viewing a system at different length scales or distances (or different energies in particle physics). In particular, at the largest length scales

it can be the case that the microscopic details of a system become unimportant; this leads to universal behaviour among disparate physical systems, their properties determined only by features such as spatial dimension and symmetry. The behaviour of the system on large length scales determines its phase behaviour, for example, if distant parts of a system are strongly correlated then we would expect to see some degree of long range order in the system, for example crystallinity. One form of renormalisation group theory, the real space renormalisation group, is based mainly on the work of Migdal [1] and L. P. Kadanoff [2, 3] and consists of removing short distance degrees of freedom by a process of decimation. This entails averaging over short distance properties to create a new system that describes how the original one looks at larger distances; this can be achieved by averaging out individual components or by averaging over a collection of components to create a new kind of object. If this averaging is repeated over and over again, it is found that the system as described by a collection of parameters will tend to a limit, called a fixed point. The limit reached depends on what the original system was, for example what its temperature was. These fixed points are understood to describe the system properties on the macroscopic scale, and certain fixed points correspond to the phases observed in experiment.

While equilibrium physics is mostly a well understood discipline, a cursory glance around us reveals that the world is generally not in a state of equilibrium; it is filled with fluid flows, electrical currents, temperature gradients, time dependent phenomena and so on. What is the correct picture for this significantly more complicated world? It is most often assumed that a picture in terms of probability distributions will serve just as well as at equilibrium, although it is rather unlikely that there is a universal probability distribution that describes all situations with the simplicity of the Boltzmann distribution due to the vast range of situations that fall under the label “nonequilibrium”. Nonequilibrium systems may be observed to undergo phase transitions as at equilibrium, although there is no general theory for comparison. Renormalisation group theory cannot be used in its usual guise, but one of the chapters of this thesis is devoted to the application of the same ideas out of equilibrium. Insight into the near equilibrium case was given by Green and Kubo in the form of their relations that link dynamic properties such as viscosity to correlation functions [4, 5]. Some more general approaches have been devised, such

as the Jarzynski [6, 7, 8] and Crooks [9, 10] relations and the assorted fluctuation theorems [11, 12, 13], that are valid arbitrarily far from equilibrium. The theory of stochastic thermodynamics due to U. Seifert [14, 15] uses the ideas and language of thermodynamics in the context of microscopic systems where fluctuations are important.

The study of time independent systems provides a large simplification. These are systems in a steady state, for which the values of macroscopic quantities fluctuate in time but average to the same constant value over any time window of long enough duration (in theoretical work this duration is normally assumed to be infinite, but in practice the phrase "long enough" depends on the details of the system). Equilibrium is the simplest example of a steady state, one without any macroscopic flow of mass, energy or any other quantity.

This thesis is concerned only with boundary driven systems in a steady state. Boundary driven systems are those whose constituents are not directly affected by any external fields but are perturbed away from equilibrium at the boundaries. The archetypal example of a boundary driven system is a sheared fluid, where the perturbation is provided by the relative movement of the walls of the container. Newtonian fluids such as water respond simply to the perturbation, by developing a constant velocity gradient across the system called the shear rate $\dot{\gamma}$. If the shear stress $\Sigma$ needed to drive the system is measured then it is found to obey $\Sigma = \eta\dot{\gamma}$, which serves to define the (constant) viscosity $\eta$. This relation between flow parameters is called the constitutive relation. Non-newtonian fluids are those which do not follow this rule and have instead a more complicated form for $\Sigma(\dot{\gamma})$. These complex fluids possess some degree of internal structure on the mesoscopic scale, larger than the size of a single molecule but not as large as the system size, and are generally described by tensorial models. Typical fluids that show non-Newtonian behaviour include polymer solutions, polymer melts and micellar solutions. The deviation from Newtonian behaviour may take many forms. Shear thinning is a decrease of the viscosity with shear rate, whereas shear thickening is the opposite. Some systems cannot support homogeneous flow for some range of shear rates or stresses and must separate out into bands of differing shear rates (shear banding) or stresses (vorticity banding).

From a microscopic point of view, constituents of the fluid near the boundary

may collide with the confining walls, but particles in the bulk of a large volume of fluid will obey the same equations of motion as at equilibrium due to the lack of direct forces from the walls. These bulk particles are in a nonequilibrium state but only due to the similarly nonequilibrium condition of the fluid around them. This suggests the interpretation of a large volume in the bulk of the fluid as the system of interest with the remaining even larger surrounding fluid being a nonequilibrium reservoir, similar to the picture in the equilibrium canonical ensemble where a system of interest is in contact with a heat bath of practically infinite size. R. M. L. Evans and coworkers have investigated the modelling of these systems and provided rules that models should obey if they wish to describe such situations [16, 17, 18, 19]; these rules and their foundation are used to derive some results in this thesis.

Chapter 2 is devoted to an application of the rules just mentioned: the behaviour of boundary driven systems as their temperature is reduced to zero. Athermal systems with a large number of constituents abound in nature, but are not described by ordinary statistical mechanics as they cannot explore their configuration space due to the lack of any thermal excitation. It is as yet unclear whether a statistical description of these systems is possible. However, driven athermal systems raise the possibility of exploration of the phase space through mechanical excitation. In this chapter, I give some background to the phenomenology and theory of granular materials before reviewing the theory of Evans et al. for boundary driven systems. The rest of the chapter discusses the application of the theory to athermal systems before testing it in boundary driven toy models for which the temperature is taken to zero.

Chapter 3 delves deeper into the theory of boundary driven systems in order to provide a partial answer to an elusive question in the field: is there such a thing as a free energy out of equilibrium, and if so, how can we calculate it? If known, this function would provide a route to calculate properties of any model such as the average current. The NCDB formalism is used to derive two results: a rather formal expression for the free energy in boundary driven systems dependent on full knowledge of the statistics of the current at equilibrium, and an equivalent but simpler expression which can be calculated using just the equilibrium transition rates and the integrated flux gained in each transition. The former is applied to an analytically tractable model, one dimensional diffusion. The latter is applied to the

"comb model", a simple toy model for which the equilibrium current distribution is unknown. However, the free energy and therefore the current can be numerically determined very simply. This result is checked against the independent analytical result for the current in the driven system.

Chapter 4 moves away from fundamental theory and introduces a toy model of a complex fluid called the rotor model. This is a one dimensional model similar to the XY model but with a full dynamical equation of motion for each constituent. In addition, it is sheared out of equilibrium into a steady state. As it is a nonequilibrium many particle interacting system, it is difficult to analyse theoretically so the first approach at understanding it is via simulation. Simulation results are given for various parameters and the phase behaviour of the model is sketched. Two important results from the simulations are the constitutive curve, i.e. the stress $\Sigma$ felt by the rotors as a function of the applied shear rate $\dot{\gamma}$, and the identification of possible order parameters describing the phases.

Chapter 5 analyses the rotor model from a theoretical perspective. The goal is to describe some of the features revealed in simulation, a difficult job due to the nonequilibrium nature of the problem. The rotor model is an interacting model, meaning it is much more realistic than the models considered in chapters 2 and 3, but also too complex for the apparatus associated with the fundamental theory to be used. The main result of this chapter is a nonequilibrium real space renormalisation group calculation which describes how the parameters of the model appear to change as the model is viewed at different length scales. This gives information about the way in which homogeneous regions of the system behave. The results obtained are compared with the simulation data.

# Chapter 2

# Boundary driven systems in the limit of zero temperature

## 2.1 Introduction

As well as the thermal systems that are most commonly encountered in statistical mechanics, nature also provides a wide variety of athermal systems, including granular media. These are typically systems that contain a large number of particles, where said particles are themselves too large to be appreciably affected by thermal fluctuations and can only be excited by driving the system in some fashion. This means that static granular assemblies are nonergodic, i.e. their phase space is unexplored, and so ordinary statistical mechanics fails to describe them. Granular systems that are driven would fall outside of the realm of equilibrium statistical mechanics anyway.

An early documentation of the uniqueness of granular media describes what is now known as Reynolds dilatancy [20]. This is the change in volume of the system in response to a change in shape or an applied strain and is a property not exhibited by simple fluids. Granular media jam, that is, develop a nonzero yield stress in an amorphous state, when their density is increased, so that they will only flow when pushed hard enough or in the right direction [21]. The stress in a high density granular medium is typically distributed inhomogeneously, with chains of grains in contact supporting large forces and others only feeling weak contact forces. Many more interesting properties are exhibited by driven granular systems. When the concentration of grains is low, they mostly interact via (inelastic) binary

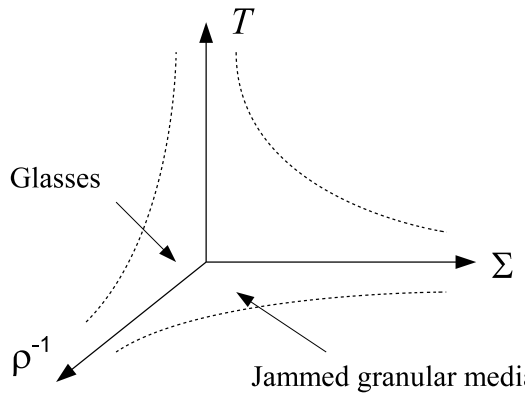


**Figure 2.1:** The jamming phase diagram of Liu and Nagel, adapted from their original paper on the matter [26].

collisions and exhibit gas-like behaviour. At higher concentrations more lasting contacts between grains are formed. Non-Newtonian behaviour is typically seen, often including Bagnold scaling [22, 23] where the shear stress varies as the square of the shear rate; shear induced size separation [24] and shear banding [25] have also been seen. These and other disparate phenomena have for the most part not been drawn together.

The connection to finite temperature materials is also unclear. Colloidal suspensions may jam at a high enough packing fraction, and molecular liquids may jam at a low enough temperature, so it is natural to ask if these phenomena are related. In 1998 A. J. Liu and S. R. Nagel proposed a unification of these phenomena via a jamming phase diagram [26]. A sketch of the phase diagram is shown in figure 2.1. The three axes are temperature $T$, applied stress $\Sigma$ and inverse density $\rho^{-1}$. The common link between all of these is that at large values jamming does not occur. An ordinary equilbrium fluid would reside in the $\Sigma = 0$ plane, whereas granular media occupy the $T = 0$ plane. Close to the origin, within the region enclosed by the dotted lines, the system is jammed in one way or another. The exact surface that bounds this region is somewhat vague, depending on the system in consideration and the time constraints of the experiment; it could be the case that a jammed system is not truly "thermodynamically" jammed, but would relax given a long enough time to an unjammed state. This relaxation time may be vastly greater than any length of time that an experimentalist would be willing to wait for, so in general some arbitrary definition must be decided upon as to what constitutes a jammed state.

The line in the $T = 0$ plane corresponds to the yield stress of an athermal

material, whereas the line in the $\Sigma = 0$ plane corresponds to the glass transition. It has been conjectured that for systems with short range repulsive interactions these two lines meet at a well defined point on the inverse density axis called point J. This corresponds to random close packing, the densest packing fraction achievable in an amorphous arrangement of particles - roughly 64% for hard spheres - although the concept of random close packing has been criticised by S. Torquato, who argues for a more precise maximally random jammed state [27]. Point J has some of the features of a critical point but many that do not correspond to equilibrium critical physics [28, 29]. The work in this chapter will be framed in terms of the Liu and Nagel phase diagram later.

The most common way of disturbing a granular system is via the imposition of a shear stress. The shearing of a granular medium is an example of a boundary driven process, as described in chapter 1. This opens up the possibility of using the theory of boundary driven systems developed by R. M. L. Evans and coworkers. This is a well founded approach to this class of systems which results in a nonequilibrium ensemble picture of a sheared system, and a principle called the nonequilibrium counterpart to detailed balance, or NCDB. This says that stochastic boundary driven systems have a number of constraints upon the transition rates between microstates, equal to the number of constraints in equilibrium (i.e. those given by detailed balance). In section 2.2 I review the NCDB formalism and comment on its use in the limit of zero temperature. The following sections apply the principle to some toy models, namely one dimensional diffusion in section 2.3 and the comb model in section 2.4.

## 2.2 The nonequilibrium counterpart to detailed balance

Theoretical models of stochastic systems are often described using a set of states between which the system moves according to some probabilistic rules. The states represent a specification of the system, for example in terms of positions, velocities, energies and so on; collectively they are called the phase space of the system. The rules consist of transition rates between different states: for two states $i$ and $j$ the transition rate $\omega_{ij}$ is the probability of moving from $i$ to $j$ per unit time. The probability of observing the system in state $i$, $p_i$, is determined by the master equation:

$$\frac{\mathrm{d}p_i}{\mathrm{d}t} = \sum_j (p_j \omega_{ji} - p_i \omega_{ij}). \tag{2.1}$$

For a particular $j$, the term in the sum represents the net current between $i$ and $j$. This equation is to be supplemented with the usual conditions of positive and normalised probabilities: $p_i \geq 0$ and $\sum_i p_i = 1$. If the rates are known, and given a suitable initial condition, then we can in principle solve this equation to find the probability distribution over the states of the system as a function of time.

We may instead consider steady states only. These are situations for which the occupation probabilities are time invariant, so that the left hand side of the master equation (2.1) is zero. One way of ensuring this is to have all the individual terms in the sum on the left hand side vanish individually:

$$p_j \omega_{ji} - p_i \omega_{ij} = 0 \quad \forall\, i,\, j. \tag{2.2}$$

This statement says that the transitions from $i$ to $j$ are balanced exactly by transitions from $j$ to $i$, so that on average there is no flow of matter, energy and so on through the system. In this way detailed balance is a necessary condition for equilibrium; it can be viewed as a restriction on the transition rates in the model if equilibrium is to be reached. For a system described by a canonical distribution, the probability of a state $i$ is known to be proportional to $e^{-\beta E_i}$ where $E_i$ is the energy of state $i$ and $\beta = 1/k_B T$ (the Boltzmann distribution). Equation (2.2) can then be rewritten as

$$\frac{\omega_{ij}}{\omega_{ji}} = e^{\beta(E_i - E_j)}. \tag{2.3}$$

There are any number of steady states other than equilibrium for which the right hand side of (2.1) is zero, but they must lead to some net flux through the system. Detailed balance does not hold, and it is not known in general whether an equivalent constraint will hold instead. Because of this lack of knowledge, it is a common practice to simply define a physically reasonable set of rates for a nonequilibrium system before investigating their consequences such as phase behaviour (see e.g. the bus route model of O'Loan et al. [30] or driven diffusive systems [31, 32]). A partial substitute for detailed balance has been derived by R. M. L. Evans and coworkers, who consider the case of boundary driven systems arbitrarily far from equilibrium.

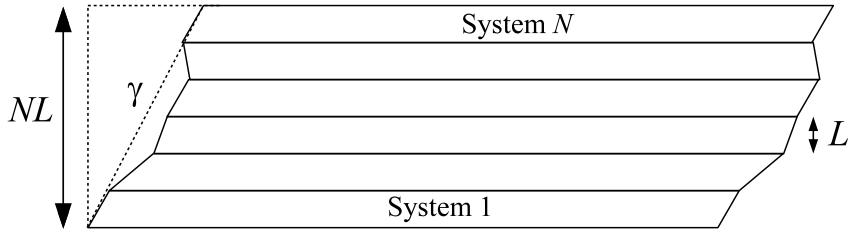


**Figure 2.2:** A large volume of sheared fluid, divided up into $N$ subsystems. Each subsystem is itself macroscopically large, in the sense that it is much larger than any correlation length.

In these systems, a flux or current, such as the shear rate in a sheared fluid, is constrained in a similar way to how constraints are applied at equilibrium to the average energy. The development of the theory is given a brief overview here; it is mostly derived from the papers of Evans et al. [18, 33, 19].

The same results have since been obtained by C. Monthus [34] and are said to apply in the more general context of all steady states, although this has to my knowledge not been verified by either analytical or numerical work; as such the applicability of this interpretation is unknown. V. Lecomte et al. have used the idea of constraining the current in a system to some non-zero value to produce a nonequilibrium system and analyse the current fluctuations [35]; likewise, the motivation for this is somewhat lacking. The advantage of NCDB and the associated ensemble is the sound physical basis and the proof of application to various toy models.

We begin with a very large region of sheared fluid, depicted in figure 2.2. This region is divided up into a large number $\mathcal{N}$ of smaller but still macroscopically large subsystems. To ensure minimal coupling between subsystems, the size $L$ of each is taken to be much larger than any correlation length in the system. Each subsystem follows a trajectory in phase space $\Gamma$ for a duration $\tau$. The number of subsystems that undergo the trajectory $\Gamma$ is denoted by $n_\Gamma$; the probability of observing the trajectory $\Gamma$ is given by a frequentist interpretation: $p(\Gamma) = n_\Gamma/\mathcal{N}$. If we now make many copies of the entire ensemble, an ensemble of ensembles, the distributions that we see will be dominated by those with the largest statistical weight $\Omega_\mathcal{N}$, where

$$\Omega_\mathcal{N} = \frac{\mathcal{N}!}{\prod_\Gamma n_\Gamma!} \tag{2.4}$$

is the number of distinct ways of rearranging the observed trajectories amongst the

subsystems. In order to find the most likely distribution, $\Omega_{\mathcal{N}}$ should be maximised. Equivalently we can maximise $\ln \Omega_{\mathcal{N}}$ in order to make use of Stirling's approximation: $\ln x! \approx x \ln x - x$, for large $x$. Converting the distribution numbers $n_\Gamma$ into probabilities $p(\Gamma)$ and applying the approximation, the quantity to maximise is the entropy of the distribution $-\mathcal{N} \sum_\Gamma p(\Gamma) \ln p(\Gamma)$. This is to be done with the constraint

$$\sum_\Gamma p(\Gamma)\gamma(\Gamma) = \langle \gamma \rangle, \tag{2.5}$$

where $\gamma(\Gamma)$ is the shear accumulated during the trajectory $\Gamma$.

In order to maximise the entropy, we require an appropriate measure on the space of trajectories. This is an unknown quantity, but we can infer that it is the same measure as that for the equilibrium set of trajectories because the subsystems follow the same equations of motion as at equilibrium. With the nonequilibrium constraint the equilibrium trajectories are reweighted depending on their accumulated shear:

$$p(\Gamma) = \frac{1}{W} p^{\mathrm{eq}}(\Gamma) e^{\nu \gamma(\Gamma)}, \tag{2.6}$$

where $\nu$ is the Lagrange multiplier associated with the shear constraint (analogous to the inverse temperature $\beta$) and $W$ is a factor assuring normalisation. Going back to a single system somewhere in the middle of figure 2.2, its trajectory will follow this distribution. The many surrounding systems play the role of a nonequilibrium reservoir or heat bath that requires both $\beta$ and $\nu$ to specify it instead of just $\beta$ as in the equilibrium case. The distribution just derived forms the basis of my analysis of boundary driven systems in this and the next chapter.

The same result could have been reached using the Bayesian statistical mechanics of E. T. Jaynes [36, 37] by interpreting the path entropy mentioned above as the Shannon information of the trajectory distribution. This is in fact how NCDB was originally derived [17], but the Gibbsian argument reproduced here puts the theory on a less controversial basis by avoiding the need for an observer's knowledge of the system, or lack thereof. Similar results have also been used in trajectory-based investigations of the glass transition and its associated dynamical heterogeneity [38, 39, 40]. In those studies the trajectories were biased towards those with low or high average mobility, but the biasing is a way to access physically unlikely trajectories rather than to generate physically correct trajectories as in NCDB.

In principle this result could be used to calculate averages and so on, but this is unlikely given that $p^{\mathrm{eq}}(\Gamma)$ is unknown. However, using the idea that a microscopic transition from state $i$ to $j$ is part of a longer trajectory, some remarkable properties of the nonequilibrium system can be derived [18]; this calculation is detailed in appendix A. Given a set of equilibrium transition rates $\omega_{ij}$ that necessarily obey detailed balance, the rates $\Omega_{ij}$ in the driven system can be expressed in terms of them:

$$\Omega_{ij} = \omega_{ij} \exp[\nu K_{ij} + q_j(\nu) - q_i(\nu)], \tag{2.7}$$

where $K_{ij}$ is the flux gained during the transition. The quantity $q_i(\nu)$ contains detailed information about the equilibrium system and is a measure of the amount of flux that can be gained in the future if the system starts in state $i$. It is the crucial difference between NCDB and mean field models, where transitions are made more or less likely according to the flux carried by that transition only.

Given the mapping (2.7) between the driven and equilibrium rates, and given the detailed balance condition that the equilibrium rates satisfy, it can be inferred that the driven rates satisfy an analogous constraint: this is the nonequilibrium counterpart to detailed balance. Similarly to ordinary detailed balance, it can be viewed as the definition of a boundary driven steady state, or at least the simplest (but still common) type of of these systems that does not have, for example, long term memory of its initial conditions. For these systems, NCDB can be viewed as a set of rules that a model must adhere to if it is to produce physically meaningful results. It is not expected that NCDB can help us to understand all systems. The assumptions that go into the theory include a steady state, a lack of long term memory, and an insensitivity to the exact details of the boundary conditions; any of these conditions may be violated in real systems.

The rules have been produced with the minimum of physical assumptions. There is some unspecified coupling between the nonequilibrium reservoir and the system of interest, the presence of which allows both the driving of the system out of equilibrium and the dissipation necessary to reach a steady state. The theory does not specify or care about exactly what the coupling is, only that it results in the specified amount of flow, just as in canonical equilibrium the exact thermostatting mechanism at the boundaries is irrelevant as long as the same energy is maintained on average. In normal thermodynamic terms, the reservoir is doing work on the system which is

maintaining a steady state by losing energy through heat flow back to the reservoir, but quantifying this energy exchange would require some more detail on the actual processes involved.

### 2.2.1 The role of the driving parameter

At this point the parameter $\nu$ may seem a little mysterious. Introduced as a Lagrange multiplier in a maximisation procedure, it has not yet been given a full physical interpretation, other than to say that it is a property of the nonequilibrium heat bath inducing the shear flow. Intuitively, it should be related to the force that is driving the system out of equilibrium - the stress in a sheared fluid, for example - but it has not been shown that this is the case.

$\nu$ plays a role similar to $\beta$ at equilibrium, in that it indicates how readily shear can be exchanged between the system and reservoir. In the usual presentation, the statistical mechanical $\beta$ is identified as a quantity that must be the same for systems in thermal contact that are in mutual equilibrium. The assumption of the equality of the statistical mechanical entropy $k_B \ln \Omega$ and the thermodynamic entropy is then required to explicitly relate $\beta$ to temperature. In the nonequilibrium situation seen here there is no thermodynamic counterpart to the theory; there is a trajectory entropy, but whether this corresponds to a measurable thermodynamic entropy is unknown.

### 2.2.2 The role of temperature

While the relation given by equation (2.7) specifies the driven rates in terms of the equilibrium rates, we may well ask: which equilibrium rates? Or more specifically: the equilibrium rates at what temperature? While the nonequilibrium reservoir will still have a temperature-like quantity that governs how energy is exchanged between system and reservoir, it is not necessarily the same as at equilibrium. This temperature is not known a priori, and has been regarded as a fitting parameter in previous studies [41].

### 2.2.3 The use of NCDB at zero temperature

NCDB gives a prescription for the transition rates in boundary driven systems by comparing the system to one at equilibrium. The equilibrium rates depend on the

temperature of the associated heat bath. If this temperature is reduced to zero, then the theory may model or at least help us to understand driven athermal systems. The matter is more subtle than this, however. As seen in the last chapter, the statistics of the current in the driven ensemble depend on the statistics of the current in the equilibrium ensemble. At equilibrium the average current is zero and most nonzero currents are effectively out in the tails of the equilibrium distribution. However, at zero temperature there is no distribution - such currents have a probability of exactly zero as there is nothing to excite the system into producing them, and the mapping to the nonequilibrium system fails. In this work, the theory is used at finite temperature and then once we have access to the statistics of the nonequilibrium system we take the temperature to zero. This corresponds to approaching the zero temperature plane along a particular route in the jamming phase diagram shown in figure 2.1. Instead of moving down the $T - \rho^{-1}$ plane to $T = 0$ and then moving to a finite stress, we first move the system off the $T - \rho^{-1}$ plane and then bring it down to the zero temperature plane.

At this point, NCDB yields a set of transition rates at zero temperature for some imposed current $J$. A further connection could be made with the jamming phase diagram by taking $J$ to zero. If we have a way of calculating the stress for a given current, then this can be monitored as $J \to 0$. If the stress is finite at $J = 0$, this would indicate a yield stress for that system.

## 2.3 One dimensional driven diffusion

To illustrate the basic idea of the method, it is first applied to a very basic model: a particle undergoing a random walk or diffusion in a discrete state space. The state space is shown in figure 2.3. The particle has the option of jumping to the states immediately to the left or right of its current position. The rates of hopping to the left or right are equal in equilibrium and are labelled $\omega$. The driven rates to the left and right, $L$ and $R$ respectively, are derived using the NCDB prescription in continuous time, equation (2.7). Each state has exactly the same propensity for future flux as every other, so $q_i = q_j \ \forall i, j$ and the only term in the exponent is the

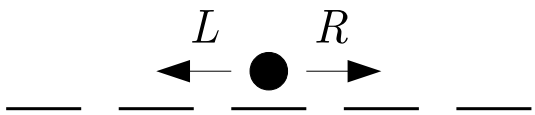


**Figure 2.3:** The state space for the one dimensional diffusion model.

term linear in $\nu$:

$$R = \omega e^{\nu}, \tag{2.8a}$$

$$L = \omega e^{-\nu}. \tag{2.8b}$$

The rates are altered so that, for positive $\nu$, hops to the right are enhanced while those to the left are suppressed.

### 2.3.1 The limit of zero temperature

The equilibrium rate $\omega$ drops to zero in the zero temperature limit, as there are no thermal kicks to move the particle into another state. The driven system, however, must have a nonzero transition rate in order to satisfy the imposed flux constraint. If a positive flux is imposed, then $R$ must remain non-zero right down to zero temperature. Inspection of equation (2.8a) then indicates that in this limit the driving parameter $\nu$ must tend to infinity in order to counterbalance the decrease in $\omega$. Clearly $\nu$ must vary with temperature in order to keep the imposed current the same, and in the limit of zero temperature if the current is to stay nonzero then $\nu$ must diverge.

$\nu$ can be related to a force using an argument from Simha et al. [19]. The transition rate in equation (2.8) can be interpreted as the solution of the Fokker-Planck equation

$$\frac{\partial p(x+\Delta x, t+\Delta t|x,t)}{\partial t} = -\frac{\partial}{\partial x}\left(A(x) + D\frac{\partial}{\partial x}\right) p(x+\Delta x, t+\Delta t|x,t), \tag{2.9}$$

where $D$ is a diffusion coefficient, $A(x)$ is related to the force acting on the particle $F$ via $F(x) = \mu A(x)$, for a friction coefficent $\mu$. For short times, the solution for a constant diffusion coefficient independent of space and time is:

$$p(x+\Delta x, t+\Delta t|x,t) = \frac{1}{\sqrt{4\pi D\Delta t}} \exp\left(-\frac{(\Delta x - A(x)\Delta t)^2}{4D\Delta t}\right). \tag{2.10}$$

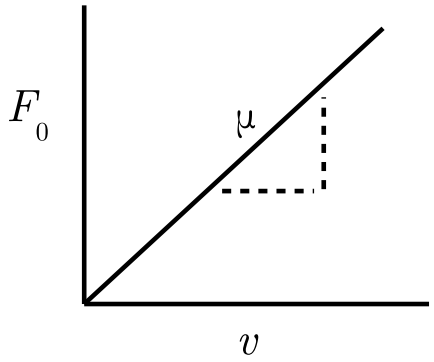


**Figure 2.4:** The flow curve at zero temperature, force $F_0$ as a function of imposed velocity $v$, for the 1D driven diffusion model. Note that the curve passes smoothly through the origin as $v \to 0$, indicating no yield stress. As noted in the text, the same flow curve results for any temperature.

From this we can identify a transition rate $\omega_{x,x+\Delta x} = p(x + \Delta x, t + \Delta t|x, t)/\Delta t$. Consideration of the equivalent transition in the other direction, $\omega_{x,x-\Delta x}$, leads to

$$\frac{\omega_{x,x+\Delta x}}{\omega_{x,x-\Delta x}} = \exp\left(\frac{A(x)\Delta x}{D}\right). \tag{2.11}$$

Assuming that this holds in the current discrete model, a comparison with equations (2.8) gives an expression for the force:

$$F = 2\nu k_B T. \tag{2.12}$$

In section 3.3.1 of the following chapter, the average velocity of a diffusing particle $v$ will be shown to be related to $\nu$ by $v = 2D\nu$. Taken together, these relations imply that $v$ is directly proportional to the applied force (i.e. we have reproduced the simple relation $F = \mu v$) and therefore $F \to 0$ as $v \to 0$ for any temperature: there is no jamming in this simple model. This is no great surprise as there is nothing to jam against - no configuration of the system (position on the line) could ever result in impeded movement. The curve of force against velocity (analogous to stress versus shear rate for a sheared fluid) is a straight line through the origin with gradient $\mu$, shown in figure 2.4.

## 2.4 The comb model

A toy model called the comb model was introduced by Evans to provide an application of the NCDB formalism [18]. This model, whose state space is shown in figure

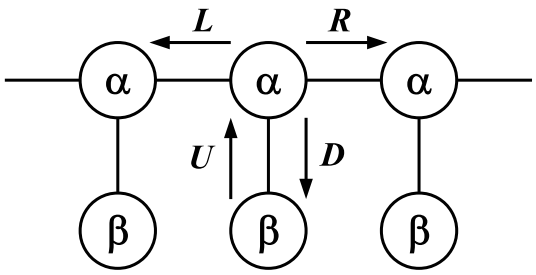


**Figure 2.5:** The state space of the comb model, consisting of the two states $\alpha$ and $\beta$ repeated in both directions. Only the $\alpha$ states possess the horizontal connections that allow the particle to change the integrated flux.

2.5, has just two states periodically repeated. The structure of the state space is different to the previous model. If a particle hopping among these states finds itself in an $\alpha$ state, it can either hop downwards into a $\beta$ state with rate $D$ or left or right into another $\alpha$ state with rates $L$ and $R$ respectively. If it is instead in a $\beta$ state then it can only hop directly upwards into its neighbouring $\alpha$ state. If we define the integrated flux as the distance travelled in the horizontal direction, then only left and right transitions contribute to the flux acquired in a trajectory. The two states $\alpha$ and $\beta$ also have differing energies: the energy of the $\beta$ states is lower by an amount $E$ compared to the $\alpha$ states.

At equilibrium, detailed balance leads to the following conditions (the equilibrium rates are distinguished from the general rates by writing them in lowercase script):

$$r = l, \tag{2.13}$$

$$u = de^{-E}, \tag{2.14}$$

where the energy is measured in units of $k_BT$. We can think of the first condition as ensuring that the system does not acquire a net flux, as the rates of hopping to the left and right are the same, and the second condition as ensuring that Boltzmann's law is recovered for state occupancies.

As in the previous section, we would expect that for positive driving hops to the right are encouraged. In addition, since no flux can be accumulated from the $\beta$ states, we would also expect the system to enhance the upwards hopping rate in order to get the particle out of these trapped states and into an $\alpha$ state where it can carry flux. The NCDB constraints on the driven rates are derived by Evans and can

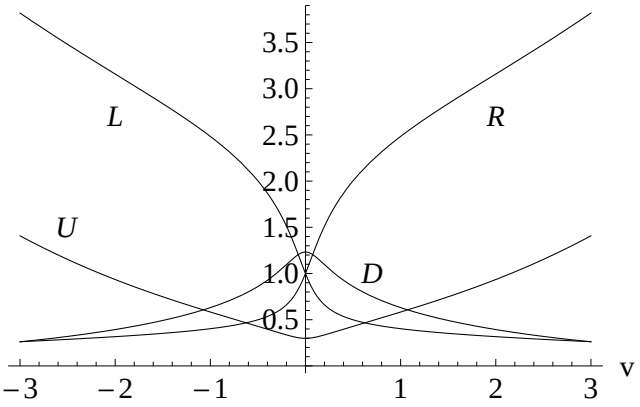


**Figure 2.6:** The nonequilibrium transition rates in the boundary driven comb model as a function of velocity $v$, given by equations (2.15).

be written as [18]:

$$R - L = \left(1 + \frac{D}{U}\right) v, \tag{2.15a}$$

$$RL = r^2, \tag{2.15b}$$

$$UD = d^2 e^{-E}, \tag{2.15c}$$

$$R + L + D - U = 2r + (1 - e^{-E})d, \tag{2.15d}$$

where $v$ is the drift velocity of the particle, that is, the imposed current. The first of these four equations amounts to a definition of the drift velocity in terms of the rates, as flux can only be acquired when in an $\alpha$ state and the occupancy of $\alpha$ states is $U/(U+D)$. The other three equations are nontrivial consequences of NCDB, and can be identified as the product constraints (equations (2.15b) and (2.15c)) and exit rate constraints (equation (2.15d)) derived by Baule and Evans [33].

A graph of the driven rates as a function of the driving parameter $v$ is shown in figure 2.6. As before, hops to the right are enhanced for positive $v$ while hops to the left are suppressed, and vice versa for negative $v$. As the magnitude of $v$ increases, upward hops are enhanced leading to a greater occupancy of the $\alpha$ states so that the system can carry more flux, whereas downward hops are suppressed in order to keep particles in the $\alpha$ states where they can flow.

### 2.4.1 The limit of zero temperature

As $T \to 0$, all the equilibrium rates tend to zero as well - there is no thermal excitation at all between states. In the driven case, the rates will not be zero due

to the imposed current that is maintained by the mechanical driving. In the limit of zero temperature then the constraints on the rates, equations (2.15), become:

$$R - L = \left(1 + \frac{D}{U}\right) v, \tag{2.16a}$$

$$RL = 0, \tag{2.16b}$$

$$UD = 0, \tag{2.16c}$$

$$R + L + D - U = 0. \tag{2.16d}$$

The solution to these equations is given by $R = U = v$, $L = D = 0$ assuming that $v > 0$; for $v < 0$ the solution has instead $L = U = -v$ and $R = 0$. Transitions in the direction opposite to the current are completely suppressed, and the particle is always found in an $\alpha$ state due to the downwards rate being zero.

To analyse the force in the system, a similar approach is taken to the simple diffusion case. I again assume that the result in equation (2.11) applies to this discrete model. The approach requires an explicit expression for the driven rates, but the system of equations (2.15) cannot be solved explicitly for the rates in terms of $v$. As with the case of diffusion I instead use the NCDB prescription in terms of the Lagrange multiplier $\nu$, equation (2.7), which results in the following rates [18]:

$$R = re^{\nu}, \tag{2.17a}$$

$$L = re^{-\nu}, \tag{2.17b}$$

$$D = \frac{d^2 e^{-E}}{de^{-E} + Q(\nu)}, \tag{2.17c}$$

$$U = de^{-E} + Q(\nu), \tag{2.17d}$$

where the flux potential $Q(\nu)$ is given by

$$Q(\nu) = r(\cosh(\nu) - 1) - \frac{d}{2}(1 + e^{-E}) + \sqrt{\left(r\left(\cosh(\nu) - 1\right) - \frac{d}{2}(1 - e^{-E})\right) + d^2 e^{-E}}. \tag{2.18}$$

Using $R$ and $L$ in place of $\Omega_{x,x+\Delta x}$ and $\Omega_{x,x-\Delta x}$ in equation (2.11) and setting $\Delta x = 1$, we find again that

$$\begin{aligned} F &= k_B T \ln(R/L) \\ &= 2\nu k_B T. \end{aligned} \tag{2.19}$$

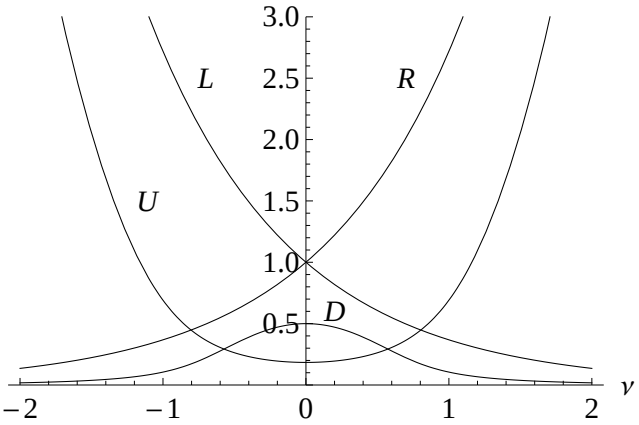


**Figure 2.7:** The nonequilibrium transition rates in the boundary driven comb model as a function of the driving parameter $\nu$, given by equations (2.17).

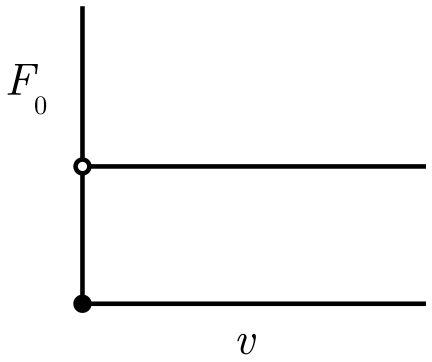


**Figure 2.8:** The zero temperature flow curve, force $F_0$ as a function of imposed velocity $v$, for the comb model. Note that in contrast to figure 2.4 the curve does not pass smoothly through the origin as $v \to 0$, but tends to a nonzero value before a discontinuous jump down to zero at $v = 0$.

The same result arises because in both models the transitions that carry flux are between identical kinds of states. Furthermore, $\nu$ can be expressed in terms of known rates from equation (2.17a) as $\ln(R/r)$, giving the force as:

$$F = 2k_BT(\ln R - \ln r). \tag{2.20}$$

The force at zero temperature

$$F_0 = -2 \lim_{T\to 0} k_BT \ln r, \tag{2.21}$$

where $F_0 = \lim_{T\to 0} F$. This follows from $\lim_{T\to 0} R = v$, a finite number. Surprisingly in this model the zero temperature force does not depend on the imposed current $v$, as the limiting form of $F$ depends on the equilibrium rate $r$ only.

Assuming a particular form for $r$ gives a physical interpretation of the limit. As

the hops between sites are an activated process, it is natural to consider an Arrhenius form for $r$:

$$r = A(T) \exp\left(-\frac{E_A}{k_B T}\right), \tag{2.22}$$

where $E_A$ is an activation energy, the height of the energy barrier restricting passage between $\alpha$ sites. The prefactor $A(T)$ varies slowly with temperature. Substituting this into equation (2.21) gives

$$F_0 = 2E_A - 2k_B \lim_{T\to 0} T \ln A(T). \tag{2.23}$$

If we assume that the second term vanishes then the force takes on a simple form. Imagine the comb model to be a coarse graining of an underlying continuous model with a potential barrier of height $E_A$ halfway between $\alpha$ sites. The distance between $\alpha$ sites in the current units is one, so the distance from the bottom of the well (the $\alpha$ state) to the top of the barrier is one half. The limiting force $2E_A$ is then simply the average gradient of that potential for one side of the barrier. However, the following conclusion may still hold if the limit is not so simple.

The above analysis indicates that the comb model at zero temperature exhibits a yield stress: flow is not possible below the force specified by equation (2.21). This is because there is no dependence of the force on the imposed velocity, except when $v = 0$ for which $F = 0$. For any $v \neq 0$, i.e., if the system is to flow at all, the force in equation (2.21) will be felt. The equivalent of a flow curve for this system, $F$ versus $v$, is simply a horizontal line and $F$ does not go to zero as $v$ goes to zero: $\lim_{v\to 0} F_0 \neq 0$. This is qualitatively different to the case of simple diffusion previously examined. Note that this result is only seen in the limit of zero temperature. At any non-zero temperature $\lim_{v\to 0} R = r$, meaning that the force as given by equation (2.20) is identically zero.

## 2.5 Conclusions

In this chapter I have outlined the use of NCDB for sheared athermal systems and applied the principle to two simple models. Some subtlety arises due to the necessity of a finite temperature when constructing the statistics of the driven system; this was discussed in terms of the more general jamming phase diagram of Liu and Nagel.

The models discussed, one dimensional diffusion and the comb model, indicate that physical results can be obtained at least for these toy models.

I have also found indications that NCDB could be used to help understand yield stress materials. By studying the force in a zero temperature system as the imposed current is taken to zero, the existence or non-existence of a yield stress in principle be determined for any particular system. It was found that for one dimensional diffusion in a continuous state space there is no yield stress, whereas the more complex comb model can exhibit a yield stress, although that can only be concluded by making an assumption on the temperature dependence of the equilibrium rates.

Further work on this topic includes the extension of the theory to more complex, realistic models.

# Chapter 3

# Free energies in boundary driven systems

## 3.1 Introduction

The question of a nonequilibrium free energy has been discussed in the literature for many years. Around sixty years ago Onsager and Machlup formulated an answer to the problem for linear deviations from equilibrium [42] in terms of the Onsager Machlup functional. More recently B. Derrida and collaborators have used large deviation techniques to investigate driven diffusive systems such as the symmetric exclusion process [43]. This is a lattice model consisting of hard core particles that can hop to the left or right nearest neighbour lattice sites as long as they are empty. It is driven by providing an influx of particles at one end and removing them at the other. Derrida et al. derived a free energy functional that gives the probability of fluctuations about the average density profile. This can be viewed as a specific case of the macroscopic fluctuation theory developed by L. Bertini and collaborators [44], which is a theory for many body systems that admit a description in terms of thermodynamic densities that obey hydrodynamical equations of motion.

In this chapter, the extension of the equilibrium free energy formalism to boundary driven systems is discussed. It is developed using the theory of boundary driven systems described in section 2.2. In section 3.2, I give a recap of the equilibrium free energy formalism in order to set the stage for the nonequilibrium version. My own work starts in section 3.3 where I derive a free energy for boundary driven systems, before giving an example of a toy model for which this free energy formalism can

be used analytically to obtain a physical result. The result is then compared to the same model under direct driving. In 3.4 I derive an alternative expression for the free energy which is more useful for application to complex problems, and then test it against another toy model where the current can be analytically determined by independent means.

## 3.2 Free energies at equilibrium

In this section, the definition and use of free energies in statistical mechanics is laid out to provide a context for the upcoming nonequilibrium calculation.

The probability distribution for microstates at equilibrium is well known:

$$p(\mathbf{x};\beta) = \frac{1}{Z} e^{-\beta U(\mathbf{x})}, \tag{3.1}$$

where $\mathbf{x}$ labels a microscopic configuration of the system, $U(\mathbf{x})$ is the energy of microstate $\mathbf{x}$, $\beta^{-1} = k_B T$ with $T$ the temperature of the associated heat bath, and $Z$ is the canonical partition function which ensures that the distribution is normalised:

$$Z = \int \mathrm{d}\mathbf{x}\, e^{-\beta U(\mathbf{x})}. \tag{3.2}$$

In the following I will be interested in the thermodynamic limit $N \to \infty$ and so will use the energy density $u = U/N$ for clarity.

An experimenter does not have the required resolution to find out which microstate the system happens to be in at a given time and even if they did it would not be of much use. Instead, they measure macroscopic quantities that can be given in terms of a function of the microscopic configuration of the system. We are able in principle to find the probability distribution for any observable that we like. Here we deal with a general macroscopic observable $M$ with an associated function over microstates $M(\mathbf{x})$, and the probability that it takes on a particular value $M_0$:

$$p(M = M_0;\beta) = \frac{1}{Z} \sum_{\substack{\mathbf{x} \\ M(\mathbf{x})=M_0}} e^{-N\beta u(\mathbf{x})}. \tag{3.3}$$

This is simply the result of summing the probabilities of all microstates that are consistent with the value of $M$ being $M_0$. We now rewrite equation (3.3) by defining

two quantities:

$$f_N^{\mathrm{eq}}(\beta) = -\frac{1}{N}\beta^{-1}\ln Z, \quad \text{and} \tag{3.4}$$

$$\tilde{f}_N^{\mathrm{eq}}(M_0,\beta) = -\frac{1}{N}\beta^{-1}\ln \sum_{\substack{\mathbf{x} \\ M(\mathbf{x})=M_0}} e^{-\beta H(\mathbf{x})}. \tag{3.5}$$

The first of these is identified with the thermodynamic equilibrium free energy density. The second depends on the quantity we wish to measure and is also often referred to as a free energy. This is the quantity that appears in, for example, the Landau theory of phase transitions. Here I will call $\tilde{f}_N^{\mathrm{eq}}(M_0,\beta)$ an observable dependent free energy in order to distinguish it from the usual free energy $f_N^{\mathrm{eq}}(\beta)$.

With these definitions, equation (3.3) becomes:

$$p(M = M_0;\beta) = e^{-N\beta[\tilde{f}^{\mathrm{eq}}(M_0,\beta) - f^{\mathrm{eq}}(\beta)]}. \tag{3.6}$$

For large $N$, it is assumed that $f_N$ and $\tilde{f}_N$ are independent of $N$ (i.e. the free energies are extensive); these limits are denoted by $f$ and $\tilde{f}$ respectively. If this is the case, then as the number of particles in the system tends to infinity (i.e. as we take the thermodynamic limit), the probability distribution of $M$ becomes more and more sharply peaked about the value of $M$ that minimises $\tilde{f}(M,\beta) - f(\beta)$. In this case, it is overwhelmingly likely that the experimenter will measure $M$ to have the value that satisfies:

$$\frac{\partial}{\partial M_0}[\tilde{f}^{\mathrm{eq}}(M_0,\beta) - f^{\mathrm{eq}}(\beta)] = \frac{\partial}{\partial M_0}\tilde{f}^{\mathrm{eq}}(M_0,\beta) = 0. \tag{3.7}$$

This is the principle of minimisation of free energy. In addition to this, if there is only one value of $M$, say $M^*(\beta)$, that provides a minimum to the exponent then the probability of seeing that value will tend to one in the thermodynamic limit, so we must have

$$\tilde{f}^{\mathrm{eq}}(M^*(\beta),\beta) \approx f(\beta) \tag{3.8}$$

in the limit of a large number of particles.

The key points here are that the most probable value of a macroscopic observable is given by the minimisation of its corresponding free energy, the free energy comes from the normalisation factor in the distribution, and the observable dependent free

energy comes from the unnormalised probability of the macroscopic observable being considered. Recall also that the free energy contains the information necessary to calculate averages of the system, for example the energy density and its fluctuations:

$$\langle u \rangle_N = \frac{\partial(\beta f_N^{\rm eq})}{\partial \beta}, \tag{3.9}$$

$$\langle U^2 \rangle_N - \langle U \rangle_N^2 = \frac{\partial^2(\beta F_N^{\rm eq})}{\partial \beta^2}, \tag{3.10}$$

where I have used $U = Nu$ and defined the extensive free energy $F_N = Nf_N$. Corresponding relations will hold for the nonequilibrium free energy derived next.

## 3.3 Free energies in boundary driven steady states

In this section, I follow an identical path to the one just seen but starting from the distribution of trajectories instead of the distribution of microstates. In the driven system, the probability of an individual trajectory $\Gamma$ of length $\tau$ is given by

$$p_\tau(\Gamma;\nu) = \frac{1}{W} p_\tau^{\rm eq}(\Gamma) e^{\nu J(\Gamma)\tau}, \tag{3.11}$$

where $p_\tau^{\rm eq}(\Gamma)$ is the equilibrium probability distribution for the trajectory, and $W$ is the normalisation factor associated with this distribution:

$$W = \sum_\Gamma p_\tau^{\rm eq}(\Gamma) e^{\nu J(\Gamma)\tau}. \tag{3.12}$$

Now consider the current $J$ instead of the arbitrary quantity $M$ as the macroscopic variable of interest: given a driving strength $\nu$, what current will an experimenter observe in the system? As in the previous section, we can write down the probability for the current $J(\Gamma)$ to take on a value $J_0$:

$$p_\tau(J = J_0;\nu) = \frac{1}{W} \sum_{\substack{\Gamma \\ J(\Gamma)=J_0}} p_\tau^{\rm eq}(\Gamma) e^{\nu J(\Gamma)\tau}. \tag{3.13}$$

In the sum, we can factor out $e^{\nu J(\Gamma)\tau} = e^{\nu J_0 \tau}$ and note that

$$\sum_{\substack{\Gamma \\ J(\Gamma)=J_0}} p_\tau^{\rm eq}(\Gamma) = p_\tau^{\rm eq}(J_0). \tag{3.14}$$

As the system must be seen to have some current, integrating (3.13) over all currents gives an expression for the normalisation factor:

$$W = \int_{-\infty}^{\infty} \mathrm{d}J_0 \, p_\tau^{\mathrm{eq}}(J_0) e^{\nu J_0 \tau}. \tag{3.15}$$

We can then rewrite the distribution as

$$p_\tau(J = J_0; \nu) = \frac{p_\tau^{\mathrm{eq}}(J_0) e^{\nu J_0 \tau}}{\int_{-\infty}^{\infty} \mathrm{d}J_0 \, p_\tau^{\mathrm{eq}}(J_0) e^{\nu J_0 \tau}}. \tag{3.16}$$

Following the ideas of the last section, we identify a free energy density like quantity $f_\tau(\nu)$ that comes from the normalisation factor, and a current dependent free energy $\tilde{f}_\tau(J_0, \nu)$ that comes from the unnormalised probability, where

$$f_\tau(\nu) = -\frac{1}{\tau} \ln \int_{-\infty}^{\infty} \mathrm{d}J_0 \, p_\tau^{\mathrm{eq}}(J_0) e^{\nu J_0 \tau}, \tag{3.17}$$

$$\tilde{f}_\tau(J_0; \nu) = -\frac{1}{\tau} \ln [p_\tau^{\mathrm{eq}}(J_0) e^{\nu J_0 \tau}]. \tag{3.18}$$

The trajectory duration $\tau$ plays the role of the system size $N$ in the previous section. As in the previous section, for large $\tau$ I assume that $f_\tau$ and $\tilde{f}_\tau$ are independent of $\tau$; these limits are denoted by $f$ and $\tilde{f}$ respectively. The analysis in the previous section can be copied practically verbatim to find that the most probable current $J^*$ is the one that minimises the generalised free energy $\tilde{f}(J_0, \nu)$, and in the limit of large $\tau$ we have $\tilde{f}_\tau(J^*(\nu), \nu) \approx f_\tau(\nu)$.

We may also use the definition of $f_\tau(\nu)$ in equation (3.17) directly to find the average integrated current:

$$\begin{aligned} -\frac{\partial f_\tau}{\partial \nu} &= \frac{\int_{-\infty}^{\infty} \mathrm{d}J_0 \, p_\tau^{\mathrm{eq}}(J_0) e^{\nu J_0 \tau} J_0}{\int_{-\infty}^{\infty} \mathrm{d}J_0 \, p_\tau^{\mathrm{eq}}(J_0) e^{\nu J_0 \tau}} \\ &= \langle J \rangle_\tau. \end{aligned} \tag{3.19}$$

Taking the infinite $\tau$ limit will then give the steady state current. Compared to the equilibrium case, the current $J$ plays the role of the energy density $u$ and the trajectory duration $\tau$ plays the role of $N$. Likewise, the fluctuations of the integrated

current $K = J\tau$ are given by

$$\langle K^2 \rangle_\tau - \langle K \rangle_\tau^2 = \frac{\partial^2 F_\tau}{\partial \nu^2}, \tag{3.20}$$

where as in the previous section I have defined $F_\tau = \tau f_\tau$.

$\tilde{f}(J_0; \nu)$ is related to the properties of the current at equilibrium as follows. From the definition:

$$\begin{aligned} \tilde{f}(J_0; \nu) &= \lim_{\tau \to \infty} -\frac{1}{\tau} (\ln p_\tau^{\mathrm{eq}}(J_0) + \nu J_0 \tau) \\ &= I(J_0) - \nu J_0, \end{aligned} \tag{3.21}$$

where the "rate function" for the large deviations of the current at equilibrium is defined by [45]

$$I(J_0) = -\lim_{\tau \to \infty} \frac{1}{\tau} \ln p_\tau^{\mathrm{eq}}(J_0). \tag{3.22}$$

There is a strong connection between this work and large deviation theory that is expanded upon below in section 3.4.3. By differentiating the expression for $\tilde{f}$, we find that the most probable current is that which satisfies

$$\frac{\mathrm{d}}{\mathrm{d}J_0} I(J_0) = \nu, \tag{3.23}$$

so that the most likely current is the one that makes the slope of the equilibrium rate function equal to the driving parameter $\nu$.

### 3.3.1 One dimensional driven diffusion

As an illustration the above quantities are calculated for the case of a particle diffusing on a line. In contrast to the diffusion model of the previous chapter I consider a continuous space model, for mathematical ease. Here, the integrated current $K$ is the distance travelled by the particle $x$, and the corresponding current is the average velocity $v = x/\tau$. The equilibrium probability distribution for the distance travelled $x_0$ in a trajectory of length $\tau$ is given by the solution of the diffusion equation:

$$p_\tau^{\mathrm{eq}}(x_0) = \frac{1}{\sqrt{4\pi D \tau}} \exp\left( -\frac{x_0^2}{4D\tau} \right), \tag{3.24}$$

where $D$ is a diffusion coefficient. For the present purposes this is expressed in terms of the velocity (current) $v$ instead:

$$p_\tau^{\mathrm{eq}}(v_0) = \frac{1}{\sqrt{4\pi D\tau}}\exp\left(-\frac{v_0^2\tau}{4D}\right). \tag{3.25}$$

The steady state free energy is calculated from equation (3.17) as

$$\begin{aligned} f_\tau(\nu) &= -\frac{1}{\tau}\ln\left[\frac{1}{\sqrt{4\pi D\tau}}\int_{-\infty}^{\infty}\mathrm{d}v_0\exp\left(-\frac{v_0^2\tau}{4D}+\nu v_0\tau\right)\right] \\ &= -\frac{1}{\tau}\ln\left[\frac{1}{\sqrt{4\pi D\tau}}\sqrt{4\pi D\tau}\exp\left(D\nu^2\tau\right)\right] \\ &= -D\nu^2+\frac{1}{\tau}\ln\sqrt{4\pi D\tau}. \end{aligned} \tag{3.26}$$

As expected, $f_\tau(\nu)$ is independent of $\tau$ for large trajectory durations, being equal to $-D\nu^2$. The current dependent free energy is similarly calculated:

$$\begin{aligned} \tilde{f}_\tau(v_0,\nu) &= -\ln\left[\frac{1}{\sqrt{4\pi D\tau}}\exp\left(-\frac{v_0^2\tau}{4D}+\nu v_0\tau\right)\right] \\ &= \frac{1}{\tau}\ln\sqrt{4\pi D\tau}+\frac{v_0^2}{4D}-\nu v_0, \end{aligned} \tag{3.27}$$

which again in the long time limit is independent of $\tau$, being equal to $v_0^2/4D-\nu v_0$. This can be found equivalently from equation (3.21) after noting that the distribution for the velocity, equation (3.25), has a large deviation form: $p_\tau^{\mathrm{eq}}(v_0) = e^{-I(v_0)\tau}$, meaning that the large deviation function for the equilibrium current is $v_0^2/4D$. Subtracting $\nu v_0$ from this gives the above result.

To find the most probable distance travelled we must minimise the current dependent free energy $\tilde{f}(v_0,\nu)$ with respect to the velocity, which gives:

$$v^*(\nu) = 2D\nu. \tag{3.28}$$

Substituting this into the expression for $\tilde{f}_\tau$, we see that the latter is indeed equal to the long time limit of $f_\tau(\nu)$. The fluctuations of the distance travelled (the integrated current) can also be obtained via equation (3.20) to give $\langle x^2\rangle_\tau - \langle x\rangle_\tau^2 = 2D\tau$.

This procedure is in some sense a "top down" process: we work in terms of a globally conserved quantity, the average velocity $v$, and don't worry about the microscopic laws needed to drive the system. As the system is so simple, we can

compare this to a "bottom up" method of solving the problem: diffusion under the action of a constant force $\Sigma$, corresponding to a linear potential $-\Sigma x$. The probability distribution for a delta function initial condition is as follows:

$$p_\tau(v_0) = \frac{1}{\sqrt{4\pi D\tau}} \exp\left(-\frac{(v_0 - \Sigma/\mu)^2\tau}{4D}\right), \tag{3.29}$$

where $\mu$ is a coefficient of friction. The solution looks just like that of the ordinary diffusion equation but in a moving frame of reference. The average velocity in the steady state is calculated to be:

$$\langle v \rangle = \int_{-\infty}^{\infty} \mathrm{d}v_0 \, v_0 p_\tau(v_0) \quad = \frac{\Sigma}{\mu}. \tag{3.30}$$

Comparing this to the expression derived from equation (3.28), we can identify $2D\nu = \Sigma/\mu$, or

$$2\nu = \frac{\Sigma}{k_B T}, \tag{3.31}$$

where I have used the fluctuation dissipation relation $D = k_B T/\mu$. The driving parameter $\nu$ is then proportional to the slope of the potential in units of $k_B T$. It is clear that $\nu$ should be connected to a force (or stress for a sheared fluid), as it is the property of the outside world that drives the system out of equilibrium and it is conjugate to the current (or shear rate for a sheared fluid). Note also that this reproduces the result of the previous chapter for one dimensional diffusion.

It should be emphasised that these results have been derived from first principles using a well founded free energy principle for a class of out of equilibrium systems: a rare achievement. Although the current results are obviously related to NCDB, they focus on a different aspect. The main result taken from the NCDB formalism is the distribution of trajectories, which has a physical basis greater than many *ad hoc* nonequilibrium methods. If the trajectories of real systems follow this distribution, then the results presented here should apply.

## 3.4 An alternative formulation of the nonequilibrium free energy

While the previous calculation is a success in terms of defining a free energy away from equilibrium, it may not be very useful for the majority of systems. The full time dependence of the equilibrium system must be known to find the quantity $p_\tau^{\mathrm{eq}}(J)$, a task that usually cannot be done exactly. In one particular presentation of NCDB [18], a relation between Greens functions was used in order to solve a model without having to explicitly calculate the probability of currents at equilibrium; this was extended by A. Baule in order to give a general procedure for NCDB calculations [33]. The following calculation uses the same relation and ideas to arrive at a different expression for $f(\nu)$. This approach is valid for systems that have a discrete set of states and are modelled by a Markov process.

First, the expression for $f$, equation (3.17), is rewritten in the long time limit as

$$\begin{aligned} f(\nu) &= \lim_{\tau\to\infty} -\frac{1}{\tau}\ln\int_{-\infty}^{\infty} \mathrm{d}J_0\, p_\tau^{\mathrm{eq}}(J_0)e^{\nu J_0\tau} \\ &= \lim_{\tau\to\infty} -\frac{1}{\tau}\ln\int_{-\infty}^{\infty} \mathrm{d}J_0 \sum_i p^{\mathrm{eq}}(i)p_\tau^{\mathrm{eq}}(J_0|i)e^{\nu J_0\tau} \\ &= \lim_{\tau\to\infty} -\frac{1}{\tau}\ln\sum_i f_i(\tau,\nu), \end{aligned} \tag{3.32}$$

where $f_i(\tau,\nu)$ is defined by

$$f_i(\tau,\nu) = \int_{-\infty}^{\infty} \mathrm{d}J_0\, p^{\mathrm{eq}}(i)p_\tau^{\mathrm{eq}}(J_0|i)e^{\nu J_0\tau}. \tag{3.33}$$

$p^{\mathrm{eq}}(i)$ is the probability of being in state $i$ at equilibrium, and $p_\tau^{\mathrm{eq}}(J_0|i)$ is the probability of the system exhibiting a flux $J_0$ given that it begins in state $i$. It will be easier in the following to deal with probabilities of integrated flux $K_0 = J_0\tau$; as the two quantities are simply related, the integrals in the above expressions hold with $K_0$ substituted for $J_0$.

The probabilities $p_\tau^{\mathrm{eq}}(K_0|i)$ for different values of $i$ can be related to each other as follows. One way for the system to acquire the required flux in the time $\tau$ is to hang around in state $i$ for some time $\tau - t$ before jumping to a different state $j$. The probability of waiting in state $i$ for a time $t$ depends on the stochastic process; in order to proceed I assume the process in question is Markovian. For a continous

time Markov process this probability is given by

$$h_i(t) = \pi_i e^{-\pi_i t}, \tag{3.34}$$

where $\pi_i = \sum_j \omega_{ij}$ is the total exit rate from state $i$. The likelihood of jumping to state $j$ is given by $\omega_{ij}/\pi_i$; the jump results in a contribution $K_{ij}$ to the flux. From $j$, the system then needs to make up the remaining flux, $K_0 - K_{ij}$, in the remaining time $t$; the probability of this is $p_\tau^{\rm eq}(K_0 - K_{ij}|j)$. The system could jump at any time and to any connected state, so summing over these variables we obtain

$$p_\tau^{\rm eq}(K_0|i) = C_i \int_0^\tau {\rm d}t\, h_i(\tau - t) \sum_j \frac{\omega_{ij}}{\pi_i} p_\tau^{\rm eq}(K_0 - K_{ij}|j). \tag{3.35}$$

$C_i$ is a normalisation constant, calculated by integrating over all $K_0$:

$$C_i = \frac{1}{1 - e^{-\pi_i t}}. \tag{3.36}$$

This equation is now converted into one for the functions $f_i(\tau, \nu)$. Multiplying equation (3.35) by the occupation probability $p_i^{\rm eq}$, on the right hand side detailed balance is used to write $p_i^{\rm eq}\omega_{ij} = p_j^{\rm eq}\omega_{ji}$. Multiplying by $e^{\nu K_0}$ and integrating over $K_0$ requires a shift in the integration variable on the right hand side. Finally the expression (3.34) for $h_i$ is used, to give the result

$$f_i(\tau, \nu) = \frac{e^{-\pi_i \tau}}{1 - e^{-\pi_i \tau}} \int_0^\tau {\rm d}t\, e^{\pi_i t} \sum_j \omega_{ji} e^{\nu K_{ij}} f_j(t, \nu). \tag{3.37}$$

From here, the factor in front of the integral is taken to the left hand side and then the equation is differentiated with respect to $\tau$ to get rid of the integral:

$$\pi_i e^{\pi_i \tau} f_i + e^{\pi_i \tau} \frac{\partial f_i}{\partial \tau} - \frac{\partial f_i}{\partial \tau} = e^{\pi_i \tau} \sum_j \omega_{ji} e^{\nu K_{ij}} f_j(\tau, \nu). \tag{3.38}$$

For long times, the term without a factor of $e^{\pi_i \tau}$ is neglected to give a simple equation for $f_i(\tau, \nu)$:

$$\frac{\partial f_i}{\partial \tau} = \sum_j M_{ij} f_j, \tag{3.39}$$

where $M_{ij}$ are the entries of the square matrix $M$:

$$M_{ij} = \begin{cases} \omega_{ji} e^{\nu K_{ij}}, & \text{if } i \neq j, \\ -\pi_i, & \text{if } i = j. \end{cases} \tag{3.40}$$

This is a set of linear, constant coefficient differential equations for the $f_i$. The solution may be written as

$$f_i(\tau, \nu) = \sum_k c_k v_{k,i} e^{\lambda_k \tau}, \tag{3.41}$$

where $\lambda_k$ and $\mathbf{v}_k$ are the eigenvalues and corresponding eigenvectors of $M$, the latter of which have entries $v_{k,i}$, and $c_k$ are constants of integration. As we are only interested in long times, the sum over $k$ will eventually be dominated by the most positive eigenvalue $\lambda^*$. We may therefore write

$$f_i(\tau, \nu) \approx c^* v_i^* e^{\lambda^* \tau}. \tag{3.42}$$

With this solution in hand we turn back to the expression for $f(\nu)$, equation (3.32). Substituting in, we find that

$$\begin{aligned} f(\nu) &= \lim_{\tau \to \infty} -\frac{1}{\tau} \ln \sum_i r_i \\ &= \lim_{\tau \to \infty} -\frac{1}{\tau} \ln \sum_i c^* v_i^* e^{\lambda^* \tau} \\ &= \lim_{\tau \to \infty} -\frac{1}{\tau} \ln (c^* \sum_i v_i^*) + \lim_{\tau \to \infty} -\frac{1}{\tau} \lambda^* \tau \\ &= -\lambda^*. \end{aligned} \tag{3.43}$$

This expression provides a way to calculate the nonequilibrium free energy if all the equilibrium rates are known, given the feasibility of computing $\lambda^*$.

This method has clear advantages over the previous result, equation (3.17), as it does not involve solving the equilibrium dynamics for $p^{\text{eq}}(J)$; the only information needed is the equilibrium rates $\{\omega_{ij}\}$. The state space for any realistic model will likely be enormous, corresponding to a very large matrix $M$, but one need only find the largest eigenvalue of $M$. In addition $M$ may well be a sparse matrix, allowing the use of faster solution methods.

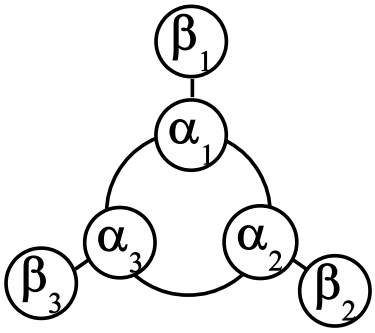


**Figure 3.1:** The cyclic state space used in the calculation of the free energy for the comb model.

The method relies on the fact that the system is modelled by a Markov process and has discrete states. A naïve extension of the above result to continuous state spaces would give an integral equation, where the eigenvalues are now eigenvalues of the integral operator that will involve the probability of moving between two points in the continuum of states. The mathematics becomes more complicated, but it could be sidestepped using a discretisation of phase space and an application of the above method.

### 3.4.1 The comb model

The validity of this approach is tested using the comb model seen in section 2.4, for which the steady state current is known analytically. A system consisting of three $\alpha$ and three $\beta$ states with periodic boundary conditions is used, so that state $\alpha_3$ is connected to state $\alpha_1$. This state space is shown in figure 3.1. Three is the minimum number of $\alpha$ states that will allow periodic boundary conditions without multiple connections between two states. As there are six states in total, $M$ is a $6 \times 6$ matrix. In order to cut down the number of parameters, the units used in this section differ from those in the previous chapter and follow Evans [18]. Rates are normalised by the equilibrium horizontal hopping rate so that $r = l = 1$, $d = \rho$ and $u = \rho e^{-E}$. The equilibrium exit rate from an $\alpha$ state is given by $r + l + d = 2 + \rho$, while from a $\beta$ state it is $u = \rho e^{-E}$. The rates in terms of the driving parameter $\nu$ are used;

putting equations (2.17) into the current units:

$$R = e^{\nu}, \tag{3.44a}$$

$$L = e^{-\nu}, \tag{3.44b}$$

$$D = \frac{\rho^2 e^{-E}}{\rho e^{-E} + Q(\nu)}, \tag{3.44c}$$

$$U = \rho e^{-E} + Q(\nu), \tag{3.44d}$$

where the flux potential $Q(\nu)$ is given by equation (2.18) in the current units:

$$Q(\nu) = \cosh(\nu) - 1 - \frac{\rho}{2}(1 + e^{-E}) + \sqrt{\left((\cosh(\nu) - 1) - \frac{\rho}{2}(1 - e^{-E})\right) + d^2 e^{-E}}. \tag{3.45}$$

Putting it all together, $M$ is as follows:

$$M = \begin{pmatrix} -(2+\rho) & e^{\nu} & e^{-\nu} & \rho e^{-E} & 0 & 0 \\ e^{-\nu} & -(2+\rho) & e^{\nu} & 0 & \rho e^{-E} & 0 \\ e^{\nu} & e^{-\nu} & -(2+\rho) & 0 & 0 & \rho e^{-E} \\ \rho & 0 & 0 & -\rho e^{-E} & 0 & 0 \\ 0 & \rho & 0 & 0 & -\rho e^{-E} & 0 \\ 0 & 0 & \rho & 0 & 0 & -\rho e^{-E} \end{pmatrix}. \tag{3.46}$$

This has six eigenvalues, of which we require the most positive one. The quantities $E$ and $\rho$ are fixed, and the eigenvalues are solved for numerically as a function of $\nu$. The most positive eigenvalue for each $\nu$ is selected to produce a graph of $f(\nu)$; this is shown in figure 3.2 for particular values of $E$ and $\rho$. Following equation (3.19), the derivative of this function is computed numerically to find the average current (velocity) $J$. From section 2.4, we know that the current satisfies

$$\begin{aligned} J &= \frac{U}{U+D}(R - L) \\ &= 2\sinh(\nu)\frac{(\rho e^{-E} + Q(\nu))^2}{(\rho e^{-E} + Q(\nu))^2 + \rho^2 e^{-E}}, \end{aligned} \tag{3.47}$$

The numerical and analytical results are compared in figure 3.3; for all values of $E$ and $\rho$ tested, the two curves are indistinguishable. Alternatively, it can be seen numerically that $f(\nu)$ is exactly the same function as $-Q(\nu)$. Given that $f = -Q$, and that by definition $\frac{\mathrm{d}Q}{\mathrm{d}\nu} = J$ [18], then the correct current must also follow from

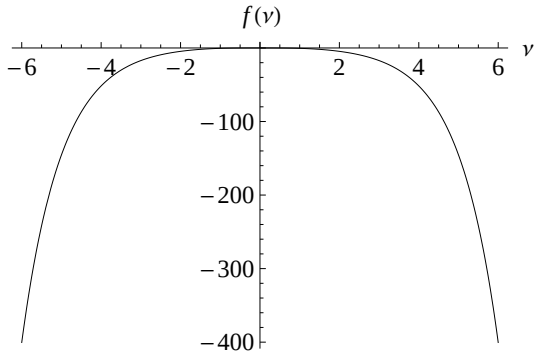


**Figure 3.2:** The nonequilibrium free energy $f(\nu)$ for the comb model for the parameters $\rho = E = 1$.

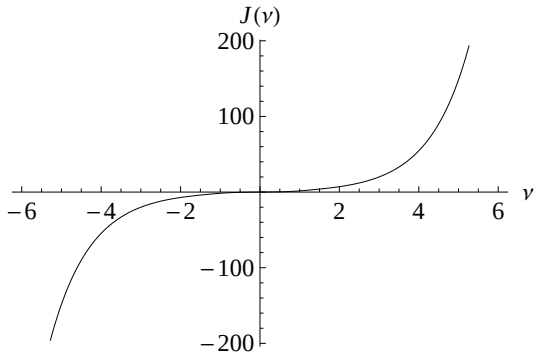


**Figure 3.3:** The average current (velocity) $J(\nu)$ for the comb model for the parameters $\rho = E = 1$.

the negative derivative of $f$.

### 3.4.2 Comparison to the theory of Evans

As noted above, in the comb model the free energy $f$ turns out to be identical to the negative of the flux potential $Q$. This is in fact a general result, despite an apparent difference in their definitions. As seen in equation (3.32), $f$ is an average of the quantity $f_i$ over all microstates, where the average is taken using the equilibrium microstate distribution. According to Evans [18] $Q$ is an average of the same quantity but using the driven microstate distribution (see for example equations (19) and (20) of the cited paper). One might expect these to be different quantities as the microstate distribution is certainly altered by the driving in general, but the infinite time limit ensures that there is no inconsistency. After a long enough time the system will have forgotten its initial microstate and the initial transient behaviour becomes insignificant when compared with the steady state behaviour.

### 3.4.3 Connection to large deviation theory

A connection between NCDB and large deviation theory was made earlier in this section when the rate function for the fluctuations of the current $I(J_0)$ was introduced. The approach taken in this thesis has been to deliberately avoid phrasing things in terms of large deviations and instead drawing the parallel with the familiar case of equilibrium physics. However, the calculations seen in this chapter can all be phrased as large deviation results if desired. Indeed, the generalisation of the free energy away from equilibrium is the rate function and equilibrium free energies can be expressed in this way as well [45].

The functions $f_\tau$ and $\tilde{f}_\tau$ were introduced by way of a definition, but then assuming the existence of a long time limit is tantamount to assuming a large deviation principle. The calculation of $f$ in terms of the eigenvalue $\lambda^*$ of the matrix $M$ has been obtained in the large deviation literature, although in the context of quantifying the fluctuations of an additive process given a large deviation principle for the paths of a stochastic system. In the current work there is an explicit connection to a whole class of physical systems and a fundamental significance to the fluctuations of the current.

## 3.5 Conclusions

In this chapter I derived a free energy formalism for boundary driven systems using a physically motivated expression for the probability distribution of trajectories in such systems. This free energy generates physical results for the case of one dimensional diffusion. This result requires a knowledge of the current statistics at equilibrium. For Markovian systems with a finite state space I then expressed the free energy as an eigenvalue of a matrix related to the transition matrix of the Markov process; this is expected to be much more useful for actual calculations as it only requires knowledge of the local equilibrium rates. I have numerically tested this version of the free energy against the comb model, for which analytical results are known, and found an excellent agreement.

While the work in this chapter has provided strong evidence for the validity and applicability of the free energy formalism, the models that I used for the test were very simple single particle models. A stronger test would be to apply the theory

to more complicated interacting systems. A prime candidate is the one dimensional simple exclusion process, a lattice model consisting of hard core particles that can hop to neighbouring lattice sites as long as they are empty. Similarly to the comb model, if the left and right hopping rates are equal then it is an equilibrium model called the symmetric simple exclusion process. This has been studied using large deviation techniques [43], although generally with a different method of driving than that considered here. Exclusion processes generally are model systems for nonequilibrium steady states and much is known about them [32]. A. Simha et al. have studied the two particle symmetric exclusion process using NCDB [19], but two particles is the only case for which analytical results were obtained. The study of the symmetric simple exclusion process using the free energy formalism, particularly the approach in section 3.4, could prove to be very fruitful. In addition, it would be most useful to form a general connection with the free energy at equilibrium. This is a difficult problem as the free energy derived here is based on trajectories rather than microstates, but if achieved it could be a vital calculational tool as much is known about equilibrium free energies.

Finally, the free energy concept could be combined with the ideas of the previous chapter in order to produce a free energy approach to sheared athermal systems. As discussed in that chapter, there is little in the way of a unifying framework for athermal systems, but this approach could provide some general insight into the field.

# Chapter 4

# The rotor model: a simulation study

## 4.1 Introduction

The most common example of a boundary driven system is a sheared fluid. Typically a fluid is placed between two boundaries that are then moved relative to each other; in the most common cases the boundaries are either concentric cylinders (Taylor-Couette flow), a cone and plate or two parallel plates. The rheological or flow properties such as the stress for a given shear rate or shearing protocol can then be measured. As mentioned in chapter 1 the simplest fluids are Newtonian fluids such as water, but many fluids will exhibit more complex behaviour in the form of viscoelasticity, a response to perturbations that is partly viscous and partly elastic in character leading to a dependence of the flow properties such as viscosity on the speed at which they are perturbed. The complex flow is due to the presence of some mesoscopic structure, on a scale smaller than the sample size but much bigger than the atomic scale. For example, if a polymer solution is sheared then it could encourage the individual polymer chains to align with each other more than they otherwise would. This change in structure then has a feedback effect on the flow itself, for example, by making it easier to shear, leading to a complex relationship between the macroscopic and mesoscopic scales. This mutual dependence can result in nonequilibrium phase transitions [46]. As well as measuring rheological properties, the mesostructural properties can be investigated directly using a number of techniques, including flow birefringence [47, 48], nuclear magnetic resonance [49, 50]

and small angle neutron scattering [51, 52].

Examples of complex fluids are polymer solutions [53, 54], colloidal suspensions [55, 56] and surfactant solutions [57, 47], of which the latter provide a particularly interesting case. Surfactant molecules have a polar headgroup and a non-polar tail, usually a hydrocarbon chain. These parts of the molecule are hydrophilic and hydrophobic respectively, meaning that the molecules will often huddle together to hide away their hydrophobic tails while maximising the exposure of the headgroup to the solvent, in structures called micelles. The formation of micelles results in a loss of translational entropy and so will only happen at a critical micelle concentration where the energy gain from protecting the hydrophobic tails from the water outweighs the entropic penalty for doing so. The structures formed include lamellae and vesicles. Wormlike micelles are long cylindrical arrangements of surfactant molecules that behave in many respects like polymers, being effectively one dimensional chains, but the chains can break and combine so they cannot be modelled as having a constant size. Wormlike micelle solutions can be observed to undergo shear banding [47]. Another unusual phase is the so-called onion phase in which multilayered spherical vesicles are formed [57].

The properties of complex fluids are typically captured theoretically using constitutive models, normally tensorial models that define the stress tensor in terms of the mesoscopic structure, for example the (diffusive) Johnson-Segalman model [58, 59]. The dynamics of the structure is specified and then the model can be solved for the flow properties either in or out of the steady state, usually numerically. An interesting case is that of shear banding, mentioned in chapter 1, where two macroscopic regions of the fluid exist at a common shear stress but different shear rates. This is indicated theoretically by a negatively sloping constitutive curve as shown in figure 4.1; the negative slope means a small fluctuation to a higher shear rate is not penalised and the system would run away to higher shear rates. As the shear rate is increased from zero, the stress is seen to increase until it reaches a particular value $\Sigma^*$. After that point, the system separates out into two bands of low shear rate $\dot{\gamma}_1$ and high shear rate $\dot{\gamma}_2$, of sizes determined by the overall shear rate: $f_1\dot{\gamma}_1 + f_2\dot{\gamma}_2 = \dot{\gamma}$, where $f_1$ and $f_2$ are the fractions of the system occupied by the low and high shear rate bands respectively. If the shear rate continues to be increased the stress remains constant up until the upper value $\dot{\gamma}_2$, after which the flow is once

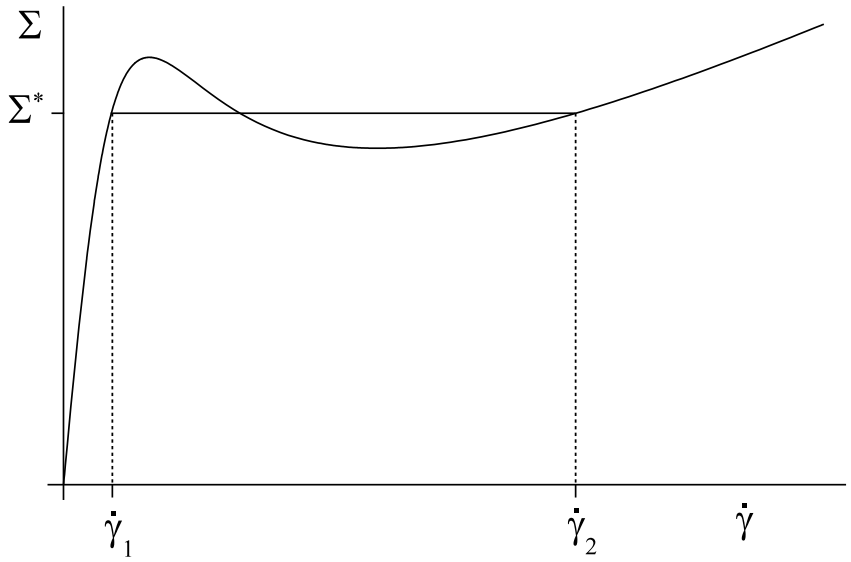


**Figure 4.1:** A typical theoretical constitutive curve for a shear banding fluid.

more homogeneous and the stress starts to increase again. The range of shear rates for which homogeneous flow is not stable covers up all of the negative slope in the underlying theoretical curve.

While tensorial models are needed to describe real fluids, simpler non-tensorial models have made appearances in the literature, such as the toy model investigated by P. D. Olmsted and others which involves only the shear stress [60, 61], and can reproduce features such as the instability in the constitutive curve described above. In a similar vein, a toy model of a sheared complex fluid is considered in this chapter. The rotor model was used by Evans et al. to test the predictions of NCDB [41]. The version investigated here is simplified in that the potential used is easier to work with, both analytically and numerically. I first define the model in section 4.2 and link it to other models in statistical mechanics. The rest of the chapter describes the results of the simulation of the model.

## 4.2 The model

The model consists of a linear chain of rotors that interact with nearest neighbour forces. At any moment in time, each rotor $j$ is characterised by its angle $\theta_j(t)$ relative to an arbitrary zero line, and its angular velocity $\dot{\theta}_j(t)$; these will normally be referred to as positions and velocities. The torque $f_{i,j}$ acting between nearest neighbour rotors with labels $i$ and $j$ has three components: conservative, dissipative

and stochastic. The conservative force is a simple periodic function:

$$f^c_{i,j} = \alpha \sin(\theta_i - \theta_j), \tag{4.1}$$

where $\alpha$ is a constant; the dissipative force is linear in the angular velocity difference:

$$f^d_{i,j} = \mu(\dot{\theta}_i - \dot{\theta}_j), \tag{4.2}$$

where $\mu$ is a constant coefficient of friction; and the stochastic force is written as

$$f^s_{i,j} = \sigma \xi_{i,j}(t), \tag{4.3}$$

where $\sigma$ is a constant that measures the strength of the stochastic force. As I will mostly be using $\sigma^2$ in what follows, I shall call $\sigma^2$ the noise strength.

The first two expressions depend only on relative angles and velocities, whereas the third force is uncorrelated with the state of the system and will be given in more detail below. As the forces on the rotors only depend on relative velocities, the system is Galilean invariant: an identical constant velocity may be added to every rotor and the model will not change its behaviour. The dependence on relative angles likewise means that the zero of angle is unimportant. Note also that the first two forces are manifestly odd in the sense that $f^c_{i,j} = -f^c_{j,i}$, and similarly for $f^d_{i,j}$, so that Newton's third law holds for these forces. For convenience, $f^s_{i,j}$ is also defined to satisfy Newton's third law: $\xi_{i,j}(t) = -\xi_{j,i}(t)$. With this restriction, angular momentum is exactly conserved in the model.

Each $\xi_{i,j}(t)$ is a Gaussian white noise process. White noise is a stochastic process with zero mean whose values at different times are completely uncorrelated, and the Gaussian qualifier refers to the fact that at any moment in time the value of the noise is drawn from a Gaussian distribution. As a result the term $\xi_{i,j}(t)$ satisfies the following:

$$\langle \xi_{i,j}(t) \rangle = 0, \tag{4.4}$$

$$\langle \xi_{i,j}(t) \xi_{i',j'}(t') \rangle = (\delta_{i,i'}\delta_{j,j'} - \delta_{i,j'}\delta_{j,i'})\delta(t - t'), \tag{4.5}$$

where $\delta(t - t')$ is the Dirac delta function. The unusual form of the correlation

takes into account the fact that stochastic forces on different rotors are uncorrelated except for when the two forces are between the same pair of rotors, in which case the restriction to follow Newton's third law comes into play.

The stochastic force $f^s_{i,j}$ mimics the effect of coupling to a heat bath. The fluctuation dissipation theorem relates the noise strength $\sigma^2$ to the temperature of the heat bath and the friction coefficient $\mu$:

$$\sigma^2 = 2\mu k_B T. \tag{4.6}$$

This relation ensures that with zero driving the system will arrive in a Boltzmann distribution with temperature $T$. The simulation data in this chapter uses the thermal energy $k_B T$ instead of $\sigma^2$ to characterise the strength of the thermal noise.

The forces chosen are of the simplest form available. A similar model could be defined with the friction given by a different odd function, or some other conservative force that is periodic with period $2\pi$, but the linear friction and sinusoid are the easiest to work with. The conservative force used here is derived from a potential $U(x)$:

$$U(x) = -\alpha \cos(x). \tag{4.7}$$

With the forces thus defined, the equation of motion of a single rotor is as follows:

$$\begin{aligned} I\ddot{\theta}_i &= f_{i+1,i} + f_{i-1,i} \\ &= \alpha[\sin(\theta_{i+1} - \theta_i) + \sin(\theta_{i-1} - \theta_i)] + \mu[\dot{\theta}_{i+1} - 2\dot{\theta}_i + \dot{\theta}_{i-1}] + \sigma[\xi_{i+1,i} + \xi_{i-1,i}], \end{aligned} \tag{4.8}$$

where $I$ is the moment of inertia of the rotor, which is identical for all of them.

This is clearly not a model of a real fluid, but is instead a toy model that will hopefully yield much interesting physics and has qualitative similarities to a real fluid. A complex fluid consists of components that will interact with each other if they are close enough, meaning that to slide past each other these components must overcome potential barriers in a similar way. In order to move past each other (that is, go through a relative rotation), the rotors similarly have to overcome a potential barrier.

### 4.2.1 Connection to previous models in statistical mechanics

The rotor model as defined above has connections to many other models, a few of which are mentioned here. It should be noted that even though for example the conservative forces may be of the same form as other models, the rotor model is a full dynamical system with dissipation and inertia, in addition to which it will be driven out of equilibrium by boundary driven shear.

#### The XY model

The XY model is a well known lattice based model whose constituents are the two dimensional spins $s = (s_x, s_y)$. There is a coupling between spins that is usually given by their scalar product: $H(s_i, s_j) = \alpha(1 - s_i \cdot s_j) = \alpha(1 - \cos(\theta_i - \theta_j)$. At equilibrium in one dimension, the spins are disordered except at zero temperature; this is a common although not completely general property of one dimensional systems in statistical mechanics [62]. At equilibrium in dimensions greater than two, the model has a critical value of the coupling below which it is disordered but above which it is in an ordered phase, and in dimension two, the situation is somewhat more complicated [63].

The equilibrium rotor model is equivalent to the one dimensional XY model, so knowledge of the equilibrium XY model specifies the equilibrium behaviour of the rotor model. Once it is driven away from equilibrium it is something new. In addition to the coupling in the XY model there is a dynamic coupling between rotors by way of friction.

#### The Kuramoto model

The Kuramoto model [64] is a simple model of phase coupled oscillators. The equation of motion for a rotor $j$ in the original Kuramoto model is given by

$$\dot{\theta}_i = \omega_j + K \sum_{j=1}^{N} \sin(\theta_j - \theta_i). \tag{4.9}$$

The numbers $\omega_j$ are the natural frequencies of the oscillators, the rate of progression of phase if there were no coupling between oscillators. They are typically random numbers drawn from some continous distribution; in the rotor model this distribution would be a delta function centred on zero as the rotors want to be at rest if

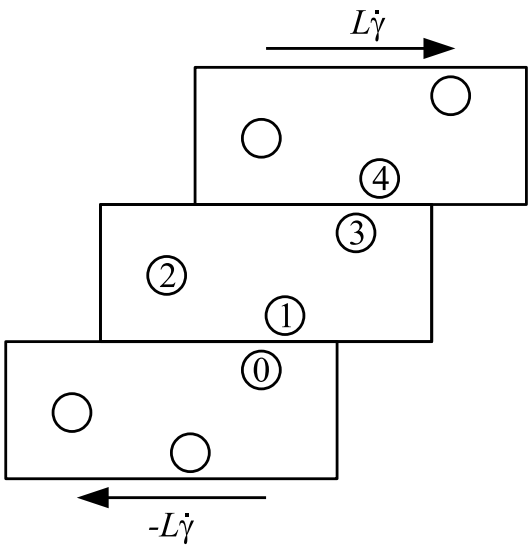


**Figure 4.2:** The sliding block representation of Lees-Edwards bondary conditions. The angular coordinate runs horizontally, while the spatial coordinate runs vertically.

possible. By comparing with the equation of motion (4.8), we see that this corresponds to the overdamped case of the rotor model. The interaction term is of a global type: the motion of a single oscillator is coupled to all others, unlike in the rotor model where the interactions are of nearest neighbour form.

The original model was created as a simple model of synchronisation, and can be solved in the large $N$ limit to find regimes where the oscillators are all synchronised, partially synchronised, or all unsynchronised. This is quite a feat for a fully nonlinear model; the rotor model is considerably more complicated and will not yield to the same techniques. The Kuramoto model does however provide us with a complex quantity that describes the synchronisation of the oscillators, namely

$$ke^{i\psi} = \frac{1}{N}\sum_{j=1}^{N} e^{i\theta_j}. \tag{4.10}$$

$k$ is a number between zero and one that measures the phase coherence of the oscillators; synchronisation is indicated by a nonzero value of $k$.

### 4.2.2 Driving the system out of equilibrium

As defined so far, the system will remain in equilibrium with the angular difference between neighbouring rotors following a Boltzmann distribution. On average, neighbouring rotors will have zero angular difference and zero relative velocity. In order

to produce a boundary driven system, the ends of the system are turned relative to one another at a constant rate, in the same way that a constant shear rate can be produced in a fluid confined by two parallel plates, by moving them at constant non-zero relative velocity.

Lees-Edwards boundary conditions were first introduced in order to perform molecular dynamics simulations of fluids undergoing planar shear [65]. The boundary conditions used in the rotor model are very similar to this situation but with angular variables. The sliding block representation of the boundary conditions is shown in figure 4.2. With ordinary periodic boundary conditions, a rotor at one end of the system would interact with an image of the rotor at the other end. With Lees-Edwards boundary conditions, the images are moved (rotated) at a constant speed, with the upper and lower images moving in opposite directions. If the system contains $N$ rotors, then the rotors numbered 1 and $L$ will interact with imaginary rotors that we may label 0 and $N+1$. Instead of having $\theta_0 = \theta_N$ and $\theta_{N+1} = \theta_1$, we have:

$$\theta_0 = \theta_N - N\dot{\gamma}t \tag{4.11}$$

and

$$\theta_{N+1} = \theta_1 + N\dot{\gamma}t, \tag{4.12}$$

where $N\dot{\gamma}t$ is the total shear applied to the system at time $t$. It is easy to see, for example by summing the difference in velocities between neighbouring rotors across the entire system (i.e. including the pair of rotors 1 and 0 or $N$ and $N+1$, but not both), that the system as a whole now has a non-zero shear rate of size $\dot{\gamma}$. These boundary conditions, like ordinary periodic boundary conditions, do not introduce any edge effects; in this scheme the rotor labelling is nothing more than convention.

### 4.2.3 The continuum limit

The rotor model is unusual in that it is not clear how to go about taking the continuum limit. Naively taking the limit of small inter-rotor distance in the equations of motion and introducing a field $\theta(x)$ leads to a topologically different system than the microscopic one. In the original system, if a rotor turns relative to a neighbour by an angle of $2\pi$ then the system is in exactly the same state as it was originally in terms of forces. In the continuous system, if two areas of the chain undergo a

relative rotation of $2\pi$ then the fluid in between gets twisted as well. This produces a restoring force that wants to untwist the chain back to its original position. This does not bode well for shearing the system; it would be similar to endlessly twisting up a rubber tube and a steady state would not be reached as a constantly increasing stress would be required. The conclusion is that the rotor model is an intrinsically discrete model and must be treated as such.

## 4.3 Simulation results

With no hope of exactly solving the model analytically, the equations of motion are numerically timestepped in order to find the properties of the steady state. The model as described contains five parameters: the moment of inertia $I$, the amplitude of the potential $\alpha$, the friction coefficient $\mu$, the noise strength $\sigma^2$ and the shear rate $\dot{\gamma}$. In the following $I$ and $\alpha$ are set equal to one, which amounts to a particular choice of units for moment of inertia and time. We are left with a three dimensional parameter space to explore, consisting of $\mu, \sigma^2$ and $\dot{\gamma}$.

### 4.3.1 Simulation method

The equations of motion (4.8) with the boundary conditions described in section 4.2.2 were numerically timestepped using an algorithm described in appendix B. Apart from the velocity profiles in the following section, each data point shown is the average of three independent simulations, that is, three simulations. All results shown are for systems of 512 rotors unless otherwise noted; some simulations were repeated with 1024 rotors but no significant deviations in behaviour from the smaller system size were found.

The initial conditions for the model were designed to be as unbiased as possible. The initial positions were randomly drawn from a uniform distribution over the interval $[-\pi, \pi]$. The initial velocities were given according to uniform flow with an additional random velocity, the latter being drawn from a Gaussian distribution with a variance determined by the temperature. Some simulations were repeated with the initial velocities given just by the random velocity, without an overall velocity gradient; these appeared to reach the same steady state but took longer to get there.

After startup, the model was given a duration of $10^5$ time units to reach a steady

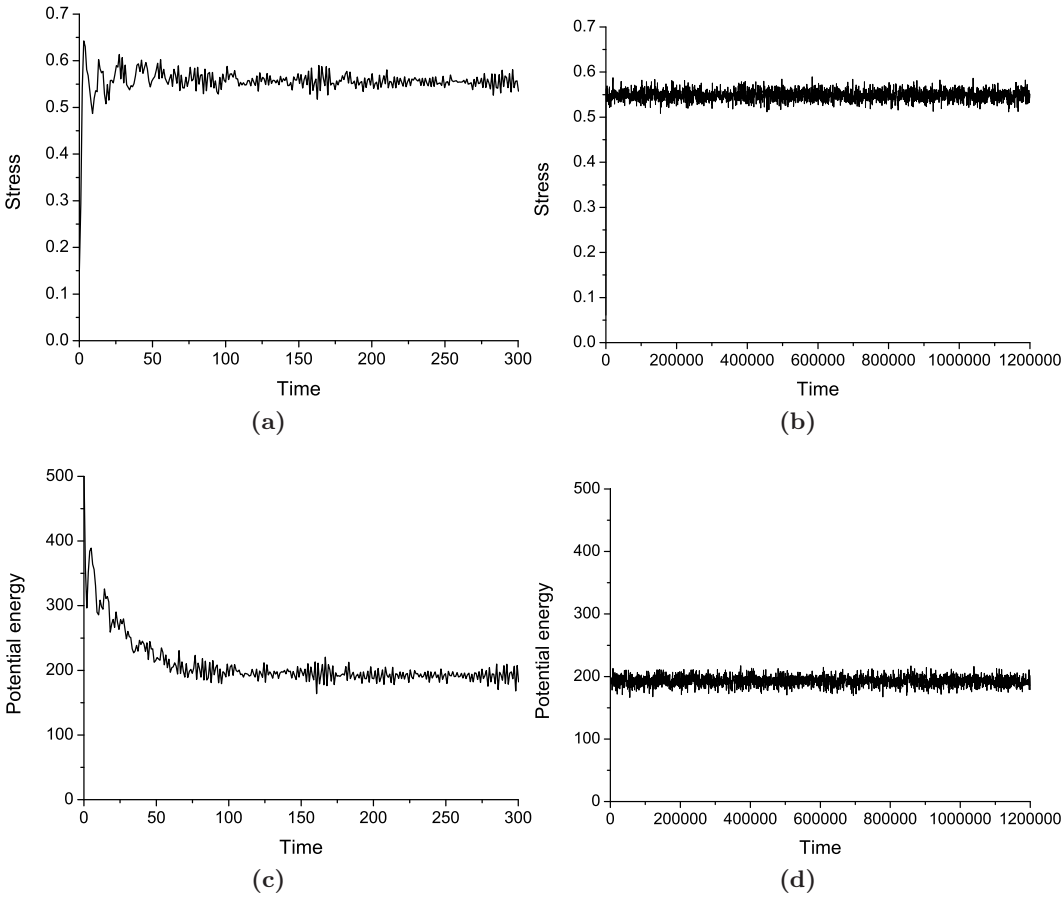


**Figure 4.3:** Time series for the stress and potential energy in a typical simulation.

state; in practice, all simulations appeared to settle down much more quickly than that. In all cases the average stress, potential energy and other quantities rapidly approached a constant value plus fluctuations and so the system was considered to be in a steady state for all intents and purposes; however, see the discussion in the following section about what constitutes a steady state in this model. Typical time series of the stress and internal energy are shown in figure 4.3, at early times and over the course of the whole simulation.

### 4.3.2 Velocity profiles

The most visually obvious output of the simulations is the velocity profile in the fluid. Typical examples for the parameters $k_BT = 0.01$ and $\mu = 0.2$ are shown in figure 4.4. For low enough $\dot{\gamma}$, $\mu$ and $\sigma^2$ neighbouring rotors can lock together, staying at a fixed relative angle on average and thus behaving like a solid under strain. Following the terminology of Büttiker et al. [66], the pair of rotors is then

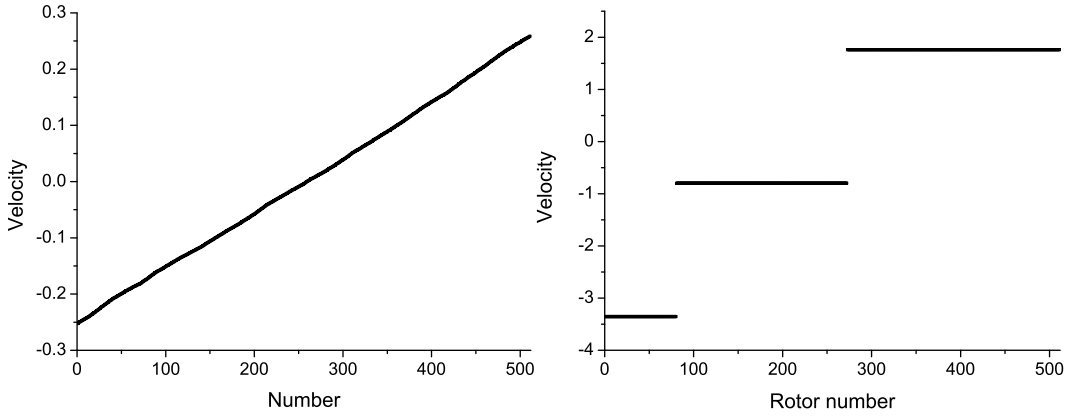


**(a)** $\dot{\gamma} = 0.001$




**(b)** $\dot{\gamma} = 0.01$

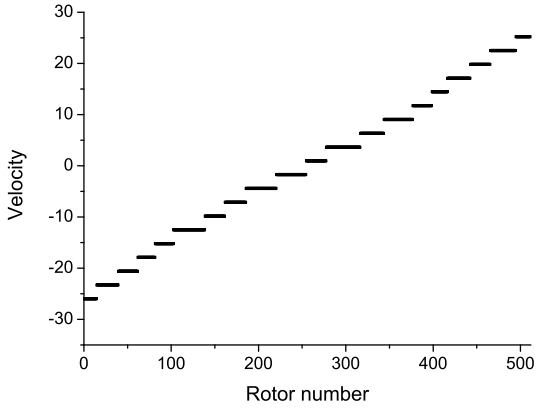


**(c)** $\dot{\gamma} = 0.1$

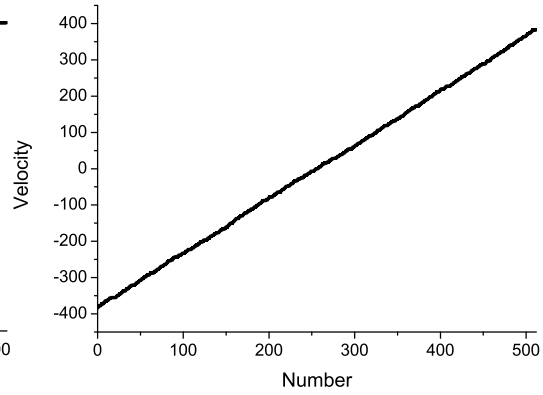


**(d)** $\dot{\gamma} = 1.5$

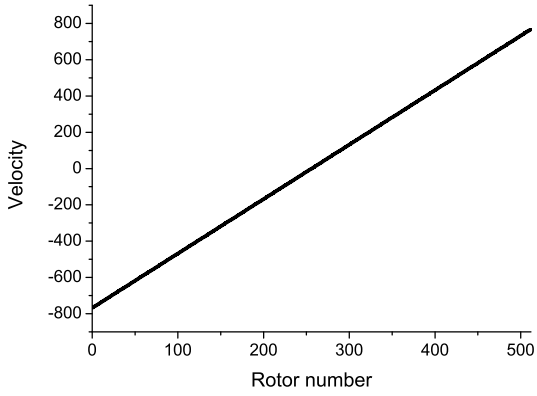


**(e)** $\dot{\gamma} = 3.0$

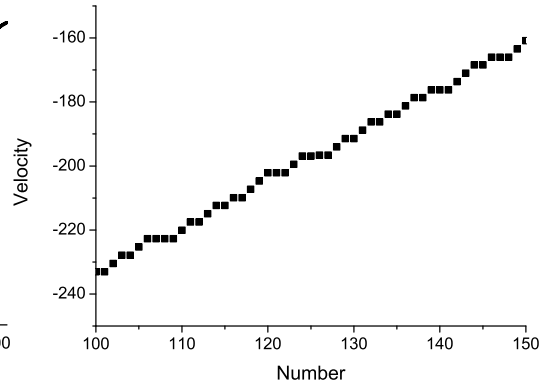


**(f)** $\dot{\gamma} = 1.5$

**Figure 4.4:** Examples of time averaged velocity profiles for $k_BT = 0.01$ and $\mu = 0.2$. Plot (f) is a blowup of a region of (d), shown so that the locked rotors are apparent.

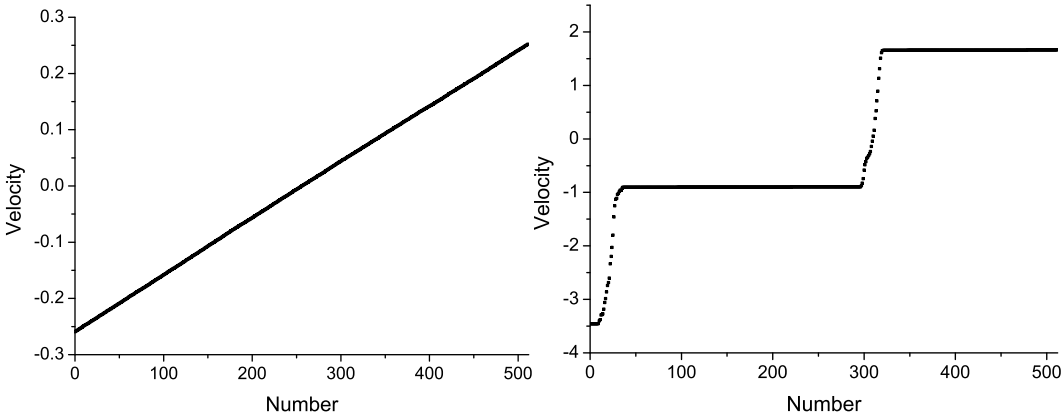


**(a)** $\dot{\gamma} = 0.001$




**(b)** $\dot{\gamma} = 0.01$

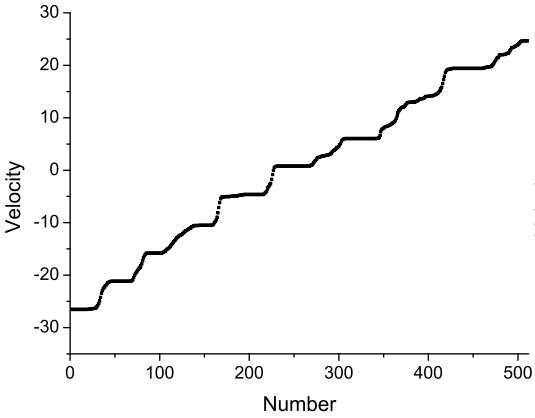


**(c)** $\dot{\gamma} = 0.1$

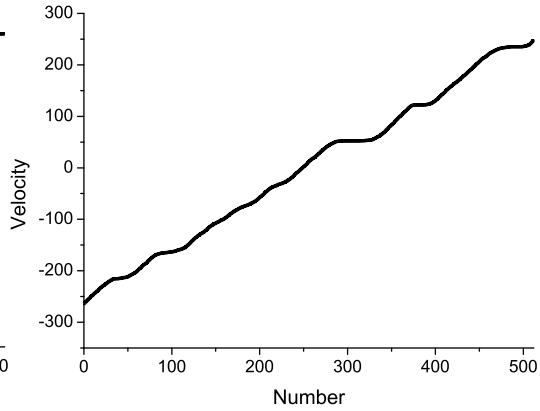


**(d)** $\dot{\gamma} = 1.0$

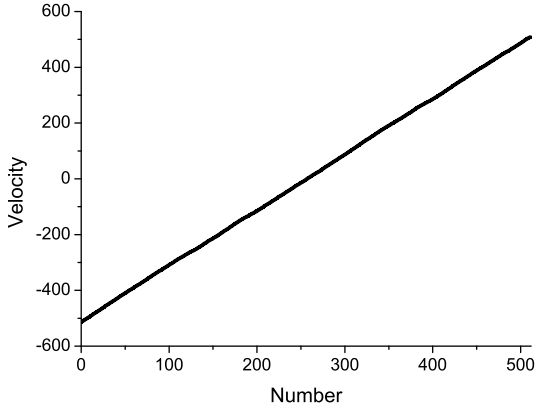


**(e)** $\dot{\gamma} = 2.0$

**Figure 4.5:** Examples of time averaged velocity profiles for $k_BT = 0.05$ and $\mu = 0.2$.

called locked; if it is not locked, it is running. The entire system cannot lock as it must sustain a shear rate somehow, so some degree of running will always occur. Note that the converse is not true: locked states cannot always occur, as the locked rotors feel only a conservative force on average due to their lack of relative velocity. The conservative force is sinusoidal and therefore bounded (by one in the current units); if the average stress exceeds one then no rotors can stay locked. This provides an upper bound on the existence of such profiles, although the actual limit is lower due to fluctuations.

At very low shear rates, of the order of $10^{-3}$, the system exhibits uniform flow (figure 4.4a). At around $\dot{\gamma} = 0.005$ there are a small number of solid regions separated by single running pairs of rotors (figure 4.4b). As the shear rate is increased these solid regions break up into smaller regions still separated by isolated pairs of running gaps (figure 4.4c). Eventually there are some regions that contain more than two consecutive rotors in relative rotation, while the solid regions become of smaller size (figure 4.4d). At high enough shear rates the profile is always uniform, with an average relative velocity that is the roughly the same for all neighbours (figure 4.4e); no more solid regions are seen from $\dot{\gamma} \approx 2.75$ onwards. The solid regions are very robust, existing for the entire averaging time of $10^6$ time units without breaking.

At the higher temperature $k_BT = 0.05$ and the same friction coefficient 0.2, there is a similar progression of large solid regions splitting into smaller ones before disappearing as $\dot{\gamma}$ is increased. In this case the extra thermal noise has the effect of blurring the boundaries between solid regions so that the jump in velocity between steps occurs over a liquid-like region. The progression is shown in figure 4.5. Uniform flow for this averaging time is seen at a lower value of $\dot{\gamma}$, approximately 1.5. In addition to this, there is again a uniform phase seen at the lowest shear rates. At $k_BT = 0.1$ and $\mu = 0.2$ no solid regions are seen in the profiles at any shear rate tested.

The low shear rate uniform regimes are due to thermal fluctuations that result in a lack of long term memory. If the shear rate is very low, then neighbouring rotors undergo full relative rotations (slip) very rarely at a rate determined by $\dot{\gamma}$. If the time between slips is so long that the system has forgotten which rotor pair slipped last (i.e. if that time is longer than some appropriate correlation time), then every rotor is equally likely to slip next. The velocity profiles shown are therefore dependent

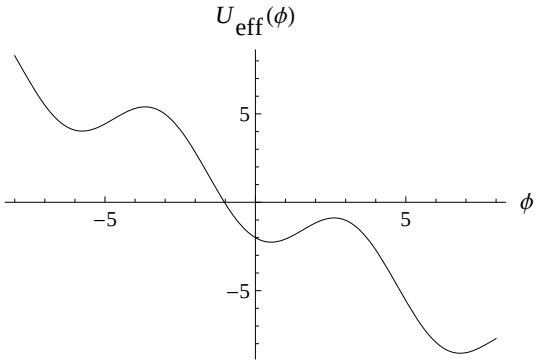


**Figure 4.6:** The effective potential used in the calculation of the escape rate in a solid region for the parameters $\alpha = 1$, $\Sigma = 0.5$.

on the interplay between shear rate, the correlation time and the averaging time. In particular, at any finite temperature locked states cannot be a part of the true steady state as any noise in the system will eventually cause them to break. When averaged over the longest periods of time all states should appear uniform at any nonzero temperature.

An order of magnitude estimate of the breaking due to thermal noise can be obtained via the use of Kramers escape rate theory [67, 68]. In its simplest guise this is concerned with the thermally activated escape of a particle from a metastable state of a one dimensional potential, i.e. a potential well. For a deep enough well or low enough temperature, the particle will effectively be in equilibrium in the metastable state and it will only rarely be excited over a barrier and out of the well. In general the rate of escape $r_K$ from the metastable state follows an Arrhenius form:

$$r_K = Ae^{-\Delta U/k_B T}, \tag{4.13}$$

where $\Delta U$ is the height of the potential barrier blocking its escape, and $A$ is a prefactor that contains some more details about the system. For moderate to strong friction $\mu$, $A$ was found by Kramers to be

$$A = \left( \sqrt{\frac{\mu^2}{4} + \omega_b^2} - \frac{\mu}{2} \right) \frac{\omega_0}{2\pi\omega_b}, \tag{4.14}$$

where $\omega_0$ is the curvature of the potential at the bottom of the well and $\omega_b$ the curvature at the top of the barrier. While this expression is not valid for low friction, in this analysis I use it for all $\mu$ - I am only looking for a very rough approximation to

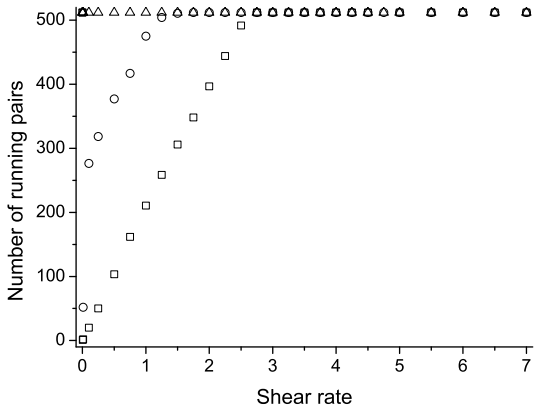


**Figure 4.7:** The number of running pairs measured in simulation for $\mu = 0.2$. Different symbols denote different temperatures $k_BT$: squares, 0.01; circles, 0.05; triangles, 0.1.

the escape rate, and the dominant behaviour is given by the exponential in equation (4.13).

In the current situation, the role of the particle position is played by the relative angle between neighbouring rotors $\phi$. In the solid region it lives in a potential that is roughly given by $U_{\text{eff}}(\phi) = -2\alpha\cos(\phi) - 2\Sigma\phi$, where $\Sigma$ is the average stress in the system. The linear term reflects the fact that the system is under strain and so there is a nonzero force $\Sigma$ from each neighbour on average. A plot of $U_{\text{eff}}(\phi)$ is show in figure 4.6. In the solid region the rotors lie at a preferential angle such that $\phi$ spends most of its time in the bottom of the potential wells. Note that there are no minima for $\Sigma \geq \alpha$, corresponding to the fact that the solid region has an upper bound to the stress that it can support due to the boundedness of the potential. The difference between the escape rates to the right and left wells then gives an estimate for the thermal shear rate $\dot{\gamma}_K$.

The inverse of this shear rate $t_K = \dot{\gamma}_K^{-1}$ gives an estimate of the time between thermally activated hops. If the averaging window used is much larger than $t_K$ then many thermally activated breakages will occur and a uniform phase will be seen. For $k_BT = 0.01$ and $\mu = 0.2$, with a stress $\Sigma = 0.55$ taken from the simulations, $t_K$ is found to be $2 \times 10^{26}$: vastly greater than the averaging time of $10^6$. For $k_BT = 0.01$ and $\Sigma = 0.59$ (the latter also determined empirically) we find $t_K \approx 2.5 \times 10^5$. This is fairly close to the averaging time so that some breakage is seen, concentrated around the areas with the largest fluctuations, the ends of the solid regions. For $k_BT = 0.1$ and $\Sigma = 0.5$, $t_K \approx 8600$ or nearly two orders of magnitude less than

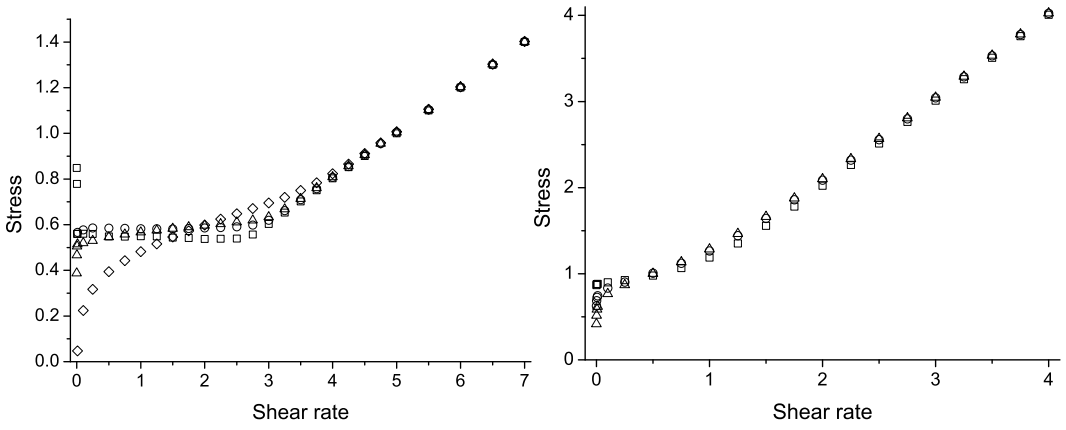


**(a)** $\mu = 0.2$ **(b)** $\mu = 1.0$

**Figure 4.8:** Constitutive relations measured in the rotor model for a range of temperatures and friction coefficients. Different symbols denote different temperatures $k_BT$: squares, 0.01; circles, 0.05; triangles, 0.1; diamonds, 0.5.

the averaging time, so we would expect to see more thermal breakage and thus a roughly uniform flow. This analysis is only approximate as the requisite conditions for Kramers' theory may not always hold and fluctuations in the solid regions are neglected, but is corroborated by the simulation results. The number of running pairs seen is plotted in figure 4.7 for $\mu = 0.2$ and various temperatures; running in the simulations was defined as having undergone a relative rotation of at least $2\pi$ over the averaging period.

Increasing $\mu$ to 1.0 destroys the solid regions previously seen. A higher friction coefficient would result in a higher average stress for the same velocity profile; if that stress is now too high to support solid regions then the same profiles will not be valid. This leaves open the possibility of observing solid regions at lower shear rates, but this has not been observed down to shear rates of $10^{-4}$.

### 4.3.3 Constitutive relation

One of the most important things to measure from a rheological perspective is the constitutive equation of the fluid, the stress $\Sigma$ as a function of shear rate $\dot{\gamma}$. Examples for various parameters are shown in figure 4.8. In all cases, at high shear rates the relation takes the Newtonian form $\Sigma \approx \mu\dot{\gamma}$; $\mu$ plays the role of the viscosity of the "fluid".

The curves for $k_BT = 0.01$, 0.05 and 0.1 at $\mu = 0.2$ (figure 4.8a) consist of three distinct regions. At low shear rates $\Sigma$ changes rapidly as a function of $\dot{\gamma}$

before levelling out to a rough stress plateau, then at high shear rates we see the Newtonian behaviour just mentioned. For $k_BT = 0.01$ the plateau ends at roughly the same value of shear rate that uniform flow sets in, although that is not the case for $k_BT = 0.05$. At the higher temperature of $k_BT = 0.5$ the plateau is effectively lost although the curve is still nonlinear. In general the plateau region is where we find some locked gaps; as the shear rate is increased, more and more begin to run in order to accommodate the imposed shear rate at roughly the same stress. When all the gaps are running, no more locked pairs of rotors can be broken and so the only way of sustaining an increased shear rate is for the average relative velocity to increase; this comes with a necessary increase in the frictional part of the stress.

At very low shear rates, the plateau in the $k_BT = 0.01$, $\mu = 0.2$ curve is preceded by a sudden increase in stress. A negative slope in the constitutive curve indicates that the system may not be in its steady state by the same argument used to predict shear banding instabilities from theoretical models: the negative slope means that any small fluctuation away from the steady state shear rate will not be opposed. Initially it was thought that this is due to finite size effects, but simulations of a system of 1024 rotors instead of 512 show the same behaviour. The reason for this remains unknown.

At $\mu = 1.0$ (figure 4.8b there is no clear plateau for the shear rates tested, although the $k_BT = 0.01$ curve does begin to level off, indicating a possible plateau at lower $\dot{\gamma}$. The curves for higher temperatures show a decrease towards zero at low shear rates before any plateau sets in.

### 4.3.4 Synchronisation and the Kuramoto order parameter

The Kuramoto order parameter $k$ is shown in figure 4.9. This is the real part of the time average of the complex quantity defined in equation (4.10). At low shear rates $k$ is generally higher; when the majority of gaps are locked, $k$ is close to one as nearly all rotors are rotating in a group of the same speed.

For $\mu = 0.2$ at the two lowest temperatures, figure 4.9a, there is again an apparent change at roughly $\dot{\gamma} = 2.75$ after which $k$ levels out from an initial decrease. At the lowest temperature, $k_BT = 0.01$, the decrease in $k$ is basically linear up until this point. At the highest temperature shown, $k_BT = 0.5$, the decrease is smoother, similar to the smoother behaviour of $\Sigma(\dot{\gamma})$ when compared to lower temperatures.

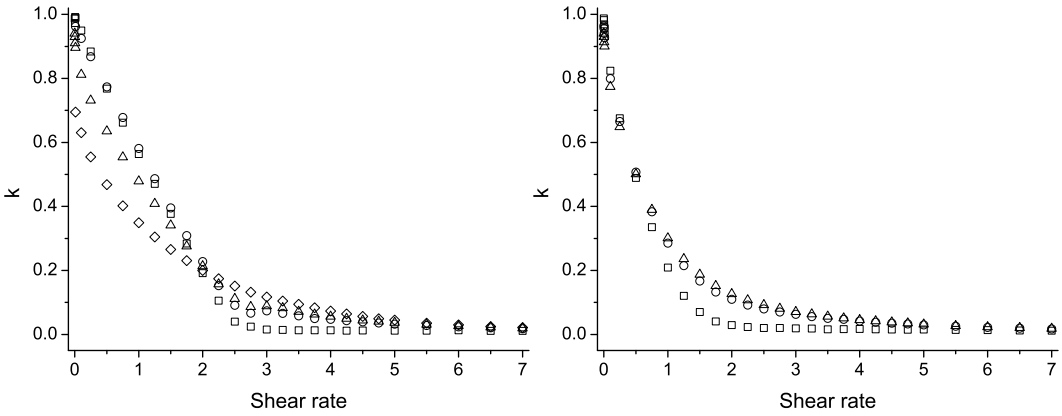


**(a)** $\mu = 0.2$ **(b)** $\mu = 1.0$

**Figure 4.9:** The Kuramoto order parameter $k$ measured in simulation for a range of temperatures and friction coefficients. Different symbols denote different temperatures $k_BT$: squares, 0.01; circles, 0.05; triangles, 0.1; diamonds, 0.5.

Increasing $\mu$ again destroys the structure seen at low temperature to give a smooth curve, as seen in figure 4.9b.

This order parameter alone may indicate a transition at $\dot{\gamma} \approx 2.75$ for $\mu = 0.2$ for $k_BT = 0.01$ and 0.05; for the lower of the two temperatures, this value is in line with the qualitative changes in the velocity profile and constitutive curve, namely, the loss of any locked gaps and the destruction of the stress plateau. $k$ might exhibit a singularity in that its derivative could be discontinuous at the transition point, if the linear decrease changes abruptly to a horizontal line across the axis. Further simulations on a larger system are needed to confirm this. The picture is not so clear cut at higher temperatures; $k_BT = 0.05$ exhibits locked gaps and a stress plateau, but after its initial decrease $k$ is significantly above zero, although it does become small eventually, and also exhibits a small bump. The $k_BT = 0.1$ system behaves in a similar fashion. The reason for the bump is unclear as it does not seem to correspond with any other change in behaviour.

### 4.3.5 The internal energy

The internal energy density $u$ is defined as $N^{-1}\sum_j(1-\cos(\theta_{j+1}-\theta_j))$, where $N$ is the number of rotors in the system. The addition of one is for convenience, so that when all the rotors are aligned $u$ it reaches its minimum value of zero. Note that the kinetic contribution to the total energy is not included, as it is not Galilean invariant

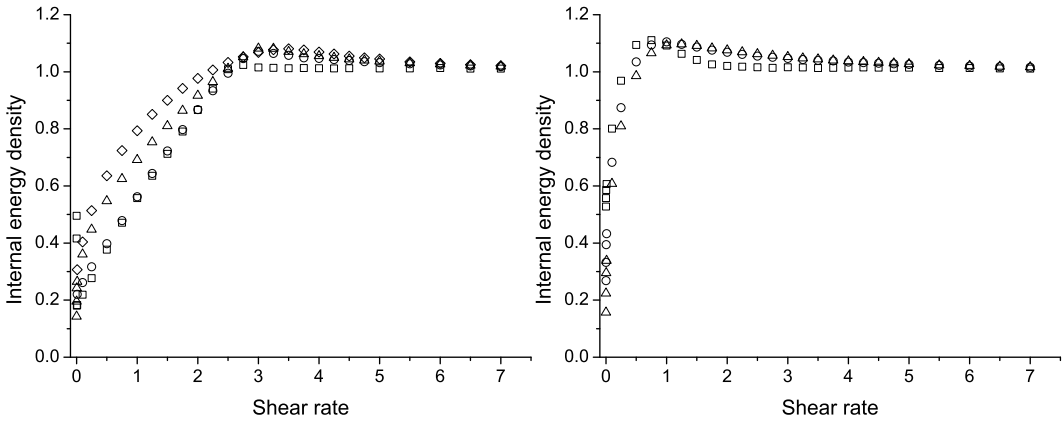


**(a)** $\mu = 0.2$ **(b)** $\mu = 1.0$

**Figure 4.10:** The internal energy density measured in simulation for a range of temperatures and friction coefficients. Different symbols denote different temperatures $k_BT$: squares, 0.01; circles, 0.05; triangles, 0.1; diamonds, 0.5.

and therefore not very informative as it is different in each frame of reference. The time averaged energy density is shown in figure 4.10 for various parameters. There is again some odd behaviour for $k_BT = 0.01$, $\mu = 0.2$ at the lowest shear rates just like in the constitutive curve, but apart from that all plots show an increase towards $u = 1$, a slight overshoot, and an approach back to one.

At high and low $\dot{\gamma}$ the reason for this behaviour is clear. Thinking in terms of relative angles, if a pair of rotors undergo a full relative rotation then they have to overcome a potential barrier. While the journey up the barrier is determined by the shear rate and is therefore slow, the way down the slope on the other side will be quick in comparison. The relative angle then languishes close to the bottom of the potential for a while until it is required to slip again. In addition, any rotors locked together provide an effectively constant contribution to the potential energy, the size of which depends on the stress. While the potential energy density always lies below two, the locked pairs of rotors effectively lower that bound. In contrast, at high shear rates and uniform flow every relative angle follows the path $\dot{\gamma}t$ to a close approximation with only small deviations from it. The potential is sampled almost uniformly in time and so $\overline{\cos(\theta_{j+1} - \theta_j)} \approx \overline{\cos(\dot{\gamma}t)} = 0$, where an overbar denotes a time average. The overshoot in between is in a region where the rotors move past each other fast enough so that they sample the potential better than at low shear rates but still with some asymmetry in the time spent moving up and down the barrier. Note that the point of crossing the line $u = 1$ roughly corresponds with the

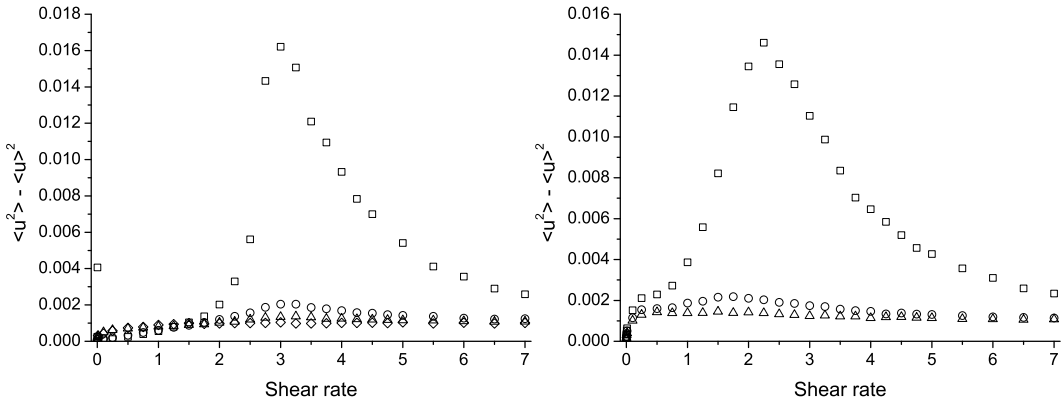


**(a)** $\mu = 0.2$ **(b)** $\mu = 1.0$

**Figure 4.11:** The fluctuations of the internal energy density measured in simulation for a range of temperatures and friction coefficients. Different symbols denote different temperatures $k_BT$: squares, 0.01; circles, 0.05; triangles, 0.1; diamonds, 0.5.

notable features of the previous sections.

The variance of the internal energy density is given by $\overline{u^2} - \bar{u}^2$. The data are shown in figure 4.11. For $\mu = 0.2$ (figure 4.11a) a clear peak is seen for $k_BT = 0.01$ at roughly $\dot{\gamma} = 3$, but for $k_BT = 0.05$ the peak is very small and at the higher temperatures shown it is not distinguishable. The peak is reminiscent of a second order phase transition, where at the critical point the fluctuations of the internal energy, and accordingly the heat capacity, diverge. A similar peak can be seen in figure 4.11b for $\mu = 1.0$, shifted to a slightly lower value of $\dot{\gamma}$, despite the fact that there are no other indications of a transition there for that friction coefficient.

The fluctuations of the internal energy (not energy density) at $k_BT = 0.01$ and $\mu = 0.2$ for different system sizes are shown in figure 4.12. The different plots are scaled by the system size for comparison. A classic indicator of a phase transition is a peak in the heat capacity, or the energy variance. In general the peak will get sharper as the system becomes larger, indicating a well defined point where the phase transition happens. Figure 4.12 does not show this, but instead shows that all three system sizes give a very similar result. This indicates that even for a system size of 256 rotors, we have essentially already converged to thermodynamic or large system size behaviour of this quantity.

The variance as shown does not appear to diverge in the large system limit as might be expected for a phase transition. This is to be expected as the internal energy of the rotor model is bounded for any given system size, meaning that its

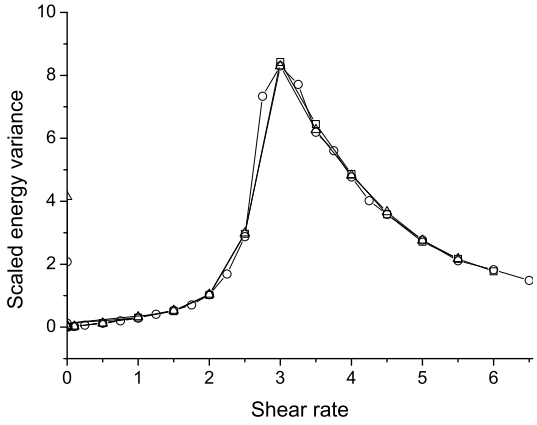


**Figure 4.12:** The fluctuations of the internal energy measured in simulation for the parameters $k_BT = 0.01$ and $\mu = 0.2$ for different system sizes, scaled by the simulation size. The squares are the data for $N = 256$, circles $N = 512$, and triangles $N = 1024$.

variance cannot grow arbitrarily.

### 4.3.6 The velocity correlation function

The velocity correlation function, defined by $C(j,k) = \langle(\dot{\theta}_j - \langle\dot{\theta}_j\rangle)(\dot{\theta}_k - \langle\dot{\theta}_k\rangle)\rangle$, gives more evidence for a transition at $\dot{\gamma} \approx 2.75$. Some correlation functions for $k_BT = 0.01$, $\mu = 0.2$ are shown in figure 4.13; $C$ is plotted as a function of distance $d = k-j$. At low shear rates the correlation is rather short ranged; increasing the shear rate up to 2.5 leads to much longer range correlations. At $\dot{\gamma} = 2.75$ the correlations abruptly disappear. Note that in the run up to the transition $C(j,k)$ does not decay away to zero within the system, indicating that finite size effects are probably important; larger simulations with 1024 rotors instead of 512 show similar statistics.

## 4.4 Conclusions

In this chapter I have studied an idealised model of a complex fluid through simulation. It was hoped that the rotor model would exhibit some qualitative properties of a real fluid and help to develop intuition about boundary driven systems in general, and it does indeed provide some rich behaviour, much of which is strongly reminiscent of real fluids. Repeat simulations and simulations started with different initial conditions indicate that the model shows reproducible steady state behaviour, meaning that the statistical mechanics seen in the previous chapters could apply. At low shear rates and thermal noise the model shows a strong departure from Newtonian

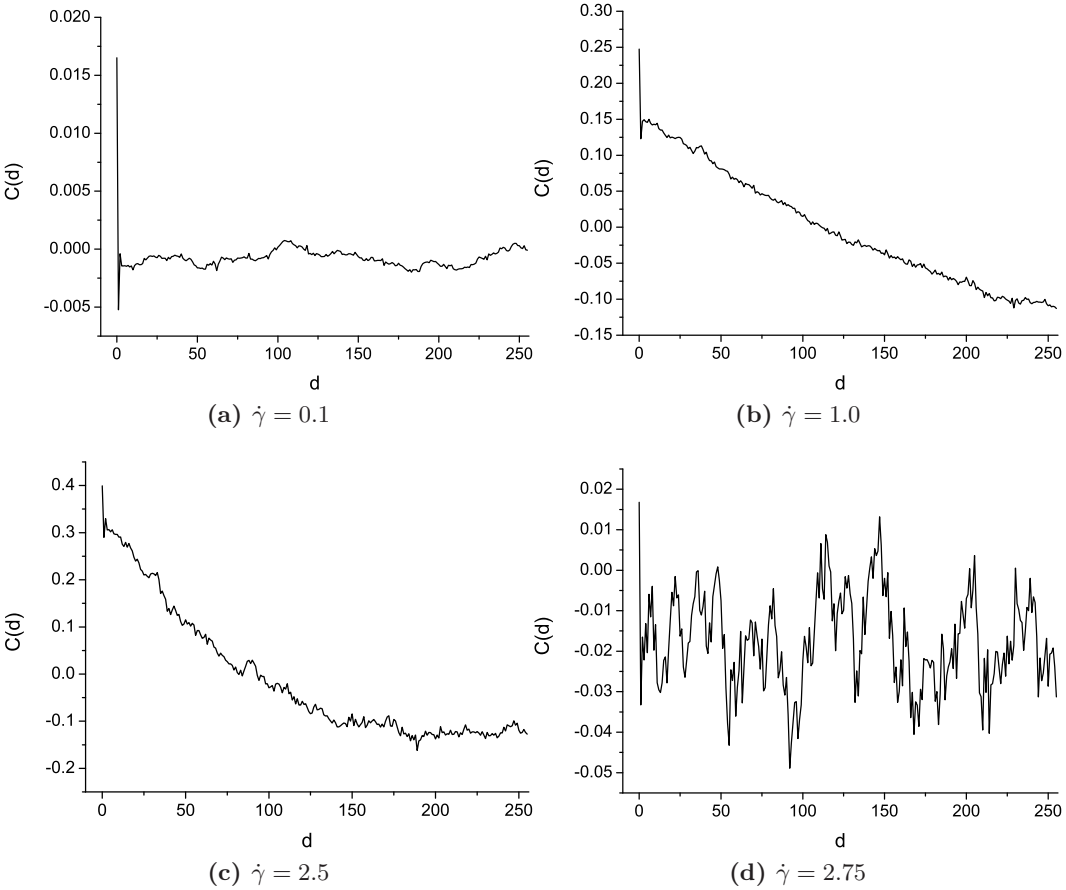


**(a)** $\dot{\gamma} = 0.1$ **(b)** $\dot{\gamma} = 1.0$

**(c)** $\dot{\gamma} = 2.5$ **(d)** $\dot{\gamma} = 2.75$

**Figure 4.13:** The velocity-velocity correlation function measured in simulation for $k_BT = 0.01$ and $\mu = 0.2$.

flow, as shown by the inhomogeneous velocity profiles and the nonlinear constitutive curves, at least for moderate to long timescales.

Various statistical averages indicate some sort of transition at $\dot{\gamma} \approx 2.75$ for $k_BT = 0.01$, with signatures seen in the constitutive relation and the Kuramoto order parameter $k$ and the most striking evidence coming from a peak in the variance of the internal energy. It seems very likely that there is a nonequilibrium phase transition at this point. Close to a phase transition finite size effects could come into play as correlation lengths diverge, making simulations more tricky in that region. The transition at low temperatures could persist down to zero temperature; the argument in section 4.3.2 for the eventual dissolution of solid regions at finite temperature does not hold at zero temperature, so the transition may correspond with a definitive structural change, the density of locked rotors going to zero. Zero temperature simulations are currently in progress to test this idea. Phase transitions in some one dimensional systems at equilibrium can be ruled out rigourously [62],

barring transitions at zero (as in the Ising model) or infinite temperature. The rotor model does not fall into that class of systems and so is free to undergo phase transitions.

The measured constitutive curves provide an interesting comparison with real experimental systems, where many fluids undergoing controlled shear rate experiments exhibit a stress plateau bounded by two Newtonian flow regimes [51]. The plateau is usually associated with some degree of inhomogeneity in the system; for example, the work of Cappalaere et al. just cited provides evidence for a mixture of isotropic and nematic phases of wormlike micelles in the plateau region. In addition, advancing along the plateau involves some internal restructuring such as changing the proportions of the different phases, or in the rotor model, removing some locked pairs of rotors. The linear increase of the number of running pairs shown in figure 4.7 is also reminiscent of the balance of the high and low shear rate bands in shear banding fluids, where the size of the latter is reduced in favour of the former as shear rate is increased in order to maintain the global shear rate constraint. In the rotor model the locked pairs constitute regions of extremely high viscosity as they are never seen to shear on the timescale of the current simulations.

In addition to the zero temperature simulations mentioned above, there are areas of parameter space that were not investigated in this work, such as the regimes of high temperature, high shear rate, or very low shear rate. A more complete investigation of parameter space would provide a wider picture to place the current results in and may reveal more connections to experiment; in particular, unpublished simulations of the rotor model performed by C. Hall have indicated velocity profiles of conventional shear banding type [69].

Having described some phenomenology of the rotor model, the next step is to try and give these features a theoretical explanation. This is the purpose of the next chapter of this thesis.

# Chapter 5

# The rotor model: a theoretical study

## 5.1 Introduction

Even though the rotor model is one dimensional and simple to write down, it is far from being analytically tractable; any theoretical examination of it must necessarily include some approximations. In this chapter I aim to analyse particular situations seen in simulation before applying a more general method, built on the ideas of the renormalisation group.

Renormalisation group (RG) theory is a very successful theoretical technique developed in the last century to study the large scale properties of thermal and quantum systems. Experimentally, it is seen that at a critical point there is no discontinuous change in the order parameter (e.g. volume or magnetisation) but there is instead some other singular behaviour, such as a divergence in specific heat capacity. The latter typically diverges as $|T - T_c|^{\alpha}$, where $\alpha$ here is an example of a critical exponent. Ordinary statistical mechanics fails at these points as the correlation length becomes infinite. In particular, the mean field theory of phase transitions, which deals in average values of the relevant quantities, fails to describe these transitions accurately. Important progress was made by B. Widom, who investigated some ideas about the behaviour of critical systems and reproduced the known relations between critical indices [70, 71]. Despite the apparent complexity of the critical physics, critical points exhibit universality, whereby different physical systems can behave in a similar manner around the critical point, dependent only

on the symmetries and dimension of the systems.

The renormalisation group formalism includes all of these ideas in one setting. Originating in particle physics, it was developed into a general calculational tool of statistical physics. L. P. Kadanoff investigated a real space renormalisation group method for the Ising model called the block spin transformation that reproduced Widom scaling [2]. K. G. Wilson built on these ideas and produced a theory that gives the critical behaviour of a model by integrating out high momentum variables [72, 73]. The Wilson procedure is an example of a momentum space RG calculation as opposed to a real space calculation.

This chapter is divided into three main sections. The first describes effective medium theory in the model, where I approximate the environment of an individual piece of the fluid in a simple manner to produce an analytically tractable model. The second analyses a single isolated running pair of rotors of the kind seen in the previous chapter. I ask under what conditions this arrangement may remain stable. The third uses the ideas of real space RG to carry out an approximate coarse graining procedure on the rotor model. Throughout the chapter the idea of linearisation of fluctuations is used repeatedly.

## 5.2 Effective medium theory

Effective medium theory is a way of approximating the rotor model that is similar to elementary treatments of the Ising model. With the equations of motion written in terms of the relative angles $\phi_j = \theta_{j+1} - \theta_j$, one pair of rotors is singled out. The forces from its neighbours are assumed to be constant, amounting to a force $\Sigma$ on each side - this is identified as the average stress throughout the system in steady state. This is analogous to the treatment of the Ising model that most students learn first: in evaluating the partition function, we must add up the Boltzmann factors for neighbouring spins. This is a difficult task in general, and is simplified by assuming that for one of these spins, the value of the neighbouring spins seen by it are all equal to a constant that is the mean value of the spin. In the Ising model, this value has the interpretation of magnetisation. The situation is the same here, with the significant constant being the force or stress in the system. As in the Ising model, this is a mean field model with a mean field of stress instead of magnetisation.

The work in this section is done at zero temperature; this is not very general, but will hopefully be relevant at least to small temperatures as well. The equation of motion for a relative angle $\phi_i = \theta_{i+1} - \theta_i$ is written as

$$\ddot{\phi}_j = g_{j+1} - 2g_j + g_{j-1}, \tag{5.1}$$

where the inter-rotor forces $g_j$ are found from equation (4.8):

$$g_j = f_{j+1,j} \quad = \alpha \sin(\phi_j) + \mu\dot{\phi}_j + \sigma\xi_{j+1,j}. \tag{5.2}$$

The effective medium approximation is applied as follows:

$$\begin{aligned} \ddot{\phi}_j &\approx 2\langle g \rangle - 2g_j \\ &\approx 2\Sigma - 2\alpha \sin(\phi_j) - 2\mu\dot{\phi}_j + \sqrt{2}\sigma\zeta(t). \end{aligned} \tag{5.3}$$

where the average force from one rotor on its neighbour $\langle g \rangle$ is identified as the average stress in the system $\Sigma$. The final term on the right hand side is a rewriting of the stochastic forces so that the function $\zeta(t)$ is delta-correlated white noise. The approximation corresponds to the effective potential used in section 4.3.2 and shown in figure 4.6. As can be seen, the problem has been greatly simplified to a single differential equation, an approximate equation of motion for the local dynamics of the rotor chain. This is still a difficult equation to solve exactly as it contains a sinusoidal nonlinearity, so approximate solutions are sought instead.

### 5.2.1 Harmonic expansion of the equation of motion

The relative angle $\phi(t)$ is expected to increase approximately linearly in time at some speed $s$, with fluctuations about the general trend. The following form for $\phi(t)$ is used:

$$\phi(t) = st + \sum_{m=0}^{\infty} (a_m \cos(mst) + b_m \sin(mst)). \tag{5.4}$$

Here, the fluctuations are periodic in nature with a period determined by the average relative velocity of the pair $s$. This expression can be substituted directly into the equation of motion (5.3). If the fluctuations are small, i.e. $a_m, b_m << 1$, then the nonlinear term can be expanded to first order in these coefficients and a set of linear equations results. There are two equations for each harmonic mode, which gives an

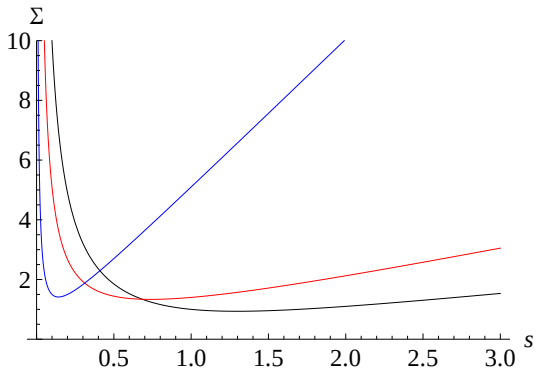


**Figure 5.1:** The stress in the rotor model as calculated in effective medium theory. The three curves correspond to different values of $\mu$: black, 0.5; red, 1; blue, 5.

infinite set of equations. In practice the upper limit on the sum is not taken to be infinity, but is truncated at some low integer $M$ to allow calculations to be done. Any harmonics higher than $M$ that appear in the equations are simply dropped, equivalent to disregarding the faster modes of the fluctuations.

With these two approximations, analytic solutions can be found. The linear system is solved for the Fourier amplitudes used, $\{a_m\}$, and the stress $\Sigma$ which is thus far unknown. This results in an expression for the stress in the system as a function of the relative velocity, $\Sigma(s)$.

The approximation is only valid for small fluctuations. This is quantified by studying the modulus of each term in the sum. For any harmonic the sine and cosine terms can be combined into one sinusoidal term with an overall prefactor which is the modulus, given as $\sqrt{a_m^2 + b_m^2}$ for the $m^{\text{th}}$ harmonic. If any modulus is greater than one, then we are not justified in neglecting the higher order products of the coefficients, for example $a_m^2$. This may occur in some regions of parameter space, given that the moduli are found as functions of the parameters of the model, but not in others. In these regions the approximation breaks down and the particular combinations of parameters that cause this are labelled invalid; regions of parameter space in which this does not happen are called valid.

In the first harmonic case, the solution is approximated via $\phi(t) = st + a\cos(st) + b\sin(st)$. After substitution into the equation of motion and linearisation treating $a$ and $b$ as small quantities, three equations are obtained via equating coefficients of

linearly independent terms:

$$a = 2(\Sigma - \mu s), \tag{5.5a}$$

$$s^2 a = 2\mu s b, \tag{5.5b}$$

$$s^2 b = 2(1 - \mu s a). \tag{5.5c}$$

The solution is easy to obtain:

$$a = \frac{4\mu}{s(s^2 + 4\mu^2)}, \tag{5.6a}$$

$$b = \frac{2}{(s^2 + 4\mu^2)}, \tag{5.6b}$$

$$\Sigma = \mu s + \frac{2\mu}{s(s^2 + 4\mu^2)}. \tag{5.6c}$$

From the last equation we see that the stress $\Sigma$ is given as a linear term $\mu s$ plus a nonlinear term that comes ultimately from the potential. For large $s$ the curve asymptotes to $\mu s$, but diverges as $s \to 0$; the approximation becomes worse for low $s$ as can be seen from the solution for $a$, so this divergence can be safely ignored. However, it doesn't necessarily rule out a portion of negative slope in the $\Sigma(s)$ curve, which is of theoretical interest as it signifies nonhomogeneous flow, as mentioned in section 4.1.

The calculation has been performed up to the third harmonic, i.e. with $M = 3$. A comparison between the approximations at first, second and third harmonics is shown in figure 5.2 reveals what at first appears to be qualitative differences between the cases: the approximation up to first or third harmonic gives a stress that diverges at low shear rates, whereas the second harmonic calculation gives a decrease to zero stress as would be physically expected. However, when resticted to the parameters for which the approximation is justifiable, the three approximations give very similar results. In view of this only the first harmonic calculation is used as higher harmonics merely add mathematical inconvenience for little or no gain.

Consider a chain of rotors undergoing uniform flow in a steady state, where each rotor is spinning at a speed $s$ relative to its neighbours. Each rotor then feels equal but opposite forces from its neighbours, of magnitude $\Sigma(s)$, which sum to zero. A real system will fluctuate about this steady state. If a rotor increases its speed by a small amount $\delta s$, then it feels a new force $-\Sigma(s + \delta s)$ from the rotor on its left

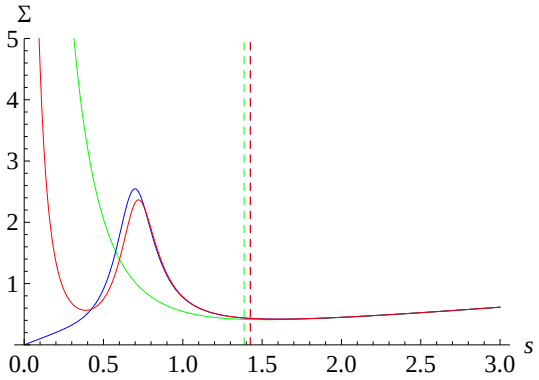


**Figure 5.2:** A comparison of the stress in effective medium theory with different highest included harmonics, for the value $\mu = 0.2$. The three curves correspond to different values of $M$: green, $M = 1$; blue, $M = 2$; red $M = 3$. The vertical lines mark the value of $s$ where the approximation becomes invalid; the lines for $M = 2$ and $M = 3$ lie on top of each other on this scale.

and $\Sigma(s - \delta s)$ from the rotor on its right. Expanding these forces to linear order and summing gives an unbalanced force on the rotor of $-2\delta s\Sigma'(s)$, with a prime denoting a derivative. From this we see that if $s$ is such that it falls on the negative slope of the $\Sigma(s)$ curve, then the fluctuation grows. This means that uniform flow at such a shear rate is unstable and therefore inhomogeneous flow must result.

An obvious question therefore is where does the minimum in the stress occur in the $\mu - s$ plane? Given the parameter values corresponding to the minimum, it is simple to check if $a$ and $b$ remain small enough in that area to trust the approximation. To find the minimum we differentiate the expression for the stress and set the resulting expression to zero. Disregarding the solution where $\mu = 0$, this ultimately leads to an equation that is a sixth order polynomial in $s$, but a quadratic in $\mu^2$. The solutions for $\mu$ as a function of $s$ at the minimum, called $s_{\min}$, are

$$\mu = \pm\frac{1}{2s_{\min}}\sqrt{1 - s_{\min}^4 \pm \sqrt{1 + 4s_{\min}^4}}, \tag{5.7}$$

where the plus/minus signs are intended to be chosen independent of each other to give four solutions. Clearly the two solutions with an overall negative sign are not relevant. The other two may be real or imaginary depending on the contents of the outer square root; it is found that only one is real for at least some values of $s_{\min}$, that with the positive sign inside the square root. This solution is only real for $s_{\min} < 6^{\frac{1}{4}}$, where $6^{\frac{1}{4}} \approx 1.565$, indicating that the minimum is never seen at higher values of $s$ than this. This curve is effectively the phase boundary, as found in this

approximation, between uniform and non-uniform flow for that region of parameter space where the approximation is valid.

Where, then, is the approximation valid? To answer this, the squared modulus is set equal to one to give a relationship between $s$ and $\mu$ which defines the boundary of validity:

$$\begin{aligned} a^2 + b^2 &= \frac{4}{s^2(s^2 + 4\mu^2)} \\ &= 1. \end{aligned} \tag{5.8}$$

This is a quadratic equation in $\mu$ and a quadratic equation in $s^2$. The solution can be expressed as $\mu$ in terms of $s$ or vice versa:

$$\mu = \pm\frac{1}{2s}\sqrt{4 - s^4}, \tag{5.9a}$$

$$s = \pm\sqrt{2}\sqrt{-\mu^2 \pm \sqrt{\mu^4 + 1}}, \tag{5.9b}$$

where the plus/minus signs are interpreted in the same way as before. Once again we only need the positive solutions, so the appropriate curve in the first case is clear. For the second case, $s$ in terms of $\mu$, we can again discard the negative solutions and then examine whether the remaining solutions are real; the useful solution is that with the positive sign inside the square root. The position of the stress minimum is compared with the boundary of validity in figure 5.3. The plot shows an area where a negative slope in the constitutive curve is included in the valid region of parameter space.

### 5.2.2 Comparison to simulation

The results are compared to simulations at $k_BT = 0.01$, the lowest temperature used, in order to limit any discrepancies due to the zero temperature used in the calculations. The result in figure 5.3 indicates that there can be inhomogeneous flow for applied shear rates of less than 1.56, depending on the value of $\mu$. This is qualitatively similar to simulation, but the region of inhomogeneous flow measured in simulation actually extends to a much higher shear rate than this theory indicates, almost up to $\dot{\gamma} = 3$ at $\mu = 0.2$; see for example figures 4.7 and 4.8. This is the opposite to what might be expected, that the zero temperature calculation would

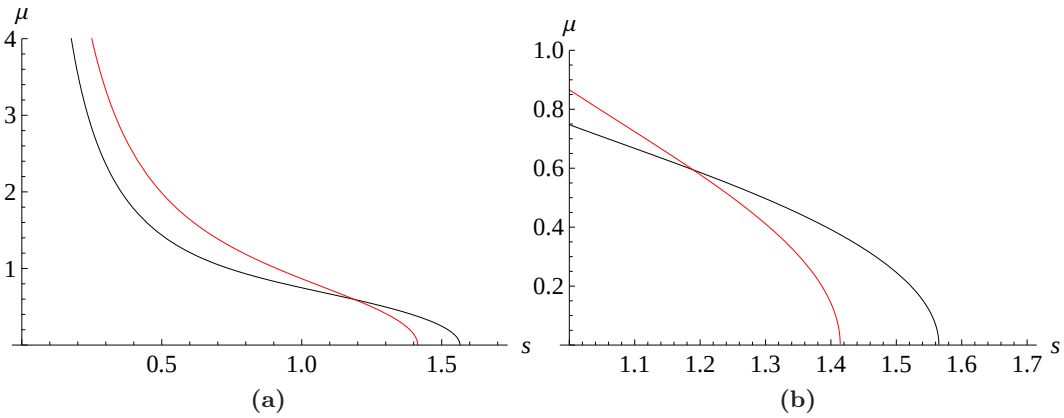


**Figure 5.3:** The position of the minimum of the $\Sigma(s)$ curve (black) and the boundary of approximation validity (red), for the first harmonic approximation. Points to the left of the red line are invalid. There is a clear area of valid $(\mu, s)$ pairs where the $\Sigma(s)$ curve has a negative slope, shown in more detail in (b).

overstate the range of inhomogeneous flow, as temperature should smear out the velocity profile to some extent. This discrepancy must then result from the mean field approximation, which omits fluctuations that would otherwise destabilise the uniform state.

Increasing $\mu$ by enough puts the system on the positive slope of the constitutive curve; the simulations at $\mu = 1$ confirm that this is the case but more simulations are needed to see where the boundary is for a given shear rate.

## 5.3 Analysis of an isolated running pair of rotors

In this section, an isolated running pair in a chain of otherwise locked rotors is studied. In contrast to the effective medium theory approximation used in the previous section, the influence of other rotors on the chosen pair is not combined into a featureless constant. Each relative angle $\phi_j$ is assumed to have a steady increase in time accompanied by small fluctuations, similar to the assumption used in effective medium theory in equation (5.4).

Instead of the single number $s$ in the previous section, we now deal with a set of average relative speeds $s_j$ and associated fluctuations $\Delta_j$:

$$\phi_j(t) = s_j t + a_0^j + \Delta_j(t). \tag{5.10}$$

$a_0^j$ is a constant for each $j$, and plays the role of the zero Fourier mode of the

fluctuations. In the previous section there was no need to include the zero mode as doing so would have just been a redefinition of the origin of time, which we are of course allowed to do. In the current case, that freedom only allows the value of one of the zero mode coefficients to be fixed, while the rest are still to be determined. Substitution into the equation of motion (5.10) gives:

$$\begin{aligned}\ddot{\Delta}_j =& \sin(s_{j+1}t + a^0_{j+1}\Delta_{j+1}) - 2\sin(s_j t + a^0_j + \Delta_j) + \sin(s_{j-1}t + a^0_{j-1} + \Delta_{j-1}) \\ &+ \mu(s_{j+1} - 2s_j + s_{j-1} + \dot{\Delta}_{j+1} - 2\dot{\Delta}_j + \dot{\Delta}_{j-1}).\end{aligned} \tag{5.11}$$

Even after linearisation with respect to the fluctuations $\Delta_j$ the above problem is practically as hard as the original one. The nature of the problem depends on the specification of the speeds $s_j$, so the simplest nontrivial choice is made: all are zero except for one. This describes a pair of rotors moving with a non-zero relative speed, sending out small amplitude waves into a surrounding chain of rotors. This is expected to be a good description of running pairs in a real system if they are far enough apart to be considered isolated and if fluctuations are small, such as for one of the steps in figure 4.4b.

The fluctuations are defined such that they don't carry any shear on average. As in the previous section a Fourier series is used, but unlike the previous section there would be no one frequency to use in a such a series in the general case. With the special case of only one rotor pair carrying shear, the frequency is clear as there is only one timescale to choose from, that associated with the velocity of the chosen pair. The fluctuations can then be given as a truncated Fourier series; in this work, only the first harmonic is included due to the amount of algebra involved. The complex exponential representation of the series is used here as opposed to the previous section, where real trigonometric functions were used:

$$\Delta_j(t) = a^j_1 e^{ist} + a^j_{-1} e^{-ist}. \tag{5.12}$$

As the fluctuation is supposed to describe a change in a real angle, the condition $a^j_1 = (a^j_{-1})^*$ is imposed, where * denotes the complex conjugate. This ensures that each $\Delta_j$ is real. The freedom in choosing one of the zero modes mentioned above is exercised by setting $a^0_0 = 0$.

With these prescriptions, the equations are solved for the Fourier coefficients. It

is assumed that the system is infinitely long and that the fluctuations decay to zero amplitude at infinity. Equating the average stress in the solid region, or equivalently averaging the acceleration and setting it to zero, gives:

$$\begin{aligned} 0 &= \overline{\sin(\Delta_{j+1})} - 2\overline{\sin(\Delta_j)} + \overline{\sin(\Delta_{j-1})} \\ &= \sin a_0^{j+1} - 2\sin a_0^j + \sin a_0^{j-1}, \end{aligned} \tag{5.13}$$

where the second equality follows after linearisation. This is solved by $a_0^j = a_0$ for all pairs $j$ inside the solid region. The average stress in the system is then $\Sigma = \sin(a_0)$, where $a_0$ is the average relative angle in the solid region (i.e. $a_0$ describes the amount of twist in the chain). It can be seen that if the average stress is larger than one, the description no longer makes sense as the average angle between rotors is now not a real number. Physically, this indicates that the stress throughout the system is large enough to overcome the barrier presented by the inter-rotor potential and that the chain should break or slip at another place; clearly this violates the assumptions in setting up this solution.

In solving the equations for the Fourier coefficients, a difficulty arises that was not seen in the previous section. While the fluctuations about the steady state are expected to be small, the zero mode coefficient that indicates the average twist in the solid region is not necessarily small. When expanding the nonlinear terms to first order in the fluctuations, the zero mode coefficient is included in the reference state that we are expanding about:

$$\begin{aligned} \sin(\phi_j) &= \sin(s_j t + a_0^j + \Delta_j) \\ &\approx \sin(s_j t + a_0^j) + \cos(s_j t + a_0^j)\Delta_j. \end{aligned} \tag{5.14}$$

Even after linearisation in the fluctuations (i.e $\{a_{\pm 1}^j\}$), this is still a nonlinear problem in the unknowns as there is, for example, a $\cos(a_0)$ term appearing in all equations for relative angles throughout the solid region, and $a_0$ is not known a priori. This is dealt with by pretending that $c = \cos(a_0)$ is a known number and then analytically solving the equations, which are still linear in the Fourier coefficients for the first harmonic. The solution is the set of coefficients given in terms of the number $c$ and the parameters $\mu$ and $s$.

Having found these expressions, another piece of information is given to us by

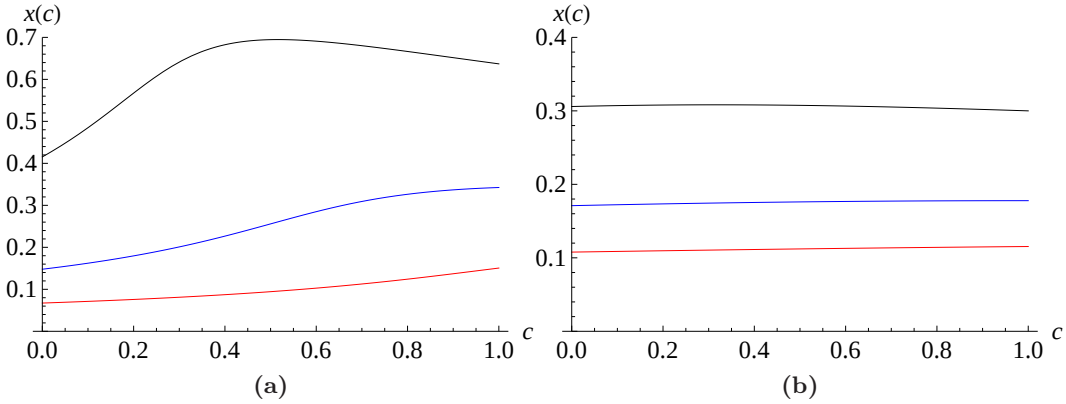


**Figure 5.4:** The function $x(c) = \Re(a_0^1)$ for (a) $\mu = 0.2$ and (b) $\mu = 1.0$. Different colours correspond to different values of $s$: black, $s = 1$; blue, $s = 1.5$; red, $s = 2$.

matching up the average stress in the solid region with the average stress inside the running pair, which must hold in the steady state. The average stress in the solid region was seen above to be $\sin(a_0)$. Using force balance on average for the shear carrying pair, we obtain:

$$0 = \overline{\sin(a_0 + \Delta_1)} - 2\overline{\sin(st + \Delta_0)} + \overline{\sin(a_0 + \Delta_{-1})} - 2\mu s \tag{5.15}$$

When the first and third terms are linearised, the familiar $\sin(a_0)$ results for each. For the second term:

$$\begin{aligned} \overline{\sin(st + \Delta_0)} &\approx \overline{\sin(st)} + \overline{\cos(st)(a_0^1 e^{ist} + a_0^{-1} e^{-ist})} \\ &\approx \frac{1}{2}(a_0^1 + a_0^{-1}), \end{aligned} \tag{5.16}$$

which is just the real part of $a_0^{\pm 1}$. It is a simple matter to express the equations to be solved in terms of the real and imaginary parts of the Fourier coefficients rather than the coefficients themselves, to allow this piece of information to be easily used. The final force balance equation is:

$$0 = \sin(a_0) - \Re(a_0^1) - \mu s. \tag{5.17}$$

As the expressions for the coefficients (or equivalently their real and imaginary parts) have been found in terms of $c$, the function $x(c)$ is known, where $x = \Re(a_0^1)$. $x(c)$ is too complicated to give as a closed form expression but is plotted for some

parameter values in figure 5.4. A trigonometric identity tells us that $\sin(a_0) = \sqrt{1-c^2}$, and we are left with an implicit equation for $c$:

$$0 = \sqrt{1-c^2} - x(c) - \mu s. \tag{5.18}$$

This equation is solved numerically, and with a value of $c$ for a given $\mu$ and $s$ the values of all the other coefficients follow.

Some example $\Sigma(s)$ curves are given in figure 5.5. Example trajectories for the middle rotor pair and some of the neighbouring pairs in the solid region are shown in figure 5.6. The problem of approximation validity arises again as in the previous section, but turns out not to be as serious. The approximation is again invalid at low values of $s$ but this affects a relatively small portion of the $\mu - s$ plane. The areas that could be expected to be susceptible are in regions that are often denied to us because for much of it $\Sigma$ is larger than one and the approximation doesn't apply anyway. All the curves include a portion of negative slope.

The interpretation of a constitutive curve with a negative slope applies as in the previous section. The situation corresponding to uniform flow there is a system where all the shear is carried by isolated running pairs, each of which has the same relative velocity $s$. The instability of the system to values of $s$ on the downward slope means that this situation is unsustainable, but again the configuration that is selected to replace it is unknown. It could be a uniform or shear banded phase, but it could still be phase with isolated running pairs, but with fewer of them or with the shear unevenly distributed between the slip planes. A region of positive slope indicates that the situation with identical velocity slip planes is stable.

The solution found gives some information as to the interaction of two slip planes in the same system. In this approximation, the slip plane disturbs its environment via linear waves that decay as they propagate. If there are two slip planes with a solid region in between, they will only interact appreciably if the fluctuations have not decayed significantly by the time they get to the other slip plane. This is quantified in figure 5.7, which shows the decay length of the fluctuations, measured in numbers of rotors, as a function of slip plane velocity for various values of the friction coefficient. For $\mu = 0.2$ and 0.5 we would expect them to be more stable as the decay length is around three rotors at most.

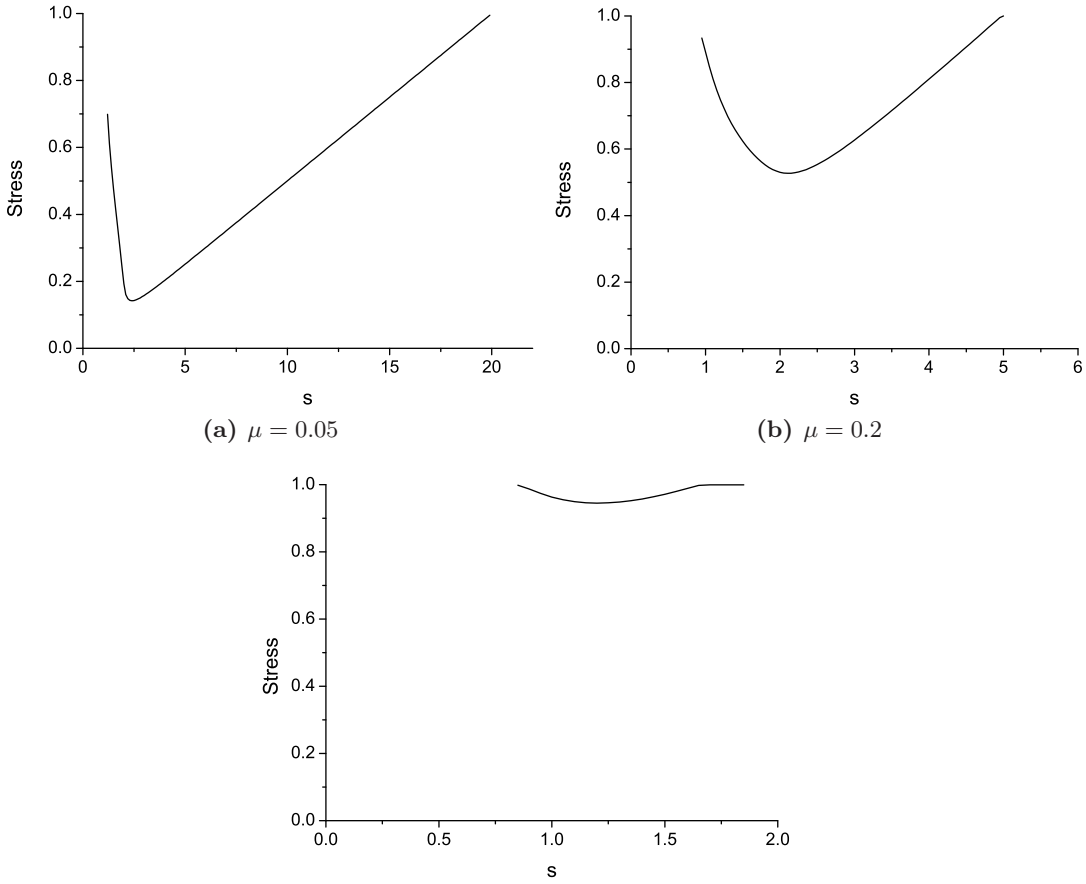


**(a)** $\mu = 0.05$ **(b)** $\mu = 0.2$

**(c)** $\mu = 0.5$

**Figure 5.5:** The stress in a system consisting of a single isolated running rotor pair. The solution only exists at stresses below one, and becomes invalid below a value of $s$ that changes with the coefficient of friction.

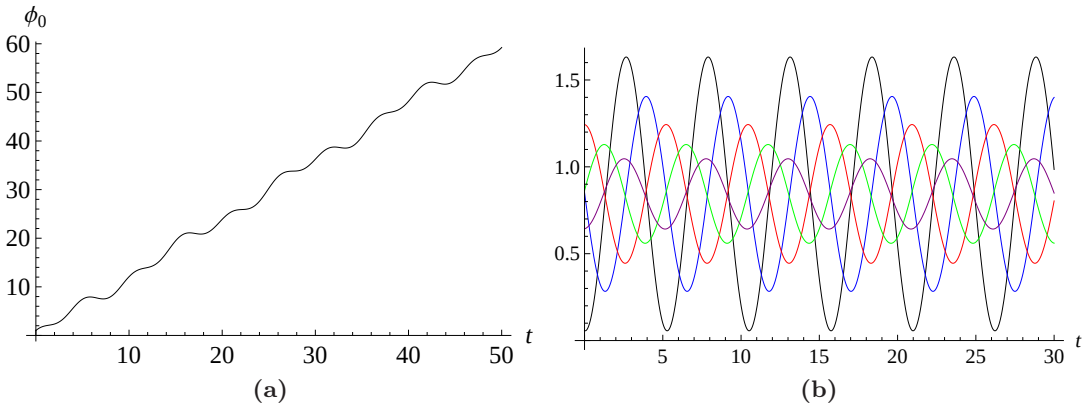


**(a)** **(b)**

**Figure 5.6:** The relative angle of (a) the running pair of rotors and (b) the first five rotor pairs to the right of the running pair as functions of time, for $s = 1.2$ and $\mu = 0.2$. The further into the solid region, the smaller the amplitude of the fluctuations about the average value. The fluctuations are successively out of phase by the same amount, indicating a travelling torsional wave.

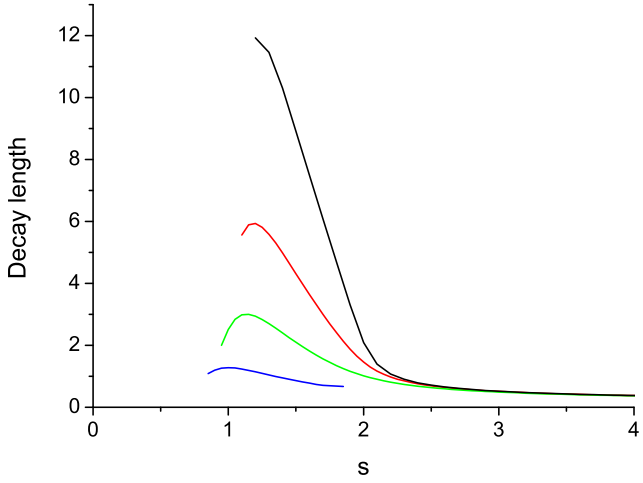


**Figure 5.7:** The decay length of the disturbances from an isolated running pair as a function of the running pair velocity $s$. Different colours indicate different values of the friction coefficient $\mu$: black, 0.05; red, 0.1; green, 0.2; blue, 0.5.

As can be seen, a lower friction coefficient means that the waves decay less quickly. As expected for linear waves, the fluctuations decay away at high frequencies. There is a cutoff at low frequencies due to the failure of the approximation as in effective medium theory, and no solutions can be found for low enough $s$ anyway. There is a peak in the decay length which is due to a resonance with the potential, where the frequency of the waves happens to be around the natural frequency of the potential. Importantly, the decay length is small for many parameter values, indicating that the slip planes can sit a few rotors apart without disturbing each other much.

### 5.3.1 Comparison to simulation

As in the previous section, the simulation data for $k_BT = 0.01$ are used as this was a zero temperature calculation. No solutions were found for $\mu = 1.0$ which is consistent with the uniform behaviour seen in simulations. For $\mu = 0.2$, there is a range of $s$ values for which a solution can be found. The solutions extend all the way up to $\Sigma = 1$ on the high $s$ side, but are not present in simulation above the plateau stress of around 0.59 (see figure 4.8a). This is due to the isolated assumption of the approximation; for large enough $\dot{\gamma}$ there are many more running pairs than locked and they cannot be considered isolated in a large chain of locked rotors - eventually there are no such large chains. The negative slope in the constitutive curves indicates

that the values on the graphs would not necessarily be the ones measured, which is good considering that the measured behaviour gives a stress plateau.

A more detailed analysis of the simulation data would be needed to identify a decay length associated with the fluctuations from an isolated running pair, but there are very clean situations such as $\dot{\gamma} = 0.01$ at $k_B T = 0.01$ and $\mu = 0.2$ where the running rotor pairs are clearly isolated and could be studied in more detail individually with the minimum of external influence.

## 5.4 Coarse graining in the rotor model

The general setup that will be used in this section is that of a single rotor $j$ coupled to two neighbours $j+1$ and $j-1$. The three rotors are described by their angles and velocities as a function of time. At the microscopic level there is an equation of motion for each rotor which involves coupling to its nearest neighbours via the force $f$. The idea is to average over the dynamics of every second rotor along the chain and express the force on the remaining rotors in terms of their next nearest neighbours instead:

$$\begin{aligned} I\ddot{\theta}_j &= f(\theta_{j+1} - \theta_j, \theta_{j-1} - \theta_j, \dot{\theta}_{j+1} - \dot{\theta}_j, \dot{\theta}_{j-1} - \dot{\theta}_j) \\ &= \tilde{f}(\theta_{j+2} - \theta_j, \theta_{j-2} - \theta_j, \dot{\theta}_{j+2} - \dot{\theta}_j, \dot{\theta}_{j-2} - \dot{\theta}_j). \end{aligned} \tag{5.19}$$

So the force that rotor $j+1$ feels due to rotor $j$ is interpreted as being due to rotor $j-1$ instead. In general, the coarse grained force $\tilde{f}$ will have a different and much more complicated form than that of $f$. This coarse graining takes us a step towards the macroscopic system by averaging over small distance properties, giving an insight into how the system behaves on a larger scale than the individual rotors. The model is only considered to be in a steady state, so that the average values of the forces from each side of rotor $j$ should always be equal and opposite, and equal in magnitude to the stress in the system $\Sigma$, regardless of which other rotors are used to express the force.

Once the average has been performed, the remaining next nearest neighbours are relabelled with consecutive numbers and the distance between them is redefined to be one lattice spacing instead of two. The latter point means that the local shear rate as calculated in the microscopic system, $(\dot{\theta}_{j+2} - \dot{\theta}_j)/2$ for example, is now the

relative velocity of nearest neighbours in the coarse grained system. The system is regarded as independent of the small distance properties that were just averaged out, so from here the same coarse graining can be repeated. In RG calculations the idea is to do this over and over to leave only the largest distance properties. Note that while the number of rotors is halved each time, a system of large enough extent will ensure that the coarse graining can be carried out an arbitrary number of times. In general, at each stage we require the physics to be identical; in the case of the Ising model this means that the partition function retains the same form, and in the scheme for the rotor model outlined here we require the new forces to be of the same form as the old. This will necessarily require some approximations, on top of those needed to solve for the dynamics of the middle rotor in the first place.

In the next section, I give the background to real space renormalisation and reproduce an equilibrium calculation for the Ising model in order to give some context for the nonequilibrium calculation. In section 5.5 I flesh out the ideas given above concerning coarse graining in the rotor model, resulting in a set of RG flow equations for the model in different flow regimes. In section 5.6 I use these equations to find the fixed points of the RG flow and interpret the results.

### 5.4.1 Real space renormalisation at equilibrium: the Ising model

The one dimensional Ising model is defined as $N$ spins positioned on sites of a regular lattice. Each spin is given a number $s_i = \pm 1$ which signifies it pointing up or down. Neighbouring spins have an energy of interaction given by $-J_0 - J s_i s_{i+1}$, where $J_0$ is a constant introduced for convenience. The partition function is given by

$$Z = \sum_{s_i=\pm 1} \prod_i e^{K_0 + K s_i s_{i+1}}, \tag{5.20}$$

where $K_0 = J_0/k_B T$, $K = J/k_B T$ and periodic boundary conditions are assumed so that $s_{N+1} = s_1$. It is common to refer to $K_0$ and $K$ as the coupling constants of the model. The decimation procedure consists of performing the sum over spin states for alternate spins, leaving a sum over half as many terms. This has the effect of averaging over the short distance properties to define a new model where the interactions are between next nearest neighbours instead. The decimation in this case is simple as the partition function factorises. Doing the sum for one of the

terms in the product over $i$ gives:

$$\sum_{s_i=\pm 1} e^{K_0+Ks_{i-1}s_i} e^{K_0+Ks_is_{i+1}} = 2e^{2K_0}\cosh(K(s_{i-1}+s_{i+1})). \tag{5.21}$$

The partition function is now a product of many of these terms. In order to make the right hand side of equation (5.21) look like the original terms, it is set equal to $e^{\tilde{K}_0+\tilde{K}s_{i-1}s_{i+1}}$; $\tilde{K}_0$ and $\tilde{K}$ are the renormalised coupling constants. By picking values of the spins $s_{i-1}$ and $s_{i+1}$ two equations are derived that can be solved to give $\tilde{K}_0$ and $\tilde{K}$ as functions of $K_0$ and $K$. The answer is:

$$\tilde{K} = \frac{1}{2}\ln\cosh(2K), \tag{5.22a}$$

$$\tilde{K}_0 = 2K_0 + \ln 2 + \frac{1}{2}\ln\cosh(2K). \tag{5.22b}$$

So the partition function can be rewritten as a sum over every other spin in such a way that it has exactly the same structure as the microscopic case, but with different values of the couplings $K_0$ and $K$. As the sum is identical in form, the procedure can be repeated over and over, with $K_0$ and $K$ changing each time. The change of the coupling constants with iteration is called the renormalisation group flow. If an iteration does not change the values of the coupling constants then we are at a fixed point of the flow: the system looks identical at larger length scales. The original system is then considered to be in a phase with the macroscopic properties of the fixed.

For the example here, the important coupling constant is $K$ which describes how likely it is that nearest neighbour spins will align. There are two fixed points for $K$, denoted by a star: $K^*$ is zero or infinity. $K^* = 0$ corresponds to an infinite temperature state where the system is completely disordered, and $K^* = \infty$ corresponds to a zero temperature state where all the spins are aligned. We still need to know what microscopic details lead to the respective fixed points, or in other words, the stability of the fixed points. It turns out that starting from any finite $K$ leads to the infinite temperature fixed point, and the only way to get to the zero temperature fixed point is to start off at zero temperature in the first place; in other words, it is unstable. For the one dimensional Ising model then, long range order only sets in at the special point of zero temperature.

The calculation shown here is rather simple; in particular, the decimation scheme results in exactly the same kind of system as we started with. This is typically not the case; particularly in higher dimensions there will normally be new couplings generated with each iteration which must be dealt with in some way. In order to keep the simple iterative structure seen above, the extra couplings may be simplified or neglected altogether in what are rather uncontrolled approximations. This will be the case for the rotor model considered next.

## 5.5 Renormalisation of the rotor model

The starting point in contrast to the previous section is the equation of motion of a single rotor:

$$I\ddot{\theta}_j = \alpha \sin(\theta_{j+1} - \theta_j) + \alpha \sin(\theta_{j-1} - \theta_j) + h(\dot{\theta}_{j+1} - \dot{\theta}_j) + h(\dot{\theta}_{j-1} - \dot{\theta}_j) + \xi_{j+1,j} + \xi_{j-1,j}. \tag{5.23}$$

Here the frictional force, ordinarily written as $\mu(\dot{\theta}_i - \dot{\theta}_j)$, is written in terms of an arbitrary function $h$. The moment of inertia is unimportant and is set equal to one from here onwards. In principle, if we knew the equivalent of the partition function for this nonequilibrium system we could sum over every second rotor as in the Ising model example, but it is unknown. In place of this, the equations of motion contain all of the physics needed to describe the system at a local scale.

Imagine an experimenter has been presented with a black box system, whose properties they wish to measure. It consists of two rotors with some unspecified medium hidden in between them. The experimenter may control the motion of the visible rotors and measure the forces on them, but cannot probe the interior. However, the apparatus does come with some helpful literature detailing the forces that the rotors feel: one that depends only on the relative angle of the rotors, one that depends only on their relative velocity and a stochastic force that is uncorrelated with the state of the system. The experimenter now wishes to characterise these forces more accurately.

First, the angle dependent force. To determine this, the experimenter must hold the rotors apart at some fixed angle and measure the average force on them. They can then collect data points which approximate the functional form of the force. If the experimenter is compelled by the accompanying literature to accept that this

force must have the form of a sinusoid, then they would fit a sinusoid to their data points to extract the constant associated with the conservative force. If the force is measured over time and the variance calculated, this experiment will also yield the variance of the stochastic forces.

The simplest method of determing the velocity dependent force is for the experimenter to turn the rotors at a constant relative velocity and measure the average resultant force. Repeating this procedure at different velocities builds up a picture of the frictional force between the two rotors.

With the knowledge that in between the two rotors is another rotor of the same type, a theorist can calculate what the experimenter might measure. Given the equation of motion (5.23), the motion of the boundary rotors $\theta_{j\pm1}$ is fixed by what the experimenter is doing, leaving a single differential equation to solve. In the following sections, the equation of motion is expressed using the variable $y$ which measures the deviation from the average motion of the boundary rotors:

$$\theta_j(t) = \frac{\theta_{j+1}(t) + \theta_{j-1}(t)}{2} + y(t) \tag{5.24}$$

In terms of $y$, the relative angles are

$$\theta_{j\pm1} - \theta_j = \pm\frac{\theta_{j+1} - \theta_{j-1}}{2} - y. \tag{5.25}$$

It should be emphasised that this is a local procedure: I only ever consider three consecutive rotors and the global shear rate constraint is not mentioned. In addition it applies only to a homogeneously flowing region and so the results may not be valid for the entire system unless it is homogeneous everywhere. If the system consists of finite size differently flowing regions then the renormalisation group transformation cannot be iterated an infinite number of times as the coarse grained system will span two flow regimes, but even if this is the case then it may still give a useful approximation if the size of the regions is large enough so that the coarse grained parameters are close to the fixed point values.

### 5.5.1 The static rotor experiment

If the two outer rotors are held apart at a fixed angle $\delta$, the rotor in between will thermalise and be distributed in angle and velocity according to a Boltzmann

distribution. On average it will be found halfway in between the two rotors at $\delta/2$ where the size of the force from each is identical. In this section the friction force $h$ is kept as a linear form with friction coefficient $\mu$. Using the fact that $\theta_{j+1}-\theta_{j-1}=\delta$ in equation (5.25), the equation of motion (5.23) can be written as:

$$\ddot{y} = -2\alpha\cos\left(\frac{\delta}{2}\right)\sin(y) - 2\mu\dot{y} + \eta, \tag{5.26}$$

where the trigonometric identities $\sin(A+B)=\sin(A)\cos(B)+\cos(A)\sin(B)$ and $\sin(A-B)=\sin(A)\cos(B)-\cos(A)\sin(B)$ have been used in rewriting the conservative force. It is derived from the potential $-2\alpha\cos(\delta/2)\cos(y)$. $\eta$ is the new stochastic force, equal to the sum of $\xi_{i+1,i}$ and $\xi_{i-1,i}$. It has a higher variance due to the contribution of two forces:

$$\begin{aligned}\langle\eta(t)\eta(t')\rangle &= \langle(\xi_{j+1,j}(t)+\xi_{j-1,j}(t))(\xi_{j+1,j}(t')+\xi_{j-1,j}(t'))\rangle \\ &= \langle(\xi_{j+1,j}(t)\xi_{j+1,j}(t')+\xi_{j-1,j}(t)\xi_{j-1,j}(t'))\rangle \\ &= 2\sigma^2\delta(t-t'),\end{aligned} \tag{5.27}$$

where the second equality takes into account that the stochastic forces from different sides of rotor $j$ are uncorrelated. Noting that the rotor also has a friction coefficient of $2\mu$, we see that the temperature that rotor $j$ experiences is unchanged, as can be seen from equation (4.6):

$$\begin{aligned}k_BT &= \frac{2\sigma^2}{2(2\mu)} \\ &= \frac{\sigma^2}{2\mu}.\end{aligned} \tag{5.28}$$

The distribution of $y$ and $\dot{y}$ is known thanks to the equilibrium conditions:

$$\rho^{\mathrm{eq}}(y,\dot{y}) = Z_y^{-1}Z_{\dot{y}}^{-1}\exp\left(-\frac{\mu\dot{y}^2}{\sigma^2}\right)\exp\left(\frac{4\alpha\mu}{\sigma^2}\cos\left(\frac{\delta}{2}\right)\cos(y)\right), \tag{5.29}$$

where the normalisation factors $Z_y$ and $Z_{\dot{y}}$ are given by

$$\begin{aligned}Z_y &= \int_0^{2\pi}\mathrm{d}y\,\exp\left(\frac{4\alpha\mu}{\sigma^2}\cos\left(\frac{\delta}{2}\right)\cos(y)\right) \\ &= 2\pi I_0\left(\frac{4\alpha\mu}{\sigma^2}\cos\left(\frac{\delta}{2}\right)\right)\end{aligned} \tag{5.30}$$

and

$$\begin{aligned} Z_{\dot{y}} &= \int_{-\infty}^{\infty} \mathrm{d}\dot{y} \, \exp\left(-\frac{\mu \dot{y}^2}{\sigma^2}\right) \\ &= \sqrt{\frac{\pi\sigma^2}{\mu}}. \end{aligned} \tag{5.31}$$

Here $I_n$ is a modified Bessel function of order $n$ [74].

Now on to what the experimenter will measure. The frictional force on the boundary rotors is zero on average, so the only contribution comes from the conservative force $\alpha \sin(\theta_j - \theta_{j-1})$:

$$\begin{aligned} \langle \alpha \sin(\theta_j - \theta_{j-1}) \rangle &= \langle \alpha \sin(y + \delta/2) \rangle \\ &= \frac{\alpha}{Z_y} \int_0^{2\pi} \mathrm{d}y \, \exp\left(\frac{4\alpha\mu}{\sigma^2} \cos\left(\frac{\delta}{2}\right) \cos(y)\right) \\ &\qquad \times [\sin(y)\cos(\delta/2) + \cos(y)\sin(\delta/2)] \\ &= \frac{\alpha}{Z_y} \int_0^{2\pi} \mathrm{d}y \, \exp\left(\frac{4\alpha\mu}{\sigma^2} \cos\left(\frac{\delta}{2}\right) \cos(y)\right) \cos(y)\sin(\delta/2). \end{aligned} \tag{5.32}$$

The integral involving $\sin(y)$ vanishes due to the integrand being odd. The remaining integral can again be expressed in terms of a Bessel function [75], to give:

$$\langle \alpha \sin(\theta_j - \theta_{j-1}) \rangle = \alpha \sin\left(\frac{\delta}{2}\right) \frac{I_1\left(\frac{4\alpha\mu}{\sigma^2} \cos\left(\frac{\delta}{2}\right)\right)}{I_0\left(\frac{4\alpha\mu}{\sigma^2} \cos\left(\frac{\delta}{2}\right)\right)}. \tag{5.33}$$

Using the fact that odd and even order modified Bessel functions are themselves odd and even respectively [74], we see that the force is periodic in the angular separation of the boundary rotors $\delta$ with period $2\pi$, and that it is odd in $\delta$ so that the coarse grained system still has equal and opposite forces between rotors.

Despite these properties, this force is clearly not the sinusoid that we want for this renormalisation group flow. It is approximated by a sinusoid via expansion in a Fourier series which is truncated after the first harmonic:

$$\begin{aligned} \langle \sin(\theta_j - \theta_{j-1}) \rangle &= \sum_n b_n \sin(n\delta) \\ &\approx b_1 \sin(\delta). \end{aligned} \tag{5.34}$$

Note that constraining the force in this way this is a somewhat arbitrary assumption, resulting in a (possibly very) lossy transformation. However, at this stage it is the

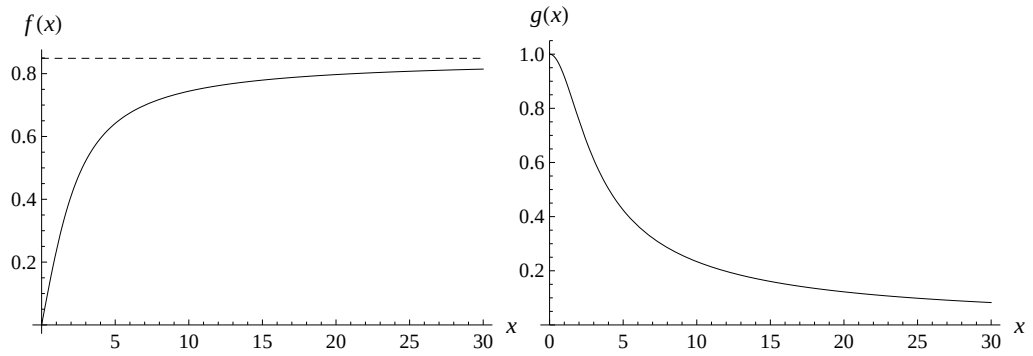


**Figure 5.8:** The functions (a) $f(x)$ and (b) $g(x)$ defined in equations (5.37) and (5.43) respectively. The dashed line in (a) represents the value $x = 8/3\pi$.

simplest route to be taken as any more complicated assumption would result in additional coupling constants to be considered.

Given this approximation, the problem of finding $\alpha$ in the experimenter's black box system is reduced to finding the first Fourier coefficient $b_1$:

$$b_1 = \frac{1}{\pi}\int_{-\pi}^{\pi} \mathrm{d}\delta \, \langle \sin(\theta_j - \theta_{j-1}) \rangle \sin(\delta). \tag{5.35}$$

This integral cannot be done analytically but has some simple properties. The final result is expressed in terms of a function defined by the integral:

$$\tilde{\alpha} = \alpha f\left(\frac{4\mu\alpha}{\sigma^2}\right), \tag{5.36}$$

where $f$ is defined by

$$f(x) = \frac{1}{\pi}\int_{-\pi}^{\pi} \mathrm{d}\delta \, \sin(\delta) \sin\left(\frac{\delta}{2}\right) \frac{I_1\left(x\cos\left(\frac{\delta}{2}\right)\right)}{I_0\left(x\cos\left(\frac{\delta}{2}\right)\right)}. \tag{5.37}$$

$f$ is plotted in figure 5.8a. As $I_1$ is odd, $f(0) = 0$. The function asymptotes to the value $8/3\pi$, and is always less than one. Equation (5.36) describes the renormalisation group flow of the quantity $\alpha$, in particular how it is coupled to the other parameters undergoing renormalisation.

Now the experimenter measures the variance of the force on a boundary rotor. The average of the squared force is given by

$$\langle (\mu(\dot{\theta}_j - \dot{\theta}_{j-1}) + \alpha \sin(\theta_j - \theta_{j-1}))^2 \rangle = \langle \mu^2 \dot{y}^2 \rangle + \langle \alpha^2 \sin^2(y + \delta/2) \rangle, \tag{5.38}$$

due to the decoupling of position and momentum degrees of freedom at equilibrium. The mean square frictional force is given by

$$\begin{aligned}\langle \mu^2 \dot{y}^2 \rangle &= \frac{\mu^2}{Z_{\dot{y}}} \int_{-\infty}^{\infty} \mathrm{d}\dot{y}\, \dot{y}^2 \exp\left(-\frac{\mu \dot{y}^2}{\sigma^2}\right) \\ &= \frac{\mu \sigma^2}{2}.\end{aligned} \tag{5.39}$$

The mean square conservative force is calculated as follows:

$$\begin{aligned}\langle \alpha^2 \sin^2(\theta_j - \theta_{j-1}) \rangle &= \langle \alpha^2 \sin^2(y + \delta/2) \rangle \\ &= \frac{\alpha^2}{Z_y} \int_0^{2\pi} \mathrm{d}y \, \exp\left(\frac{4\alpha\mu}{\sigma^2} \cos\left(\frac{\delta}{2}\right)\right) \frac{1}{2} \left(1 - \cos(2y + \delta)\right) \\ &= \frac{\alpha^2}{Z_y} \int_0^{2\pi} \mathrm{d}y \, \exp\left(\frac{4\alpha\mu}{\sigma^2} \cos\left(\frac{\delta}{2}\right)\right) \\ &\qquad \times \frac{1}{2} \left[1 - \cos(2y)\cos(\delta) + \sin(2y)\sin(\delta)\right].\end{aligned} \tag{5.40}$$

The sine term again gives an odd integrand so its contribution vanishes, while the term involving $\cos(2y)$ results in another modified Bessel function [75]:

$$\langle \alpha^2 \sin^2(\theta_j - \theta_{j-1}) \rangle = \frac{\alpha^2}{2} \left[1 - \cos(\delta) \frac{I_2\left(x \cos\left(\frac{\delta}{2}\right)\right)}{I_0\left(x \cos\left(\frac{\delta}{2}\right)\right)}\right]. \tag{5.41}$$

This quantity and $\langle \sin(\theta_j - \theta_{j-1}) \rangle^2$ are dependent on the relative angle of the boundary rotors $\delta$, but we require the stochastic force to be independent of the state of the system at all times. Referring again to the thought experiment above, it is reasonable that the experimenter may simply average over all the results that they obtain at different angles. The final answer for the variance in the coarse grained system is

$$\tilde{\sigma}^2 = \sigma^2 + \frac{\mu\sigma^2}{2} + \frac{\alpha^2}{2} g\left(\frac{4\mu\alpha}{\sigma^2}\right), \tag{5.42}$$

where the function $g$ is defined by

$$g(x) = \frac{1}{2\pi} \int_{-\pi}^{\pi} \mathrm{d}\delta \left[1 - \cos(\delta) \frac{I_2\left(x \cos\left(\frac{\delta}{2}\right)\right)}{I_0\left(x \cos\left(\frac{\delta}{2}\right)\right)} - 2\sin^2\left(\frac{\delta}{2}\right) \frac{I_1^2\left(x \cos\left(\frac{\delta}{2}\right)\right)}{I_0^2\left(x \cos\left(\frac{\delta}{2}\right)\right)}\right]. \tag{5.43}$$

$g$ is shown in figure 5.8b. It is easy to show that $g(0) = 1$, and it can be seen from the graph that $g$ is a decreasing function.

### 5.5.2 The moving rotor experiment at high shear rates

In this experiment, the boundary rotors are given a constant nonzero relative velocity. Instead of $\theta_{j+1} - \theta_{j-1} = \delta$ as in the previous section, $\theta_{j+1} - \theta_{j-1} = 2ut$ where $u$ is the local shear rate. The zero of time has been chosen so that $\theta_{j-1}$ and $\theta_{j+1}$ are both parallel to the zero angle line at $t = 0$. If $u$ is large enough, simulation and intuition indicate that the three rotors will be in a situation of uniform flow, so that the middle rotor lies in between the two outer rotors on average. The deviation from this average condition is given by $y(t)$, which is assumed to be non-increasing on average so as to fulfil the expectation of uniform flow. $y$ is written as $a_0 + \Delta(t)$, where $a_0$ is a constant and $\bar{\Delta} = 0$, where the bar denotes the time average. $\Delta$ and its time derivative $\dot{\Delta}$ are assumed to be small in order to make the equation of motion tractable. This approximation will fail at low shear rates where we might expect the middle rotor to climb slowly up its potential barrier and quickly accelerate down the other side, before oscillating in its new minimum for an appreciable amount of time. This failure will be seen in the results obtained below. The stipulation that rotor $j$ is stationary on average implies that $\bar{\dot{\Delta}} = 0$, where the bar denotes the time average.

For high enough shear rates it is assumed that the thermal noise will have a negligible impact on the physics involved and so we solve for the motion of $j$ in the zero temperature case. Substituting all of this into equation (5.23), performing the same manipulations as in the previous section, and linearising with respect to $\Delta$ gives the equation of motion

$$\begin{aligned}\ddot{\Delta} =&\alpha(\sin(ut - a_0) + \sin(-ut - a_0)) - \alpha(\cos(ut - a_0) + \cos(-ut - a_0))\Delta(t) \\ &+ h(u) + h(-u) - (h'(u) + h'(-u))\dot{\Delta}(t),\end{aligned} \tag{5.44}$$

where $h'$ is the derivative of $h$. We will assume that $h$ is an odd function, as befits a frictional force, which means that $h(u) + h(-u) = 0$ and $h'(u) + h'(-u) = 2h'(u)$.

In the steady state we expect $\Delta(t)$ to be periodic in time, so it is expanded in Fourier series with complex coefficients $a_n$:

$$\Delta(t) = \sum_n a_n e^{inut}. \tag{5.45}$$

As $\Delta$ is an angle, the coefficients incur restrictions that force $\Delta$ to be real, namely

$a_{-n} = a_n^*$. In addition, the zero frequency mode is assumed to be absent; any part of $\Delta$ with a non zero time average is absorbed into the quantity $a_0$. The series is truncated at the first harmonic in order to give a solvable equation:

$$\Delta(t) = ae^{iut} + a^* e^{-iut}, \tag{5.46}$$

where $a \equiv a_1$. The sine and cosine terms are simplified with standard trigonometric identities: $\sin(A+B)+\sin(A-B) = 2\sin(A)\cos(B)$, and $\cos(A+B)+\cos(A-B) = 2\cos(A)\cos(B)$. The product of $\cos(ut)$ and $\Delta(t)$ is found by writing the cosine as a sum of two exponentials, multiplying the exponentials together and dropping any second harmonic terms to be consistent with the truncated Fourier expansion. The equation of motion then becomes

$$\begin{aligned} -u^2(ae^{iut} + a^* e^{-iut}) = -2\alpha\sin(a_0)\cos(ut) - 2\alpha\cos(a_0)\Re(a) \\ - 2iug'(u)(ae^{iut} - a^* e^{-iut}). \end{aligned} \tag{5.47}$$

From here we equate the coefficients of linearly independent terms, giving three equations:

$$0 = -2\alpha\cos(a_0)\Re(a), \tag{5.48a}$$

$$u^2 a = \alpha\sin(a_0) + 2iuh'(u)a, \tag{5.48b}$$

$$u^2 a^* = \alpha\sin(a_0) - 2iuh'(u)a^*. \tag{5.48c}$$

Solving the latter two equations for $\Re(a)$ and $\Im(a)$ in terms of $a_0$ gives

$$\Re(a) = \frac{\alpha\sin(a_0)}{u^2 + 4h'(u)^2}, \tag{5.49a}$$

$$\Im(a) = \frac{2\alpha h'(u)\sin(a_0)}{u(u^2 + 4h'(u)^2)}. \tag{5.49b}$$

This solution for $\Re(a)$ is used in the remaining equation to get the solution for $a_0$: $\cos(a_0)\sin(a_0) = 0$, which means that

$$a_0 = \frac{m\pi}{2} \tag{5.50}$$

where $m$ is an integer.

Depending on the choice of $m$, there are two qualitatively different solutions to the equations. For $m$ odd, $\sin(a_0) = \pm 1$ leading to nonzero $\Re(a)$ and $\Im(a)$, whereas for $m$ even, $\sin(a_0) = 0$ leading to $\Re(a) = \Im(a) = 0$. In the first case the motion of the middle rotor has some fluctuations about its average path but in the other there are none at all. The two solutions are as follows:

$$\theta_{\text{odd}}(t) = \frac{m\pi}{2} + \frac{\alpha \sin(\frac{m\pi}{2})}{u(u^2 + 4h'(u)^2)}[u\cos(ut) - 2h'(u)\sin(ut)], \tag{5.51a}$$

$$\theta_{\text{even}}(t) = \frac{m\pi}{2}, \tag{5.51b}$$

for $m$ odd and even respectively.

After linearisation and neglecting second harmonic terms, the force exerted on rotor $j-1$ by rotor $j$ for these two solutions is

$$\begin{aligned}\Sigma_{\text{odd}}(t) = \alpha \sin\Big(\frac{m\pi}{2} + ut\Big) + \frac{2\alpha^2 h'(u)}{u(u^2 + 4h'(u)^2)} \\ + h(u) - \frac{2h'(u)\alpha \sin(\frac{m\pi}{2})}{u^2 + 4h'(u)^2}[u\sin(ut) + 2h'(u)\cos(ut)],\end{aligned} \tag{5.52a}$$

$$\Sigma_{\text{even}}(t) = \alpha \sin(m\pi + ut) + h(u). \tag{5.52b}$$

There is no obvious reason to choose one solution over the other, so the final results are given using an average over both. If we assume that the middle rotor will visit both solutions due to some neglected fluctuations, then we may write the relevant quantities as a weighted average over the result from each solution. The weighting is expressed via a new parameter $w$ which lies between zero and one.

The force felt as a result of uniform motion of the two outer rotors varies with time as well as shear rate (the relative velocity in the coarse grained system). However, the black box experiment stipulates that the friction should only depend on relative velocity; the natural course of action is simply to average over time. The time averaged force exerted on $j-1$ from its right hand side is

$$\begin{aligned}\bar{\Sigma} &= w\bar{\Sigma}_{\text{odd}} + (1-w)\bar{\Sigma}_{\text{even}} \\ &= h(u) + w\frac{2\alpha^2 h'(u)}{u(u^2 + 4h'(u)^2)} \\ &= \tilde{h}(u).\end{aligned} \tag{5.53}$$

As $h$ is an odd function, the friction felt by the rotors in the coarse grained system is

also odd as expected. Performing the same calculation for the other boundary rotor $j+1$ would result in the negative of this expression. The second term of the second equality in equation (5.53) diverges as $u \to 0$, a manifestation of the low shear rate problem noted at the start of the section.

**Validity of the high shear rate approximation**

It is important to have a better idea of where the current approximation breaks down. There is no hard and fast rule as to exactly which shear rates are covered by the approximation, but it was derived assuming that $\Delta(t)$ is small meaning that the Fourier coefficients should be small. This is used as a rough guide to the validity of the solution. The maximum value of $\Delta$ is

$$\max(\Delta) = 2|a| \quad = \frac{\alpha}{u\sqrt{u^2 + 4h'(u)^2}}, \tag{5.54}$$

so the corresponding condition is:

$$\frac{\alpha}{u\sqrt{u^2 + 4h'(u)^2}} < 1. \tag{5.55}$$

### 5.5.3 The moving rotor experiment at low shear rates

The calculation in the previous section is not appropriate for low shear rates, so in order to probe this regime a new approach is needed. The stochastic force is reinstated, and the friction force expressed as a linear function again; for low enough shear rates any differentiable odd function $h$ can be approximated by a straight line through the origin. Using the same prescription for $\theta_{j+1}$ and $\theta_{j-1}$ as in the previous section, the equation of motion is

$$\ddot{y} = -2\alpha\cos(ut)\sin(y) - 2\mu\dot{y} + \eta. \tag{5.56}$$

This stochastic differential equation in the overdamped limit is equivalent to a Smoluchowski equation:

$$\frac{\partial\rho}{\partial t} = \frac{1}{2\mu}\frac{\partial}{\partial y}[2\alpha\cos(ut)\sin(y)\rho] + \frac{\sigma^2}{4\mu^2}\frac{\partial^2\rho}{\partial y^2}, \tag{5.57}$$

where $\rho(y;t)$ is the probability density function for $y$ at time $t$. The aim is to solve for $\rho$ and use it to average over the behaviour of $y$.

The long term behaviour of $\rho$ should be periodic in time, and $\rho$ must always be periodic in $y$ due to the nature of the system. $\rho$ is therefore expanded in a two dimensional Fourier series:

$$\rho(y;t) = \sum_{m,n} a_{m,n} e^{imy} e^{inut} \tag{5.58}$$

With this expansion, the Smoluchowski equation can be turned into an infinite set of coupled algebraic equations for the $a_{m,n}$:

$$inua_{m,n} = m\frac{\alpha}{4\mu}(a_{m-1,n-1} + a_{m-1,n+1} - a_{m+1,n-1} - a_{m+1,n+1}) - m^2\frac{\sigma^2}{4\mu^2}a_{m,n}. \tag{5.59}$$

Some properties of $a_{m,n}$ can be determined from the properties of $\rho(y;t)$. First, at every point in time $\rho$ must be normalised:

$$\int_0^{2\pi} \mathrm{d}y\, \rho(y;t) = 1 \quad \forall t, \tag{5.60}$$

which leads to $a_{0,n} = 0$ for $n \neq 0$ and $a_{0,0} = 1/2\pi$. Second, $\rho$ must be real; taking the complex conjugate of the expansion (5.58) reveals that $a^*_{m,n} = a_{-m,-n}$. Third, $\rho$ is even in $y$; changing the sign of $y$ in equation (5.58) gives $a_{m,n} = a_{-m,n}$.

Solving the infinite set of equations (5.59) is very difficult, so the Fourier series is truncated again. The simplest nontrivial approximation is to restrict $m$ and $n$ to the values 0, +1 and -1. This gives nine linear equations to be solved, but with the help of the constraints on the coefficients the solution can be obtained easily by hand. The coefficients are:

$$a_{0,0} = \frac{1}{2\pi}, \tag{5.61a}$$

$$a_{1,1} = a_{-1,1} = \frac{\alpha}{8\pi\mu}\left(\frac{\sigma^2}{4\mu^2} + iu\right), \tag{5.61b}$$

$$a_{-1,-1} = a_{1,-1} = \frac{\alpha}{8\pi\mu}\left(\frac{\sigma^2}{4\mu^2} - iu\right), \tag{5.61c}$$

$$a_{0,1} = a_{0,-1} = a_{1,0} = a_{-1,0} = 0. \tag{5.61d}$$

The final result for $\rho(y;t)$ is

$$\rho(y;t) = \frac{1}{2\pi} + \frac{\mu\alpha}{2\pi(\sigma^4 + 16\mu^4u^2)}[(\sigma^2 - 4i\mu^2u)e^{iy}e^{iut} + (\sigma^2 + 4i\mu^2u)e^{iy}e^{-iut} + (\sigma^2 - 4i\mu^2u)e^{-iy}e^{iut} + (\sigma^2 + 4i\mu^2u)e^{-iy}e^{-iut}]. \quad (5.62)$$

The average force felt by rotor $j-1$ is as follows:

$$\begin{aligned}\langle\alpha\sin(\theta_j - \theta_{j-1})\rangle &= \langle\alpha\sin(y+ut)\rangle \\ &= \alpha\int_0^{2\pi} \mathrm{d}y\ \sin(y+ut)\rho(y;t).\end{aligned} \quad (5.63)$$

Using the solution for $\rho$ and noting that only terms constant in $y$ will survive the integration over a period, the average force is

$$\begin{aligned}\langle\alpha\sin(\theta_j - \theta_{j-1})\rangle &= 2\pi\alpha\Im(a_{-1,-1}) \\ &= \frac{4\mu^3\alpha^2u}{\sigma^4 + 16\mu^4u^2}.\end{aligned} \quad (5.64)$$

As this is the low shear rate regime, the above force is linearised in $u$ to obtain a constant friction coefficient. To get the friction in the experimenter's coarse grained system we must add the force due to the motion of the rotor which is simply $\mu u$. The final result for the low shear rate friction coefficient in the coarse grained system is

$$\tilde{\mu} = \mu + \frac{4\alpha^2\mu^4}{\sigma^4}. \quad (5.65)$$

The same calculation incorporating higher harmonics can be carried out, but the expressions involved rapidly become more complicated. If second harmonics are included then the average force is qualitatively the same but algebraically speaking significantly more complicated. In addition to this it results in unphysical behaviour for a region of parameter space that is expected to be covered by the approximations. The reason for this is unknown, but may be related to the behaviour of the different approximations in effective medium theory. In figure 5.2 the stress in the second harmonic approximation shows an unphysical divergence at low shear rates. As in the the present work, the second harmonic case is qualitatively different from the first. In addition to this, the third harmonic approximation for effective medium theory shows the same low shear rate behaviour as the first. This suggests

that, as sometimes the case with a non-rigourous approach such as this, that the simple perturbation theories used in this chapter may not be improved upon by successively taking into account higher harmonics. Instead the results point to a qualitative difference between even and odd harmonic cases. Whether the harmonic approximation interact with the linearisation approximation is unknown.

**Validity of the low shear rate approximation**

Use of the Smoluchowksi equation assumes that there is little movement during the time the velocity of the rotor equilibrates. The equilibration time for the velocity is given roughly by the Smoluchowksi timescale $\mu^{-1}$. If the rotor is driven over its potential landscape too quickly, this will not give enough time for the velocity to relax. The rate at which the rotor is driven is the shear rate $u$, with a corresponding timescale $u^{-1}$. Alternatively, if the potential varies too rapidly in space, then the rotor will be constantly trying to adjust to a new environment as it moves along and again the velocity will not relax. The timescale associated with the potential is $1/\sqrt{\alpha}$. These conditions are expressed mathematically by

$$\frac{u}{\mu} < 1 \quad \text{and} \tag{5.66a}$$

$$\frac{\alpha}{\mu^2} < 1. \tag{5.66b}$$

## 5.6 The renormalisation group flow

The RG flow equations are summarised here for convenience:

$$\tilde{\alpha} = \alpha f\left(\frac{4\mu\alpha}{\sigma^2}\right), \tag{5.67a}$$

$$\tilde{\sigma}^2 = \sigma^2 + \frac{\mu\sigma^2}{2} + \frac{\alpha^2}{2} g\left(\frac{4\mu\alpha}{\sigma^2}\right), \tag{5.67b}$$

$$\tilde{h}(u) = \left(1 + \frac{4\alpha^2\mu^2}{\sigma^4}\right)\mu u \quad \text{for low shear rates, and} \tag{5.67c}$$

$$\tilde{h}(u) = h(u) + \frac{2w\alpha^2 h'(u)}{u(u^2 + 4h'(u)^2)} \quad \text{for high shear rates.} \tag{5.67d}$$

The definition of $\mu$ in the first two equations depends on the shear rate. At low shear rates, $\mu$ is taken to be the coefficient of friction at the appropriate level of coarse

graining following the flow in equation (5.67c). At high shear rates, the coefficient of friction is taken to be $h(u)/u$. As this will in general be dependent on the shear rate $u$, which is undesirable for the stochastic and conservative forces, the $u$ dependence is replaced by a stress dependence. When the experimenter measures the force in the moving rotor experiment they are measuring the stress in the system: $\tilde{h}(u) = \Sigma$. This relation is inverted for $u(\Sigma)$ to find $h(u)/u$ as a function of $\Sigma$.

The goal is to find the fixed points of these equations which will reveal how a homogeneous region of the rotor model behaves on a large scale. These are the points in parameter space where further coarse graining does not result in movement away from that point, so for example where $\tilde{\sigma} = \sigma$ (and similarly for the other quantities). The fixed point of $\alpha$ is simple to find: as $f$ is always less than one, at each iteration $\alpha$ is multiplied by a number less than one and so always approaches zero. A fixed point is denoted by $^*$, so that $\alpha^* = 0$. In the usual language, $\alpha$ is an irrelevant variable. Typically $\mu$ and $\alpha$ appear to converge to steady values within five iterations; these are assumed to be the fixed point values.

### 5.6.1 Low shear rate renormalisation group flow

First, it is assumed that $\alpha$, $\sigma^2$ and $\mu$ in the microscopic system are nonzero and finite. From inspection of equations (5.67b) and (5.67c), $\sigma^2$ and $\mu$ will never be lower than their starting values. This leads directly to $\sigma^{*2} = \infty$ as at each iteration $\sigma^2$ is multiplied by a factor larger than one. The flow equation for $\mu$ then says that it is always increasing, but on first glance it is unclear as to whether the increase results in an infinite value of $\mu$. As the term $4\alpha^2\mu^2/\sigma^4$ has both a decreasing term on the top and an increasing one on the bottom, it is reasonable to guess that $\mu$ instead asymptotes to a finite value; this is confirmed numerically. $\mu^*$ can apparently take on a continuum of values depending on the initial value of $\mu$.

The stability of these fixed points can be investigated by linearising the flows about the fixed point. As the fixed point of $\sigma^2$ is at infinity, I use the variable $z = 1/\sigma^2$ instead, for which the fixed point is zero. The low shear rate flows in

terms of $z$ can be found from equations (5.67b):

$$\tilde{\alpha} = \alpha f(4\mu\alpha z), \tag{5.68a}$$

$$\tilde{z} = \left[\frac{1}{z}\left(1+\frac{\mu}{2}\right) + \frac{\alpha^2}{2} g(4\mu\alpha z)\right]^{-1}, \tag{5.68b}$$

$$\tilde{\mu} = \mu(1 + 4\alpha^2\mu^2 z^2). \tag{5.68c}$$

The fixed point is given by $\alpha^* = 0$, $z^* = 0$ and $\mu^*$ a finite number. Small deviations in each direction $\delta\alpha$, $\delta z$ and $\delta\mu$ are introduced about the fixed point and the flow equations are linearised in these quantities. The parameters one iteration along from these starting values are:

$$\tilde{\alpha} = 0, \tag{5.69a}$$

$$\tilde{z} = \frac{\delta z}{1 + \mu^*/2}, \tag{5.69b}$$

$$\tilde{\mu} = \mu^* + \delta\mu. \tag{5.69c}$$

The first equation is a result of $\tilde{\alpha}$ being different from zero only by a term of order $\delta\alpha^2$. The second says that, as $\mu^*$ is nonzero, $z$ decreases back toward its fixed point of zero. The third says that the new value of $\mu$ is larger than the perturbed value, or in other words the fixed point is unstable. As this is true for any value of $\mu^*$, it confirms that any nonzero value of $\mu$ can be a fixed point for the flow as long as we start from an appropriate point in parameter space.

Shown in figures 5.9, 5.10 and 5.11 are different slices through the three dimensional parameter space spanned by $\alpha$, $\mu$ and $\sigma^2$ with flows of the parameters indicated. These graphs support the analysis above. $\alpha$ always decreases from its initial value and ends up at zero quite suddenly; when this happens, the renormalisation of $\alpha$ and $\mu$ is essentially over. The most striking feature is the values of $\mu^*$ generated. In figure 5.9, we see that even a modest initial value of $\mu$ can lead to an enormous value of $\mu^*$, of the order of $10^{24}$ for $\mu = 2$ at $\sigma^2 = 1$ for example. As $\mu$ acts like a viscosity, this implies that the coarse grained system will not support a shear under any sensible timescale for some initial parameters. This is qualitatively similar to the solid regions seen in the previous chapter which are stable for the entire duration of the simulation. A larger initial value of $\sigma^2$ reduces the value of

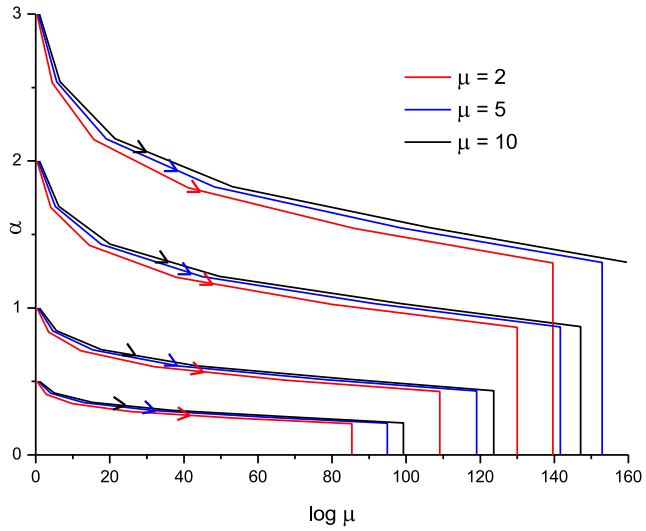


(a)

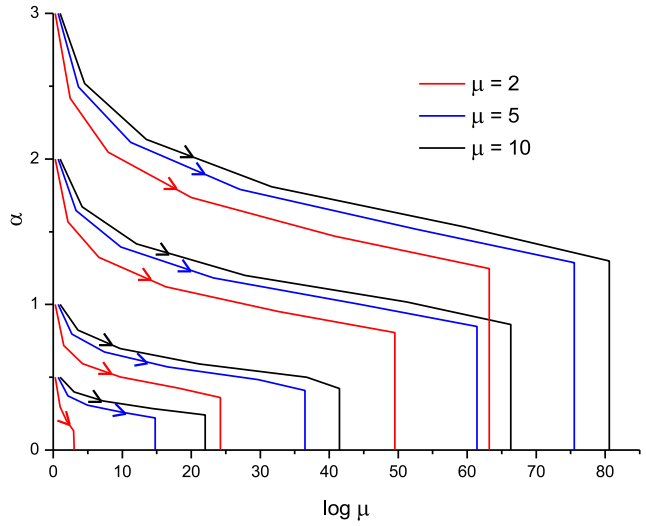


(b)

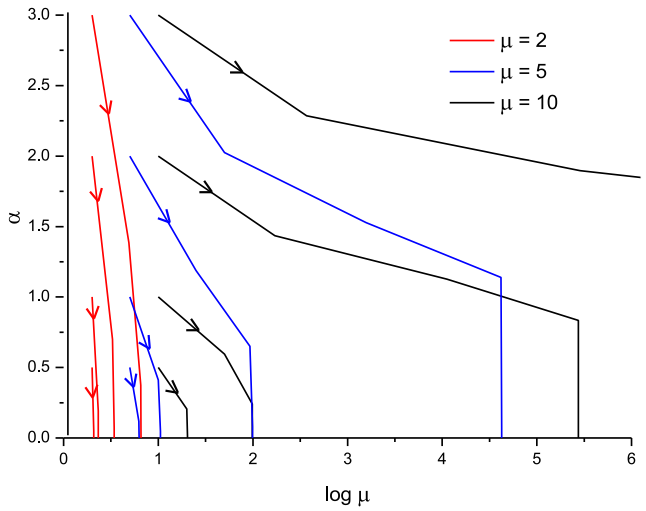


(c)

**Figure 5.9:** The low shear rate renormalisation group flow projected onto the $\alpha - \mu$ plane with initial values of $\sigma^2$ equal to (a) 0.1, (b) 1 and (c) 10. The flows start from $\alpha = 0.5$, 1, 2 and 3.

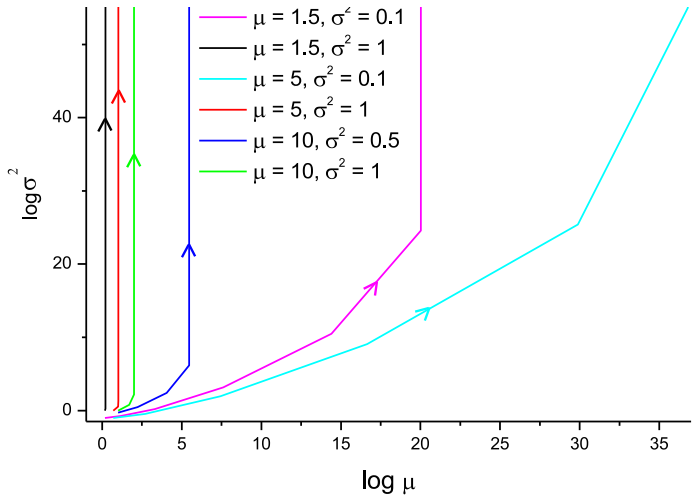


(a)

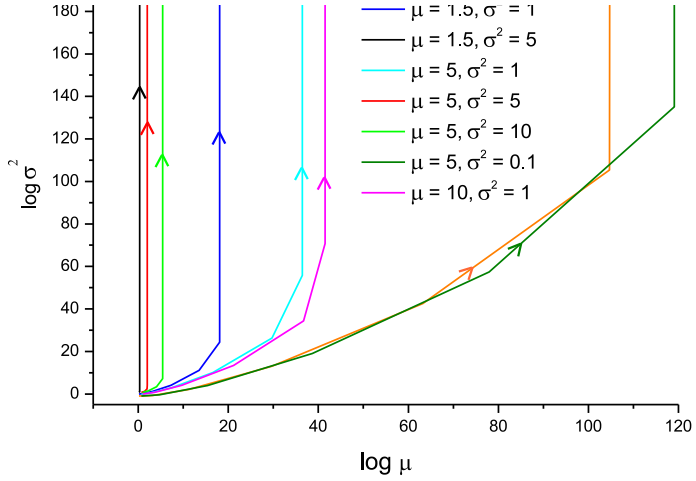


(b)

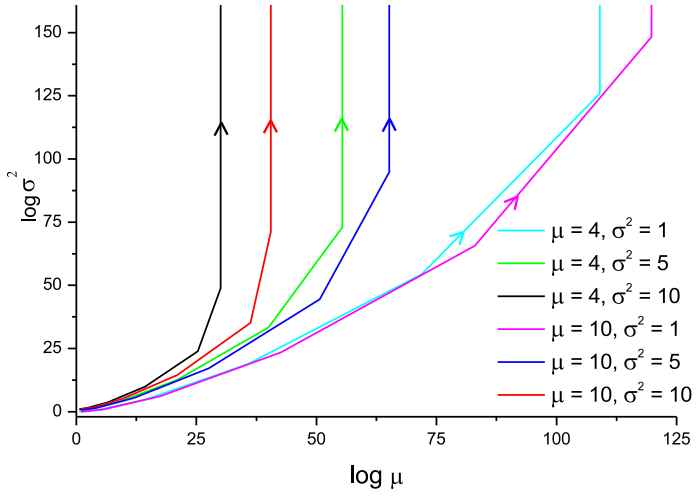


(c)

**Figure 5.10:** The low shear rate renormalisation group flow projected onto the $\sigma^2 - \mu$ plane with initial values of $\alpha$ equal to (a) 0.1, (b) 1 and (c) 10.

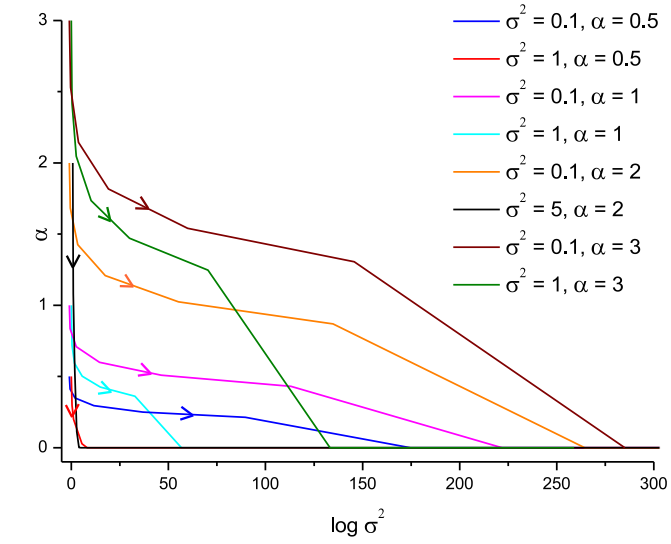


(a)

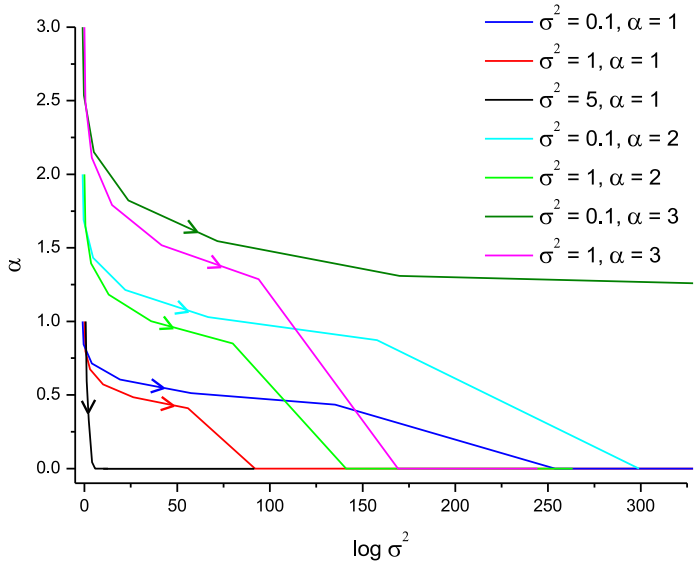


(b)

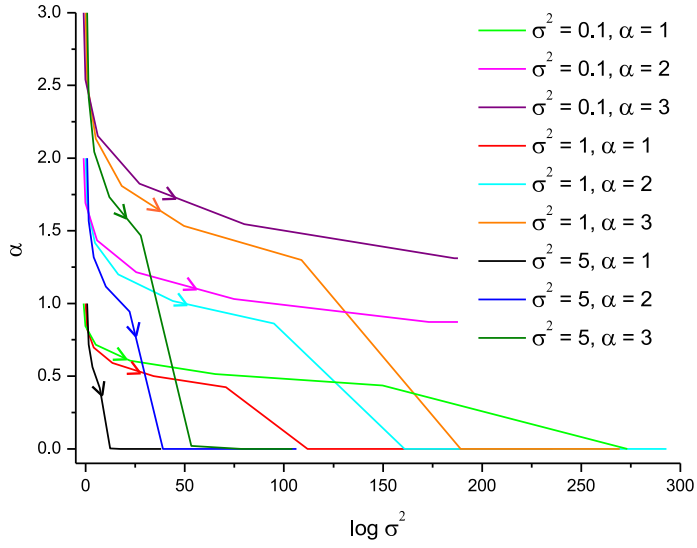


(c)

**Figure 5.11:** The low shear rate renormalisation group flow projected onto the $\alpha - \sigma^2$ plane with initial values of $\mu$ equal to (a) 2, (b) 5 and (c) 10.

$\mu^*$. Conversely, large initial values of $\sigma^2$ and small initial values of $\alpha$ can lead to more modest values of $\mu^*$, again in qualitative agreement with simulation where high temperatures destroy the solid regions.

The flows depicted are independent of the stress, although the shear rate at each iteration depends on the stress via $u = \Sigma/\mu$. Note that a lower value of $\Sigma$ brings different regions of the parameter space under the remit of the approximation. From the constraint on the local shear rate in equation (5.66a) and the constitutive relation in the linear regime, $\Sigma = \mu u$, $\mu$ is restricted to be greater than $\sqrt{\Sigma}$, so a lower stress leads to a greater region of parameter space accessible by the approximation.

If $\sigma^2$ is initially zero and $\alpha$ and $\mu$ are nonzero and finite, then the static rotor experiment will give $\sigma^2 = 0$ at any level of coarse graining; this then leads to a constant value of $\alpha$. The calculation performed for the moving rotor experiment is no longer valid at zero temperature, so the value of $\mu$ is unknown. This fixed point is unstable because, as noted above, any nonzero value of $\sigma^2$ no matter how small can only increase with the flow.

With regard to the validity of the approximation, note that if $\mu$ is increasing and $\alpha$ decreasing then the inequalities in (5.66) will continue to be met; that is, if the RG flow starts off in a region where the low shear rate approximation is valid, it will stay valid, so the fixed points found in this section are the correct ones for an initially low shear rate state. It should also be noted that the RG calculation requires at least a few iterations to converge, so that solid regions consisting of, for example, two slowly moving rotors are not really covered by the theory. This situation is seen at shear rates close to the transition to uniform flow, where the only locked pairs are isolated amongst many running pairs.

### 5.6.2 High shear rate renormalisation group flow

The flow of the frictional force at high shear rates is now the flow of $h(u)$ in function space. There is little help in finding the fixed point via the equations (5.67); setting $\alpha = \alpha^* = 0$ in equation (5.67d) just leads to $h^*(u) = h^*(u)$. Due to the relative complexity in determining the coefficient of friction in this regime it is difficult to make general statements about fixed points of the sort in the previous section. The function $h(u)$ does appear to reach a fixed point after a small number of iterations, although this can only be inferred by eye. Once the iteration process has started

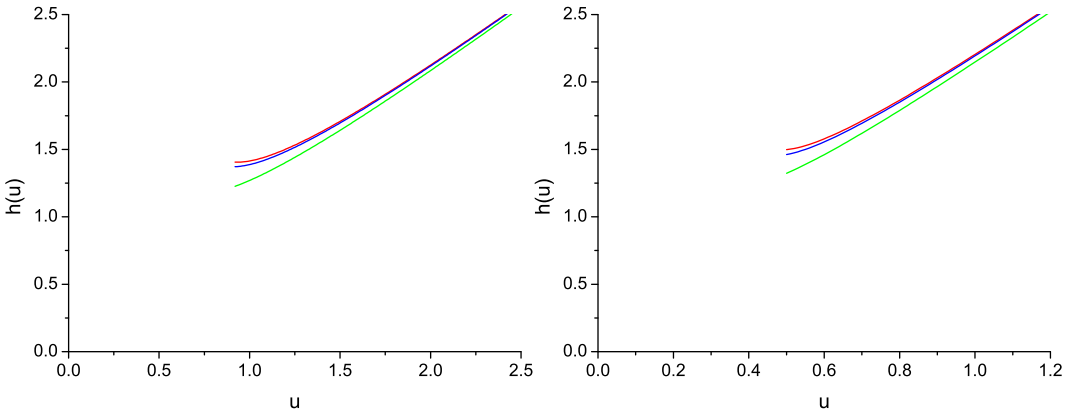


**(a)** $\mu = 1.0$ **(b)** $\mu = 2.0$

**Figure 5.12:** The RG fixed point of $h(u)$ for $\alpha = 1$. Different colours indicate different temperatures $k_BT$: red, 0.05; blue, 0.1; green 0.5.

the validity condition for this approximation, equation (5.55), must be taken into account. This leads to a cut-off for the theoretical curves at low shear rates. The available stresses give close to linear behaviour for most accessible shear rates, but often marked deviations from this as well.

Some examples of $h^*(u)$ are seen in figure 5.12. They were calculated using $\Sigma = 2$ but are very similar when calculated using other values of stress. All curves lie above the linear Newtonian curve but converge to it for high enough shear rates. The deviation at lower shear rates is most noticeable for the lower two temperatures shown, $k_BT = 0.05$ and 0.1. These appear to flatten out almost completely and could indicate the start of a region of negative slope or a plateau.

### 5.6.3 Interpretation and comparison to simulation

In general, the RG flows considered always result in a finite frictional force, an infinite temperature and zero potential at the fixed point; as previously noted, these fixed points should tell us something about the phases the model can exhibit. The finite but non-zero friction coefficient implies that the general behaviour of the model at the largest scales is viscous flow. The infinite temperature, similar to the infinite temperature fixed point in the Ising model studied earlier, indicates disorder: there is no structure in the flow visible at the macroscopic scale. This view is bolstered by the absence of a potential barrier. This simple situation is made more interesting in two ways. Firstly, the viscous flow seen may be so viscous as to be, for all practical purposes, no flow at all. Taking this into consideration, the model can show both

fluid-like and solid-like behaviour at the fixed point. Secondly, the calculation was performed for homogeneous flow only. If the flow is not homogeneous, as is often seen in simulation, the analysis does not apply, opening up the possibility for other behaviours not accounted for in the current approach.

The low shear rate RG calculation is restricted to parameters for which $\mu^2 > \alpha$. With the simulation value of $\alpha = 1$, this implies that $\mu > 1$ which is a region that was not investigated in simulation. However, the results presented show some interesting qualitative features, most promisingly the existence of extremely high viscosity states at low shear rates. The viscosities are so high that it would be very unlikely to see these very slowly moving rotors shear; although there is no overlap in this regime, the solid regions found in chapter 4 are indeed never seen to shear over the simulation timescale. The dependence of the flow on $\sigma^2$ indicates that a larger microscopic value of $\sigma^2$ leads to a reduced $\mu^*$, which would indicate less stable solid regions. This is seen in simulation, where from a situation with many locked rotor pairs, an increase in temperature leads to a smaller proportion of locked pairs.

Some discrepancies between theory and data exist for the low shear rate case. The stress independence of the low shear rate approximation means that these high viscosity states are predicted for high stresses which is not seen in the simulations. In general a higher microscopic value of $\mu$ gives a larger fixed point value $\mu^*$ (see for example figure 5.9), but simulations indicate that a larger value of $\mu$ destroys the high viscosity solid regions, the opposite of theory which would indicate that they instead become more stable. The detail missing in the theory could be the global situation, whereby an increase in $\mu$ at the same shear rate gives rise to a higher stress, meaning that if solid regions exist they must become smaller in order to spread the shear over more but slower rotor pairs. In this sense the intrinsic stability of the solid regions does increase but global constraints eliminate their existence independently of thermal fluctuations.

The high shear rate calculation again does not extend to many parameters used in simulation, although it does cover the relatively high stress regime where the local shear rate is high enough to suppress any fluctuations to a manageable level. The constitutive curve appears to always lie above the straight line Newtonian case, as in simulation. The curves shown in figure 5.13 were obtained for $\Sigma = 2.0$ but all the stresses tested gave very similar curves. Agreement with simulation is fairly

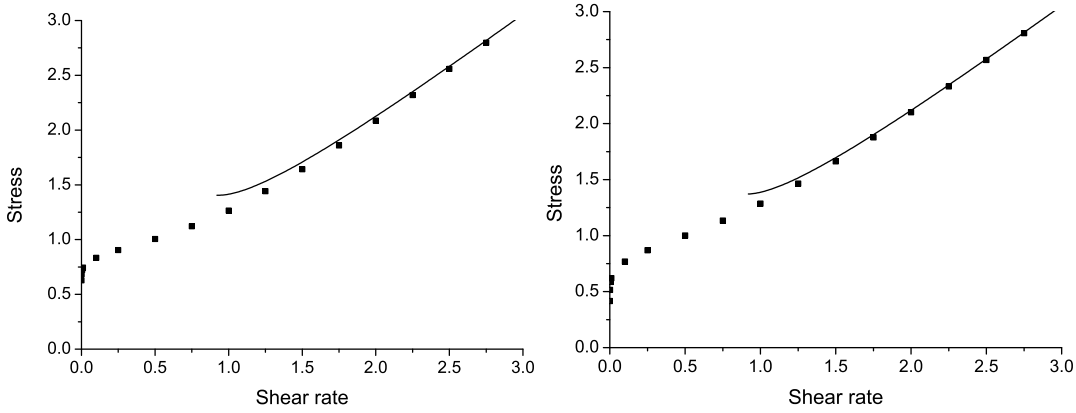


**(a)** $k_BT = 0.05$ **(b)** $k_BT = 0.1$

**Figure 5.13:** Theoretical (solid lines) and measured (data points) constitutive curves for $\mu = 1.0$ at two different temperatures. The theoretical calculations were performed at a stress of 2.

good, and gets slightly better with increasing temperature, but the theoretical curve levels out more quickly when approaching lower shear rates. This could be due to a non-monotonic region of the predicted constitutive curve, the bulk of which is not captured by the approximation, although it is currently not possible to determine if that is correct. The simulations do not seem to indicate inhomogeneous flow, as would be expected from a curve of that type.

The difference between theory and data may arise due to the neglect of some fluctuations in the RG approximation. In a true uniform flow situation, there will be many neighbouring rotors in relative rotation, sending out waves into the surrounding medium. Any particular pair would be perturbed at irregular intervals by these waves, leading to fluctuations that are not well described by a single frequency. This picture is supported by the better agreement at higher temperatures, for which the thermal noise could mimic the effects of the missing fluctuations. The fact that the approximation becomes more secure for higher friction coefficients also supports this interpretation, as this would lead to a more effective damping of perturbations meaning that fewer far away events would have a noticeable effect on the chosen pair. A temperature of 0.01, the lowest used in simulation, violated the validity condition for all parameters so an RG flow could not be determined.

The suggestion above that the flattening out of the low temperature curves could be the start of a region of negative slope seems unlikely once compared with the simulations; even at $\mu = 1.0$ the flow always appears to be uniform. However, there

is always the chance of some subtle inhomogeneity being present that is harder to detect.

## 5.7 Conclusions

In this chapter I have analysed the rotor model theoretically using three distinct but related approaches. The simplest is the effective medium theory of section 5.2, in which a single rotor pair that feels a constant average force from the other rotors is considered. The equation of motion for the relative angle of the pair was solved using an approximate harmonic expansion and a constitutive curve was produced. While being an analytically tractable approximation, solvable using pen and paper, the mean field assumption significantly underestimates the region of inhomogeneous flow.

In the next section I analysed the dynamics of an isolated running rotor pair surrounded by locked rotors, a situation seen in simulation at low shear rates, low temperature and low friction coefficient. A solution was found using a similar approximation as above, a harmonic expansion. The calculation resulted in constitutive curves for this situation and the decay length for the perturbations in the surrounding solid region. It is more difficult to compare these results with simulation, but the results indicate correctly that the situation is not stable for $\mu = 1$.

In the last part of this chapter I have performed a local nonequilibrium renormalisation group calculation for the rotor model. The calculation uses a decimation scheme in which I average over the dynamics of every other rotor, using different approximations for the averaging depending on the situtation, and further approximations in order to generate a recursion relation for the parameters of the model. The calculation yields the renormalisation group flow of the parameters $\alpha$, $\sigma^2$, $\mu$ at low shear rates and the full friction function $h(u)$ at high shear rates. A quantitative comparison of this calculation with simulation is mostly absent, as the typical simulation parameters are in a region of parameter space for which the theoretical approximations are unreliable. There is a small region of overlap in which I have calculated the theoretical constitutive curve for uniform flow at high shear rates and stresses; the agreement with simulation breaks down at the lowest shear rates available theoretically, but improves for higher shear rates and temperatures.

All the approximations used involved some kind of harmonic expansion, and all but the low shear rate RG calculation involved some linearisation of sinusoidal terms. In each case, the linearisation results in an inaccessible low shear rate regime, indicating that motion there is complicated and highly anharmonic.

# Chapter 6

# Conclusions and future work

In this thesis I have considered a variety of systems described by NCDB, namely boundary driven systems with a constrained current. The particular systems in this class ranged from completely general (chapter 3) to a specific numerical example (chapters 4 and 5).

In between these two cases was the more restricted class of athermal systems considered in chapter 2, which also served as an introduction to the NCDB formalism. There, I outlined how NCDB could be applied to sheared athermal systems and illustrated the concept for two toy models, one dimensional diffusion and the comb model. The analysis in that chapter drew on the work of Liu and Nagel and their putative jamming phase diagram in order to interpret the ordering of limits. I provided a further connection with the existing literature on athermal materials with an interpretation of yield stress in NCDB, and showed that under some assumptions the comb model can exhibit a yield stress.

The subsequent chapter was the most wide-ranging in this thesis. In it I outlined a general free energy formalism for boundary driven steady states based on the probability distribution of trajectories postulated in NCDB. The free energy density obtained is analogous to an equilibrium free energy density based on the distribution of microstates but is intensive in time as well as space. I first expressed the free energy in a rather formal way that explicitly uses the equilibrium current distribution; this is suitable for the simplest of models such as the diffusion model looked at, but may otherwise be difficult to apply in practice. I then derived an alternative expression that only requires knowledge of the equilibrium transition rates between microstates, and validated it through use of the comb model. The

formalism developed has strong connections to large deviation theory, a branch of mathematics now fairly commonplace in statistical physics.

The theory in both chapters 2 and 3 is illustrated using two simple noninteracting models, due to the complexity of real fluids and partly due to the relatively young theory. Future challenges in this direction would primarily involve addressing more complex models and developing approximate calculational techniques where necessary; one example has already been given at the end of chapter 3, that of a boundary driven simple exclusion process, that could give insight into interacting models in NCDB.

Moving away from fundamental theory, in chapters 4 and 5 I studied the rotor model, a one dimensional toy model that is designed to mimic a complex fluid. This simple one dimensional model exhibits unexpected behaviour such as the solid regions seen at low shear rate, temperature and coefficient of friction. Despite its apparent distance from any real fluid, the flow curves that are measured in simulation are remarkably similar to experimental flow curves for real complex fluids, that show non-Newtonian behaviour including the stress plateaus that are often seen in studies of shear banding fluids. The model also shows signs of a phase transition for small enough parameter values, with signatures in measured properties such as the flow curve and the variance of the internal energy.

Theoretically, the rotor model was approached in three ways: effective medium theory, the analysis of an isolated running pair of rotors, and via renormalisation group techniques. Each approach has successes and limitations. All of the approximations fail at low shear rates, bar the part of the RG calculation specifically designed for this regime. All but that one are restricted in parameter space due to the linearisation needed to make any headway theoretically; even the low shear rate RG calculation is restricted in parameter space, although for different reasons. A common theme emerges when looking at all of the techniques: the difficulty of accessing the high $\alpha$ (strongly interacting) regime, where "high" is relative to the coefficient of friction $\mu$. Unfortunately, this is where the most interesting behaviour was seen theoretically; future work would have to concentrate on cracking this area to give more insight into the phase behaviour of the model. Overall, the rotor model is a very interesting candidate for the study of boundary driven systems, nonequilibrium phase transitions and complex fluids.

Boundary driven fluids and athermal systems are commonplace in the real world and in the laboratory. This thesis has probed their underlying theoretical properties in order to help understand these important systems. While more work is needed in order to begin to apply the techniques discussed to real life situations, this has been a promising step forward along that path.

# Appendix A

# Transition rates in boundary driven systems

## A.1 The basic formulation of NCDB

This appendix gives a brief derivation of the transition rates in boundary driven systems according to the NCDB formalism; this derivation is adapted from the paper by Simha et al. [19]. The starting point is the distribution for trajectories in a subsystem of a large volume of sheared fluid, equation (2.6), and the definition of a transition rate:

$$\Omega_{ij} = \frac{p(x(t+\Delta t) = j | x(t) = i)}{\Delta t}, \tag{A.1}$$

where $x(t)$ denotes the microstate of the system at time $t$. $p(x(t+\Delta t) = j|x(t) = i)$ is the probability of being in state $j$ at time $t + \Delta t$ conditioned on the fact that it was found in state $i$ at the earlier time $t$. The precise time $t$ that we look at is immaterial as the rates are constant in the steady state, so the value of $t$ is chosen to be zero without loss of generality. A conditional probability $P(A|B)$ is defined in terms of a joint probability $P(A, B)$ via $P(A|B) = P(A, B)/P(B)$ for $P(B) \neq 0$. Given the distribution of trajectories, the probability of being in state $i$ at time 0, $p(x(0) = i)$, is obtained by summing over the probabilities of all the trajectories where $i$ appears at time 0. The probability $p(x(0) = i)$ is then

$$p_\tau(x(0) = i) = \sum_{\substack{\Gamma \\ \Gamma(0)=i}} p_\tau^{\mathrm{eq}}(\Gamma) e^{\nu\gamma(\Gamma)}, \tag{A.2}$$

where I have used the nonequilibrium trajectory distribution in equation (2.6) and used the notation $\Gamma(t)$ to denote the "value" of the trajectory $\Gamma$ at time $t$, that is, the microstate the system is in at that time if it follows trajectory $\Gamma$. The subscript $\tau$ is to remind us that the probabilities are evaluated using an ensemble of trajectories of length $\tau$. This is rewritten using a delta function to introduce an integral over $\gamma$:

$$p_\tau(x(0)=i) = \int_{-\infty}^{\infty} \mathrm{d}\gamma \sum_{\substack{\Gamma \\ \Gamma(0)=i}} p_\tau^{\mathrm{eq}}(\Gamma) e^{\nu\gamma} \delta(\gamma - \gamma(\Gamma)). \tag{A.3}$$

The constrained sum over $\Gamma$ now results in the joint probability of seeing a shear $\gamma$ at equilibrium and being in state $i$ initially:

$$\begin{aligned} \sum_{\substack{\Gamma \\ \Gamma(0)=i}} p_\tau^{\mathrm{eq}}(\Gamma)\delta(\gamma - \gamma(\Gamma)) &= p_\tau^{\mathrm{eq}}(\gamma, x(0)=i) \\ &= p_\tau^{\mathrm{eq}}(\gamma | x(0)=i) p_\tau^{\mathrm{eq}}(x(0)=i), \end{aligned} \tag{A.4}$$

where the definition of a conditional probability has been used again. The probability of the system being in microstate $i$ at time 0 and then being in microstate $j$ at time $\Delta t$, $p_\tau(x(\Delta t)=j, x(0)=i)$, is given by a similar sum over trajectories. In this case we need an extra constraint $\Gamma(\Delta t)=j$ in addition to $\Gamma(0)=i$, The result for the transition probability is then

$$\Omega_{ij} = \frac{\int_{-\infty}^{\infty} \mathrm{d}\gamma\, e^{\nu\gamma} p_\tau^{\mathrm{eq}}(\gamma | x(0)=i, x(\Delta t)=j) p_\tau^{\mathrm{eq}}(x(0)=i, x(\Delta t)=j)}{\Delta t \int_{-\infty}^{\infty} \mathrm{d}\gamma\, e^{\nu\gamma} p_\tau^{\mathrm{eq}}(\gamma | x(0)=i) p_\tau^{\mathrm{eq}}(x(0)=i)}. \tag{A.5}$$

The equilibrium rate $\omega_{ij}$ is hidden in there and may be factored out:

$$\omega_{ij} = \frac{p_\tau^{\mathrm{eq}}(x(0)=i, x(\Delta t)=j)}{\Delta t p_\tau^{\mathrm{eq}}(x(0)=i)}. \tag{A.6}$$

As the use of the driven ensemble is only valid in the limit of long trajectories, the limit of large $\tau$ is taken. The final answer is:

$$\Omega_{ij} = \omega_{ij} \lim_{\tau\to\infty} \frac{\int_{-\infty}^{\infty} \mathrm{d}\gamma\, e^{\nu\gamma} p_\tau^{\mathrm{eq}}(\gamma | x(0)=i, x(\Delta t)=j)}{\int_{-\infty}^{\infty} \mathrm{d}\gamma\, e^{\nu\gamma} p_\tau^{\mathrm{eq}}(\gamma | x(0)=i)}. \tag{A.7}$$

So the driven rates are proportional to the equilibrium rates, with the constant of proportionality being a function of the driving strength $\nu$ and dependent on the equilibrium statistics only. Since the equilibrium rates are constrained by detailed

balance, the driven rates likewise must obey the same number of pairwise constraints. This is the nonequilibrium counterpart to detailed balance. In this derivation, the underlying hypothesis is the expression for the nonequilibrium trajectory distribution, equation (2.6); if that is valid for the system in question, then the mathematics necessarily leads us to the above conclusion.

## A.2 An alternative formulation of NCDB

The expression for the driven rates derived above can be put into a more physically readable form. The derivation here is adapted from Appendix B of the paper of Evans [18]; as I will only be concerned with systems in continuous time I omit details related to discrete time models.

The equilibrium probability that appears in the numerator of equation (A.7) can be rewritten as $p^{\rm eq}_{\tau-\Delta t}(\gamma - K_{ij}|x(0)=j)$, where $K_{ij}$ is the integrated current gained from the transition $i \to j$. This is the probability of acquiring the integrated current $\gamma - K_{ij}$ in the time $\tau - \Delta t$, starting from state $j$. This equality holds because if the system has to make the transition $i \to j$ at the start of the trajectory then it has gained the integrated flux $K_{ij}$ associated with that transition, and must make up the rest of the total $\gamma$ in the remainder of the trajectory. The numerator and denominator now take on similar forms:

$$\Omega_{ij} = \omega_{ij} \lim_{\tau\to\infty} \frac{\int_{-\infty}^{\infty} {\rm d}\gamma\, e^{\nu\gamma} p^{\rm eq}_{\tau-\Delta t}(\gamma - K_{ij}|x(0)=j)}{\int_{-\infty}^{\infty} {\rm d}\gamma\, e^{\nu\gamma} p^{\rm eq}_{\tau}(\gamma|x(0)=i)}. \tag{A.8}$$

Shifting the integration variable in the numerator by $K_{ij}$ gives:

$$\Omega_{ij} = \omega_{ij} e^{\nu K_{ij}} \lim_{\tau\to\infty} \frac{\int_{-\infty}^{\infty} {\rm d}\gamma\, e^{\nu\gamma} p^{\rm eq}_{\tau-\Delta t}(\gamma|x(0)=j)}{\int_{-\infty}^{\infty} {\rm d}\gamma\, e^{\nu\gamma} p^{\rm eq}_{\tau}(\gamma|x(0)=i)}. \tag{A.9}$$

For large enough $\tau$, $p^{\rm eq}_{\tau-\Delta t}(\gamma|x(0)=j) \approx p^{\rm eq}_{\tau}(\gamma|x(0)=j)$. Defining $e^{q_i(\nu)} = \lim_{\tau\to\infty}\int_{-\infty}^{\infty} {\rm d}\gamma\, e^{\nu\gamma} p^{\rm eq}_{\tau}(\gamma|x(0)=j)$, the rates are written as

$$\Omega_{ij} = \omega_{ij} e^{\nu K_{ij} + q_j(\nu) - q_i(\nu)}. \tag{A.10}$$

The $q_i$ are factors that enhance or suppress the transition according to whether it is likely to yield a larger flux in the future.

# Appendix B

# Simulation method for the rotor model

The algorithm used to simulate the rotor model was one devised for use in dissipative particle dynamics (DPD) by Groot and Warren [76]. It is based on the velocity Verlet algorithm [77, 78], commonly used for conservative systems, where the positions $\mathbf{r}(t)$ and the velocities $\mathbf{v}(t)$ are updated as follows:

$$\begin{aligned} \mathbf{r}(t+\delta t) &= \mathbf{r}(t) + \delta t \mathbf{v}(t) + \frac{1}{2}\delta t^2 \mathbf{a}(\mathbf{r}(t)), \\ \mathbf{v}(t+\delta t) &= \mathbf{v}(t) + \frac{1}{2}\delta t[\mathbf{a}(\mathbf{r}(t)) + \mathbf{a}(\mathbf{r}(t+\delta t))], \end{aligned} \tag{B.1}$$

where $\delta t$ is the timestep used and $\mathbf{a}$ is the acceleration of the system's component parts. In the numerical analysis literature this is known as a predictor-corrector method, as the expression for $\mathbf{v}(t+\delta t)$ uses data from the next timestep in the form of $\mathbf{a}(\mathbf{r}(t+\delta t))$. This can be derived by discretising Newton's second law and using the central difference approximation for the second time derivative.

In the case of DPD and the rotor model, this algorithm cannot be applied as the force and thus the acceleration at any time depends on the velocities at that time as well as the positions. In order to overcome this, an estimate $\tilde{\mathbf{v}}$ for the velocities at the next timestep is made so that the force can be computed:

$$\begin{aligned} \mathbf{r}(t+\delta t) &= \mathbf{r}(t) + \delta t \mathbf{v}(t) + \frac{1}{2}\delta t^2 \mathbf{a}(\mathbf{r}(t), \mathbf{v}(t)), \\ \tilde{\mathbf{v}}(t+\delta t) &= \mathbf{v}(t) + \lambda \delta t \mathbf{a}(\mathbf{r}(t), \mathbf{v}(t)), \\ \mathbf{v}(t+\delta t) &= \mathbf{v}(t) + \frac{1}{2}\delta t[\mathbf{a}(\mathbf{r}(t), \mathbf{v}(t)) + \mathbf{a}(\mathbf{r}(t+\delta t), \tilde{\mathbf{v}}(t+\delta t))]. \end{aligned} \tag{B.2}$$

$\lambda$ is an empirical factor that is supposed to account for effects of the stochastic terms that appear in $\mathbf{a}$, and in the present work is set to 1/2.

The DPD algorithm was modified slightly for the present work by including a variable timestep. The distance the rotors were allowed to move in a single iteration was restricted to some number $c$. At each step, if the rotor velocities were such that an iteration at the current value of the timestep would result in one or more rotor pairs moving through a relative angle of $c$ or more, then the timestep was reduced and the step tried again. This addition ensures that rotors moving at a high speed will not miss the potential barriers between minima which could affect the dynamics. Experimentation with the value of $c$ revealed that the system was mostly insensitive to its precise value unless it became too large; for all the simulations quoted in this thesis it was set equal to 0.1. Unfortunately this leads to very slow simulations at high shear rates and temperatures, where rotors are often moving very fast. As a result this region was not investigated as thoroughly as lower temperatures and shear rates.

# Appendix C

# Equations of motion for an isolated running rotor pair

This appendix deals with the approximate solution to the equations outlined in section 5.3. In solving the equations we may concentrate on one side of the infinite chain only; here I choose to look at $j \geq 0$. Using the equations of motion (5.11) and the linearisation in equation (5.14), the equations to solve may be written as:

$$-s^2 a_1^0 = c(a_1^1 + a_1^{-1}) + ie^{ia_0^0} + i\mu s(a_1^1 + a_1^{-1} - 2a_1^0), \tag{C.1}$$

$$-s^2 a_1^1 = c(a_1^2 - 2a_1^1) - \frac{1}{2}ie^{ia_0^0} + i\mu s(a_1^0 - 2a_1^1 + a_1^2), \tag{C.2}$$

$$-s^2 a_1^j = (c + i\mu s)(a_1^{j-1} - 2a_1^j + a_1^{j+1}), \quad j \neq 0, \pm 1. \tag{C.3}$$

The last equation describes the bulk of the chain. It is a discrete wave equation, so a travelling wave solution is tried:

$$a_1^j = (Re^{ik})^j \tag{C.4}$$

Substitution into equation gives a second order difference equation that can be reduced to a quadratic equation in $Re^{ik}$ with two solutions:

$$Re^{ik} = 1 - \frac{s^2(c - i\mu s)}{2(c^2 + \mu^2 s^2)} \pm \frac{s(c - i\mu s)}{2(c^2 + \mu^2 s^2)}(q_1 - iq_2), \tag{C.5}$$

where $q_1$ and $q_2$ are given by:

$$q_{1,2} = \frac{1}{2}\sqrt{\sqrt{(s^2-4c)^2+16\mu^2 s^2} \pm s^2 - 4c}. \tag{C.6}$$

The two solutions are inverses and describe waves travelling in different directions. Infinitely far away from the middle of the chain, the disturbances must decay to zero, and only one of these waves satisfies this. The other is the solution for the other side of the chain. The general solution for $a_1^j$ in the bulk of the chain is given by $A(Re^{ik})^j$, where $A$ is a complex constant determined by matching up with the solution at the centre of the chain. The equations are solved for the real and imaginary parts of $A$, $a_1^0$ and $a_1^1$ in terms of $\mu$, $s$ and $c$.

# Bibliography


[1] A. A. Migdal. Phase transitions in gauge and spin-lattice systems. *Journal of Experimental and Theoretical Physics*, 69:1457, 1975.

[2] L. P. Kadanoff. Scaling laws for ising models near $T_c$. *Physics*, 2:263, 1966.

[3] L. P. Kadanoff. Notes on Migdal's recursion formulas. *Annals of Physics*, 100:359, 1976.

[4] M. S. Green. Markoff random processes and the statistical mechanics of time dependent phenomena. II. Irreversible processes in fluids. *Journal of Chemical Physics*, 22:398, 1954.

[5] R. Kubo. Statistical-mechanical theory of irreversible processes. i. general theory and simple applications to magnetic and conduction problems. *Journal of the Physical Society of Japan*, 12:570, 1957.

[6] C. Jarzynski. Nonequilibrium equality for free energy differences. *Physical Review Letters*, 78:2690, 1997.

[7] C. Jarzynski. Equilibrium free-energy differences from nonequilibrium measurements: A master-equation approach. *Physical Review E*, 56:5018, 1997.

[8] C. Jarzynski. Nonequilibrium work theorem for a system strongly coupled to a thermal environment. *Journal of Statistical Mechanics: Theory and Experiment*, 2004:P09005, 2004.

[9] G. E. Crooks. Nonequilibrium measurements of free energy differences for microscopically reversible Markovian systems. *Journal of Statistical Physics*, 90:1481, 1998.

[10] G. E. Crooks. Entropy production fluctuation theorem and the nonequilibrium work relation for free energy differences. *Physical Review E*, 60:2721, 1999.

[11] D. J. Evans, E. G. D. Cohen, and G. P. Moriss. Probability of second law violations in shearing steady states. *Physical Review Letters*, 71:2401, 1993.

[12] J. Kurchan. Fluctuation theorem for stochastic dynamics. *Journal of Physics A: Mathematical and General*, 31:3719, 1998.

[13] J. L. Lebowitz and H. Spohn. A Gallavotti-Cohen-type symmetry in the large deviation functional for stochastic dynamics. *Journal of Statistical Physics*, 95:333, 1999.

[14] U. Seifert. Entropy production along a stochastic trajectory and an integral fluctuation theorem. *Physical Review Letters*, 95:040602, 2005.

[15] U. Seifert. Stochastic thermodynamics: principles and perspectives. *European Physical Journal B*, 64:423, 2008.

[16] R. M. L. Evans. Rules for transition rates in nonequilibrium steady states. *Physical Review Letters*, 92:150601, 2004.

[17] R. M. L. Evans. Driven steady states: Rules for transition rates. *Physica A*, 340:364, 2004.

[18] R. M. L. Evans. Detailed balance has a counterpart in non-equilibrium steady states. *Journal of Physics A: Mathematical and General*, 38:293, 2005.

[19] A. Simha, R. M. L. Evans, and A. Baule. Properties of a nonequilibrium heat bath. *Physical Review E*, 77:031117, 2008.

[20] O. Reynolds. On the dilatancy of media composed of rigid particles in contact. *Philosophical Magazine*, 20:469, 1885.

[21] H. M. Jaeger, S. R. Nagel, and R. P. Behringer. Granular solids, liquids, and gases. *Reviews of Modern Physics*, 68:1259, 1996.

[22] R. A. Bagnold. Experiments on a gravity-free dispersion of large solid spheres in a newtonian fluid under shear. *Proceedings of the Royal Society of London. Series A, Mathematical and Physical Sciences*, 225:49, 1954.

[23] G. Lois, A. Lemaître, and J. M. Carlson. Numerical tests of constitutive laws for dense granular flows. *Physical Review E*, 72:051303, 2005.

[24] R. Khosropour, J. Zirinsky, H. K. Pak, and R. P. Behringer. Convection and size segregation in a Couette flow of granular material. *Physical Review E*, 56:4467, 1997.

[25] D. M. Mueth, G. F. Debregeas, G. S. Karczmar, P. J. Eng, S. R. Nagel, and H. M. Jaeger. Signatures of granular microstructure in dense shear flows. *Nature*, 406:385, 2000.

[26] A. J. Liu and S. R. Nagel. Jamming is just not cool any more. *Nature*, 396:21, 1998.

[27] S. Torquato, T. M. Truskett, and P. G. Debenedetti. Is random close packing of spheres well defined? *Physical Review Letters*, 84:2064, 2000.

[28] C. S. O'Hern, S. A. Langer, A. J. Liu, and S. R. Nagel. Random packings of frictionless particles. *Physical Review Letters*, 88:075507, 2002.

[29] C. S. O'Hern, S. A. Langer, A. J. Liu, and S. R. Nagel. Jamming at zero temperature and zero applied stress: The epitome of disorder. *Physical Review E*, 68:011306, 2003.

[30] O. J. O'Loan, M. R. Evans, and M. E. Cates. Jamming transition in a homogeneous one-dimensional sysyem: the bus route model. *Physical Review E*, 58:1404, 1998.

[31] S. Katz, J. L. Lebowitz, and H. Spohn. Nonequilibrium steady states of stochastic lattice gas models of fast ionic conductors. *Journal of Statistical Physics*, 34:497, 1984.

[32] B. Schmittmann and R. K. P. Zia. *Statistical mechanics of driven diffusive systems*. Academic Press, 1995. Volume 17 of Phase Transitions and Critical Phenomena.

[33] A. Baule and R. M. L. Evans. Invariant quantities in shear flow. *Physical Review Letters*, 101:240601, 2008.

[34] C. Monthus. Non-equilibrium steady states : maximization of the Shannon entropy associated to the distribution of dynamical trajectories in the presence of constraints. *Journal of Statistical Mechanics: Theory and Experiment*, page P03008, 2011.

[35] V. Lecomte, A. Imparato, and F. van Wijland. Current fluctuations in systems with diffusive dynamics, in and out of equilibrium. *Progress of Theoretical Physics Supplement*, 184:276, 2010.

[36] E. T. Jaynes. Information theory and statistical mechanics. *Physical Review*, 106:620, 1957.

[37] E. T. Jaynes. Information theory and statistical mechanics II. *Physical Review*, 108:171, 1957.

[38] R. L. Jack, J. P. Garrahan, and D. Chandler. Space-time thermodynamics and subsystem observables in a kinetically constrained model of glassy systems. *Journal of Chemical Physics*, 125:184509, 2006.

[39] L. O. Hedges, R. L. Jack, J. P. Garrahan, and D. Chandler. Dynamic order-disorder in atomistic models of structural glass formers. *Science*, 323:1309, 2009.

[40] J. P. Garrahan, R. L. Jack, V. Lecomte, E. Pitard, K. van Duijvendijk, and F. van Wijland. First-order dynamical phase transition in models of glasses: an approach based on ensembles of histories. *Journal of Physics A: Mathematical and Theoretical*, 42:075007, 2009.

[41] R. M. L. Evans, R. A. Simha, A. Baule, and P. D. Olmsted. Statistical mechanics far from equilibrium: Prediction and test for a sheared system. *Physical Review E*, 81:051109, 2010.

[42] L. Onsager and S. Machlup. Fluctuations and irreversible processes. *Physical Review*, 91:1505, 1953.

[43] B. Derrida, J. L. Lebowitz, and E. R. Speer. Large deviation of the density profile in the steady state of the open symmetric simple exclusion process. *Journal of Statistical Physics*, 107:599, 2002.

[44] L. Bertini, A. De Sole, D. Gabrielli, G. Jona-Lasinio, and C. Landim. Macroscopic fluctuation theory for stationary non-equilibrium states. *Journal of Statistical Physics*, 107:635, 2002.

[45] H. Touchette. The large deviation approach to statistical mechanics. *Physics Reports*, 478:1, 2009.

[46] V. Schmitt, F. Lequeux, A. Pousse, and D. Roux. Flow behaviour and shear induced transition near an isotropic/nematic transition in equilibrium polymers. *Langmuir*, 10:955, 1994.

[47] R. Makhloufi, J. P. Decruppe, A. Aít-Ali, and R. Cressely. Rheo-optical study of worm-like micelles undergoing a shear banding flow. *Europhysics Letters*, 32:253, 1995.

[48] J.-F. Berret, G. Porte, and J.-P. Decruppe. Inhomogeneous shear flows of wormlike micelles: A master dynamic phase diagram. *Physical Review E*, 55:1668, 1997.

[49] M. M. Britton and P. T. Callaghan. Two-phase shear band structures at uniform stress. *Physical Review Letters*, 78:4930, 1997.

[50] M. M. Britton and P. T. Callaghan. Shear banding instability in wormlike micellar solutions. *European Physical Journal B*, 7:237, 1999.

[51] E. Cappelaere, J. F. Berret, J. P. Decruppe, R. Cressely, and P. Lindner. Rheology, birefringence, and small-angle neutron scattering in a charged micellar system: Evidence of a shear-induced phase transition. *Physical Review E*, 56:1869, 1997.

[52] J.-F. Berret, D. C. Roux, G. Porte, and P. Lindner. Shear-induced isotropic-to-nematic phase transition in equilibrium polymers. *Europhysics Letters*, 25:521, 1994.

[53] P. Tapadia and S.-Q. Wang. Yieldlike constitutive transition in shear flow of entangled polymeric fluids. *Physical Review Letters*, 91:198301, 2003.

[54] P. Tapadia and S.-Q. Wang. Yieldlike constitutive transition in shear flow of entangled polymeric fluids. *Physical Review Letters*, 96:016001, 2006.

[55] L. Marshall and C. F. Zukoski IV. Experimental studies on the rheology of hard-sphere suspensions near the glass transition. *Journal of Physical Chemistry*, 94:1164, 1990.

[56] L. B. Chen, B. J. Ackerson, and C. F. Zukoski. Rheological consequences of microstructural transitions in colloidal crystals. *Journal of Rheology*, 38:193, 1994.

[57] D. Roux, F. Nallet, and O. Diat. Rheology of lyotropic lamellar phases. *Europhysics Letters*, 24:53, 1993.

[58] M. Johnson and D. Segalman. A model for viscoelastic behaviour which allows non-affine deformation. *Journal of Non-Newtonian Fluid Mechanics*, 2:255, 1977.

[59] P. D. Olmsted, O. Radulescu, and C.-Y. D. Lu. JohnsonSegalman model with a diffusion term in cylindrical Couette flow. *Journal of Rheology*, 44:257, 2000.

[60] S. M. Fielding and P. D. Olmsted. Spatiotemporal oscillations and rheochaos in a simple model of shear banding. *Physical Review Letters*, 92:084502, 2004.

[61] J. L. A. Dubbeldam and P. D. Olmsted. Two-dimensional perturbations in a scalar model for shear banding. *European Physical Journal E*, 29:363, 2009.

[62] J. A. Cuesta and A. Sánchez. General non-existence theorem for phase transitions in one-dimensional systems with short range interactions, and physical examples of such transitions. *Journal of Statistical Physics*, 115:869, 2004.

[63] L. P. Kadanoff. *Statistical physics: statics, dynamics and renormalisation.* World Scientific Publishing Co. Pte. Ltd., 2000.

[64] J. A. Acebrón, L. L. Bonilla, C. J. P. Vicente, F. Ritort, and R. Spigler. The Kuramoto model: A simple paradigm for synchronization phenomena. *Reviews of Modern Physics*, 77:137, 2005. Review article.

[65] A. W. Lees and S. F. Edwards. The computer study of transport processes under extreme conditions. *Journal of Physics C: Solid State Physics*, 5:1921, 1972.

[66] M. Büttiker, E. P. Harris, and R. Landauer. Thermal activation in extremely underdamped josephson-junction circuits. *Physical Review B*, 28:1268, 1983.

[67] H. A. Kramers. Brownian motion in a field of force and the diffusion model of chemical reactions. *Physica*, 7:284, 1940.

[68] P. Hänggi, P. Talkner, and M. Borkovec. Reaction-rate theory: fifty years after Kramers. *Reviews of Modern Physics*, 62:251, 1990.

[69] C. Hall and R. M. L. Evans. private communication.

[70] B. Widom. Surface tension and molecular correlations near the critical point. *Journal of Chemical Physics*, 43:3892, 1965.

[71] B. Widom. Equation of state in the neighbourhood of the critical point. *Journal of Chemical Physics*, 43:3898, 1965.

[72] K. G. Wilson. Renormalization group and critical phenomena. I. Renormalization group and the Kadanoff scaling picture. *Physical Review B*, 4:3174, 1971.

[73] K. G. Wilson. Renormalization group and critical phenomena. II. Phase-space cell analysis of critical behaviour. *Physical Review B*, 4:3184, 1971.

[74] M. Abramowitz and I. A. Stegun. *Handbook of Mathematical Functions*. Dover Publications Inc., New York, 1972.

[75] I. S. Gradshteyn and I. M. Ryzhik. *Table of Integrals, Series, and Products*. Academic Press, Inc., 1980.

[76] R. D. Groot and P. B. Warren. Dissipative particle dynamics: Bridging the gap between atomistic and mesoscopic simulation. *Journal of Chemical Physics*, 107:4423, 1997.

[77] L. Verlet. Computer experiments on classical fluids. I. Thermodynamical properties of Lennard-Jones molecules. *Physical Review*, 159:98, 1967.

[78] W. C. Swope, H. C. Andersen, P. H. Berens, and K. R. Wilson. A computer simulation method for the calculation of equilibrium constants for the formation of physical clusters of molecules: Application to small water clusters. *Journal of Chemical Physics*, 76:637, 1982.